

Acknowledgements

This Master's Thesis, written autumn 2018, is a co-operation between NTNU, Department of Chemical Engineering and Glencore Nikkelverk AS. All experimental work has been carried out at NTNU as a part of the crystallization research group. Professor Jens-Petter Andreassen (NTNU) has been the supervisor for this thesis, in addition to co-supervisors Ina Beate Jenssen (NTNU), Seniz Ucar (NTNU) and Oluf Bøckmann (Glencore Nikkelverk AS).

I would like to thank Jens-Petter Andreassen for his guidance, strategy and constructive criticism, which has helped me a lot in the work of this thesis. Ina Beate Jenssen and Seniz Ucar have both been very helpful in dealing with technical and laboratory related issues. Oluf Bøckmann has shown great enthusiasm throughout the project, and always quickly contributed with feedback and necessary information whenever I needed it. I would also like to thank Syverin Lierhagen for his help and feedback in regards to ICP-MS analysis and sample preparation.

Thanks to all the students in my reading room and to the rest of the K4 building for providing a good study environment. Finally, I would like to thank my family and friends for their great support over the course of the writing process.

I, Fredrik Skadsem STORØY, hereby declare that this is an independent work according to the exam regulations of the Norwegian University of Science and Technology.

Contents

Acknowledgements	i
1 Introduction and Objective	1
2 Theory	4
2.1 The Crystalline State	4
2.1.1 Dissociation and electrolyte ions	5
Ionic Strength	5
Common and diverse ion effect on crystallization	6
2.1.2 Polymorphism	6
2.2 Solubility	6
2.2.1 Metal aquo complex	7
2.2.2 Gibbs Free Energy of mixing	8
2.2.3 Expressions of solution composition	9
2.2.4 Supersaturation	10
2.3 Impurities	14
2.4 Crystal Nucleation	14
2.4.1 Primary homogeneous nucleation	15
2.4.2 Primary Heterogeneous Nucleation	17
2.4.3 Secondary Nucleation	18
2.4.4 Seeding	19
2.4.5 Induction Period and Latent time	19
2.5 Crystal Growth	20
2.5.1 Heat of crystallization	22
Agglomeration and caking	23
2.5.2 Effects of impurities on crystal growth	23
Kinetic effect	23
Thermodynamic effect	25
2.5.3 Electrical double layer	26
Zeta-potential	27

3	Experimental setup	28
3.1	Experimental overview and parameters	28
3.1.1	Saturation solubility and phase diagram of Nickel sulfate	28
3.1.2	Impurity selection and concentration	28
	De-clumping and dry-milling	29
3.1.3	Temperature	29
3.1.4	Saturation level and solution volume	30
3.1.5	Seeding ratio and particle diameter of seeds	30
3.1.6	Chemicals	31
3.2	Batch Reactor and filtration setup	31
3.3	60°C batch crystallization experiment	34
3.4	Partial filtration setup	37
3.4.1	Expectations from partial dissociation	38
3.5	Solubility setup	39
3.6	Analytical procedures	40
3.6.1	X-ray diffraction (XRD)	40
3.6.2	Inductively coupled plasma mass spectrometry (ICP-MS)	41
3.6.3	Scanning Electron Microscopy (SEM)	42
4	Results from experiments	43
4.1	Impurity uptake from experiments	43
4.1.1	Plot setup	43
	Error bars	45
4.1.2	SEM photographs	46
4.2	Impurity content in samples containing multiple impurities	46
4.3	Na^+ as a crystallization impurity on Nickel sulfate	51
4.3.1	Na^+ at 25°C without any other deliberately added impurities	51
4.3.2	Na^+ at 25°C with Cl^- , and Mg^{2+} in equal proportions	52
4.3.3	Na^+ as a crystallization impurity at 60°C in the presence of Mg^{2+} and Cl^- in equal proportions	54
4.4	Cl^- as a crystallization impurity on Nickel sulfate	54
4.4.1	Cl^- at 25°C	54
4.4.2	Cl^- at 25°C with equal proportions of Na^+ and Mg^{2+}	55
4.4.3	Cl^- at 60°C with equal proportions of Na^+ and Mg^{2+}	57
4.5	Mg^{2+} as a crystallization impurity on Nickel sulfate	58
4.5.1	Mg^{2+} at 25°C	58
4.5.2	Mg^{2+} at 25°C with equal proportions of Na^+ and Cl^-	59
4.5.3	Mg^{2+} at 60°C with equal proportions of Na^+ and Cl^-	60

4.6	Impurities and induction time estimations	61
4.7	Impurity uptake and crystal purity	61
4.7.1	Impurity uptake rate	62
4.8	XRD results	62
4.9	Results from the solubility tests	62
4.10	Crystal yields of crystallization experiments	64
5	Discussion	69
5.1	Interpretation of Results	69
5.1.1	The Structure of the solution	69
5.1.2	Structure formers and structure breakers	69
5.1.3	XRD diagram discussion	74
5.1.4	SEM photographs discussion	74
5.1.5	Effects of pH on the saturation solubility of ionic compounds .	75
5.1.6	Impurities' effect on each other	76
5.2	Effectiveness of the partial filtration method	76
5.2.1	Possible explanations	78
6	Summary and Conclusion	80
7	Recommendation for further work	82
A	Physical Properties of Nickel sulfate	83
A.0.1	Properties of Nickel sulfate hexahydrate ($NiSO_4 * 6H_2O$)	83
B	Solution Compositions and induction times	87
B.1	25°C Batch Reactor Solution composition	87
B.2	60°C batch reactor solution composition	89
C	Detailed Experimental Procedures	91
C.1	25°C batch reactor experimental procedure	91
C.2	60°batch experiment procedure	92
C.3	Partial dissociation experiment procedure	93
C.4	Solubility experiment procedure	93
D	X-ray diffraction patters	95
D.1	X-ray diffraction patterns compound identification	95
E	Scanning electron microscope pictures	105
E.1	Na^+ only SEM photographs	105
E.2	Cl^- only SEM photographs	105

E.3 Mg^{2+} only SEM photographs	105
F Health Safety and Environment	110
Bibliography	111

List of Figures

2.1	Solubility-Supersolubility diagram showing pathways to crystallization (Andreassen, 2015)	11
2.2	Saturation solubility diagram of Sodium Sulfate (Na_2SO_4) (Lohninger, 2011)	13
2.3	Nucleation types (Andreassen, 2015)	15
2.4	Visualized impurity adsorption and retardation of movement of the monolayer. (Kubota, Yokota, and Mullin, 1996).	24
3.1	SEM pictures a) and b) show declumped Nickel sulfate hexahydrate seeds containing no impurities.	31
3.2	Batch crystallizer used in experiments (not to scale)	33
3.3	Vacuum filtration setup (chem.libretexts.org, 2017)	34
3.4	Sketch of High temperature Crystallization (not to scale)	35
3.5	Sketch of partial filtration setup (not to scale)	38
3.6	Sketch of the solubility setup (not to scale)	40
4.1	Plots a) and b) display the concentrations of crystallized $NiSO_4 \cdot 6H_2O$ salts <i>before</i> partial dissociation) from solutions containing 3, 5 and 10 g/kg of solution of Na^+ , Cl^- , and Mg^{2+} at 25°C. Plot a) and b) display the same information, but use different units on the x-axis.	44
4.2	Plots a) and b) display the concentrations of crystallized $NiSO_4 \cdot 6H_2O$ crystals <i>after</i> partial dissociation. The crystals are precipitated at 25°C from solutions containing 3, 5 and 10 g/kg of solution of Na^+ , Cl^- , and Mg^{2+} . Plot a) and b) display the same information, but use different units on the x-axis.	44
4.3	Final crystals from experiment with 3 grams per kg of Na^+ , Cl^- and Mg^{2+} at 25°C before and after partial dissociation. Scale bar of 500 μm shown as reference	45
4.4	Final crystals from experiment with 5 grams per kg of Na^+ , Cl^- and Mg^{2+} at 25°C before and after partial dissociation. Scale bar of 500 μm shown as reference	46

4.5	Final crystals from experiment with 10 grams per kg of Na^+ , Cl^- and Mg^{2+} at 25°C before and after partial dissociation. Scale bar of 500 μm shown as reference	47
4.6	Plots a) and b) display the concentrations of crystallized $NiSO_4 * 6H_2O$ (<i>before</i> partial dissociation) from solutions containing 3, 5 and 10 g/kg of solution of Na^+ , Cl^- , and Mg^{2+} . These crystals were precipitated at 60°C. Plot a) and b) display the same information, but use different units on the x-axis.	48
4.7	Final crystals from experiment with 3 grams per kg of Na^+ , Cl^- and Mg^{2+} at 60°C before and after partial dissociation. Scale bar of 500 μm shown as reference	48
4.8	Final crystals from experiment with 5 grams per kg of Na^+ , Cl^- and Mg^{2+} at 60°C before and after partial dissociation. Scale bar of 500 μm shown as reference	49
4.9	Final crystals from experiment with 10 grams per kg of Na^+ , Cl^- and Mg^{2+} at 60°C before and after partial dissociation. Scale bar of 500 μm shown as reference	49
4.10	Plots a) and b) display the concentrations of crystallized $NiSO_4 * 6H_2O$ crystals <i>after</i> partial dissociation. The crystals are precipitated at 60°C from solutions containing 3, 5 and 10 g/kg of solution of Na^+ , Cl^- , and Mg^{2+} . Plot a) and b) display the same information, but use different units on the x-axis.	50
4.11	Na^+ [g] per Ni^{2+} [g] in crystallized $NiSO_4 * 6H_2O$ plotted against Na^+ concentration of the solution before crystallization at 25°C in the presence of no other deliberately added impurities. Plot a) and b) display the same information, but use different units on the x-axis.	51
4.12	Na^+ [g] per Ni^{2+} [g] in crystallized $NiSO_4 * 6H_2O$ plotted against Na^+ concentration of the solution before crystallization at 25°C in the presence of Cl^- and Mg^{2+} as other deliberately added impurities. Plot a) and b) display the same information, but use different units on the x-axis.	52
4.13	Na^+ [g] per Ni^{2+} [g] in crystallized $NiSO_4 * 6H_2O$ plotted against Na^+ concentration of the solution before crystallization at 60°C in the presence of Cl^- and Mg^{2+} as other deliberately added impurities. Plot a) and b) display the same information, but use different units on the x-axis.	53

4.14	Cl^- [g] per Ni^{2+} [g] in crystallized $NiSO_4 \cdot 6H_2O$ plotted against Cl^- concentration of the solution before crystallization at 25°C in the presence of no other deliberately added impurities. Plot a) and b) display the same information, but use different units on the x-axis.	55
4.15	Cl^- [g] per Ni^{2+} [g] in crystallized $NiSO_4 \cdot 6H_2O$ plotted against Cl^- concentration of the solution before crystallization at 25°C in the presence of Na^+ and Mg^{2+} as other deliberately added impurities. Plot a) and b) display the same information, but use different units on the x-axis.	56
4.16	Cl^- [g] per Ni^{2+} [g] in crystallized $NiSO_4 \cdot 6H_2O$ plotted against Cl^- concentration of the solution before crystallization at 60°C in the presence of Na^+ and Mg^{2+} as other deliberately added impurities. Plot a) and b) display the same information, but use different units on the x-axis.	57
4.17	Concentration of solution before crystallization plotted against Na^+ [g] per Ni^{2+} [g] in crystallized $NiSO_4 \cdot 6H_2O$ at 25°C with no other deliberately added impurity. Plot a) and b) display the same information, but use different units on the x-axis.	58
4.18	Concentration of solution before crystallization plotted against Na^+ [g] per Ni^{2+} [g] in crystallized $NiSO_4 \cdot 6H_2O$ at 25°C with no other deliberately added impurity. Plot a) and b) display the same information, but use different units on the x-axis.	59
4.19	Concentration of solution before crystallization plotted against Na^+ [g] per Ni^{2+} [g] in crystallized $NiSO_4 \cdot 6H_2O$ at 25°C with no other deliberately added impurity. Plot a) and b) display the same information, but use different units on the x-axis.	60
4.20	XRD pattern of $NiSO_4 \cdot 6H_2O$ crystallized from a supersaturated solution at 25°C with deliberately added impurities of 10 g/kg of Na^+ , Cl^- , and Mg^{2+} overlaid with the XRD pattern of Magnesium sulfate .	63
4.21	Solubility of aqueous Nickel sulfate with deliberately added 5g/kg of sulfuric acid (H_2SO_4) at 25, 50 and 75°C plotted alongside theoretical solubility of Nickel sulfate with no impurities.	63
4.22	Solubility of aqueous Nickel sulfate at 25°C with various impurities at different concentration. The saturation solubility at 25°C is shown for reference.	65
4.23	Solubility of aqueous Nickel sulfate at 60°C with various impurities at different concentration. The saturation solubility at 60°C is shown for reference.	65

A.1	Lattice parameters of Nickel sulfate (Hassanein, 2018; Beevers and Lipson, 1932)	83
A.2	Phase diagram of Nickel sulfate (Hassanein, 2018)	85
A.3	Pitzer model of a pure Nickel sulfate aqueous solution to estimate activity coefficients at different temperatures. (Hassanein, 2018)	85
D.1	XRD pattern of Nickel sulfate hexahydrate crystallized from a supersaturated solution at 25°C with deliberately added impurities of 10 g/kg of Na^+ , Cl^- , and Mg^{2+} overlaid with the XRD pattern of Nickel sulfate hexahydrate	96
D.2	XRD pattern of Nickel sulfate hexahydrate crystallized from a supersaturated solution at 25°C with deliberately added impurities of 10 g/kg of Na^+ , Cl^- , and Mg^{2+} overlaid with the XRD pattern of Magnesium chloride ($MgCl_2$)	96
D.3	XRD pattern of Nickel sulfate hexahydrate crystallized from a supersaturated solution at 25°C with deliberately added impurities of 10 g/kg of Na^+ , Cl^- , and Mg^{2+} overlaid with the XRD pattern of Sodium chloride ($NaCl$)	97
D.4	XRD pattern of Nickel sulfate hexahydrate crystallized from a supersaturated solution at 25°C with deliberately added impurities of 10 g/kg of Na^+ , Cl^- , and Mg^{2+} overlaid with the XRD pattern of Sodium sulfate (Na_2SO_4)	97
D.5	XRD pattern of Nickel sulfate hexahydrate crystallized from a supersaturated solution at 25°C with deliberately added impurities of 10 g/kg of Na^+ , Cl^- , and Mg^{2+} overlaid with the XRD pattern of Nickel chloride ($NiCl_2$)	98
D.6	XRD pattern of Nickel sulfate hexahydrate crystallized from a supersaturated aqueous solution of 3g Na^+ per kg of solution at 25°C.	98
D.7	XRD pattern of Nickel sulfate hexahydrate crystallized from a supersaturated aqueous solution of 5g Na^+ per kg of solution at 25°C.	99
D.8	XRD pattern of Nickel sulfate hexahydrate crystallized from a supersaturated aqueous solution of 10g Na^+ per kg of solution at 25°C.	99
D.9	XRD pattern of Nickel sulfate hexahydrate crystallized from a supersaturated aqueous solution of 3g Cl^- per kg of solution at 25°C.	100
D.10	XRD pattern of Nickel sulfate hexahydrate crystallized from a supersaturated aqueous solution of 5g Cl^- per kg of solution at 25°C.	100
D.11	XRD pattern of Nickel sulfate hexahydrate crystallized from a supersaturated aqueous solution of 10g Cl^- per kg of solution at 25°C.	101

D.12	XRD pattern of Nickel sulfate hexahydrate crystallized from a super-saturated aqueous solution of 3g Mg^{2+} per kg of solution at 25°C. . . .	101
D.13	XRD pattern of Nickel sulfate hexahydrate crystallized from a super-saturated aqueous solution of 5g Mg^{2+} per kg of solution at 25°C. . . .	102
D.14	XRD pattern of Nickel sulfate hexahydrate crystallized from a super-saturated aqueous solution of 10g Mg^{2+} per kg of solution at 25°C. . .	102
D.15	XRD pattern of Nickel sulfate hexahydrate crystallized from a super-saturated aqueous solution of 3g Na^+ , Cl^- , and Mg^{2+} per kg of solution at 25°C.	103
D.16	XRD pattern of Nickel sulfate hexahydrate crystallized from a super-saturated aqueous solution of 5g Na^+ , Cl^- , and Mg^{2+} per kg of solution at 25°C.	104
D.17	XRD pattern of Nickel sulfate hexahydrate crystallized from a super-saturated aqueous solution of 10g of Na^+ , Cl^- , and Mg^{2+} per kg of solution at 25°C.	104
E.1	Final crystals from experiment with 3 grams per kg of Na^+ at 25°C before and after partial filtration. Scale bar of 500 μm shown as reference	105
E.2	Final crystals from experiment with 5 grams per kg of Na^+ at 25°C before and after partial filtration. Scale bar of 500 μm shown as reference	106
E.3	Final crystals from experiment with 10 grams per kg of Na^+ at 25°C before and after partial filtration. Scale bar of 500 μm shown as reference	106
E.4	Final crystals from experiment with 3 grams per kg of Cl^- at 25°C before and after partial filtration. Scale bar of 500 μm shown as reference	107
E.5	Final crystals from experiment with 5 grams per kg of Cl^- at 25°C before and after partial filtration. Scale bar of 500 μm shown as reference	107
E.6	Final crystals from experiment with 10 grams per kg of Cl^- at 25°C before and after partial filtration. Scale bar of 500 μm shown as reference	108
E.7	Final crystals from experiment with 3 grams per kg of Mg^{2+} at 25°C before and after partial filtration. Scale bar of 500 μm shown as reference	108
E.8	Final crystals from experiment with 5 grams per kg of Mg^{2+} at 25°C before and after partial filtration. Scale bar of 500 μm shown as reference	109
E.9	Final crystals from experiment with 10 grams per kg of Mg^{2+} at 25°C before and after partial filtration. Scale bar of 500 μm shown as reference	109

List of Tables

3.1	Chemicals used in this project	32
4.1	Induction times for experiments at 25°C at intervals of 20 seconds . . .	61
4.2	Percentage impurity uptake rate from concentration in solution to crystal (slope of plot a) in figures 4.1 to 4.19. If the solution concentration has "(PD)" following it, then the crystals are partially dissociated	66
4.3	Impurity uptake [weight percentage] in precipitated $NiSO_4 * 6H_2O$ from solutions at 25°C with single, varying concentrations of Na^+ , Cl^- or Mg^{2+} . If the solution concentration has "(PD)" following it, then the crystals are partially dissociated	67
4.4	Impurity uptake [weight percentage] in precipitated $NiSO_4 * 6H_2O$ from solutions at 25°C with 3, 5 and 10 g/kg of solution of Na^+ , Cl^- and Mg^{2+} . If the solution concentration has "(PD)" following it, then the crystals are partially dissociated	67
4.5	Impurity uptake [weight percentage] in precipitated $NiSO_4 * 6H_2O$ of experiments at 60°C with 3, 5 and 10 g/kg of solution of Na^+ , Cl^- and Mg^{2+} . If the solution concentration has "(PD)" following it, then the crystals are partially dissociated	68
4.6	Crystal yields from crystallization experiments	68
5.1	Physical properties of cations and anions at 298K (Jibbouri, 2002) . . .	71
5.2	The average impurity content across all tests <i>before</i> partial filtration, the average impurity content of all tests after partial filtration and the difference from before to after	77
5.3	The percentage of impurity uptake removed by partial filtration for each impurity and the average efficiency of partial filtration for each element across all tests.	77
A.1	The saturation solubility of anhydrous Nickel sulfate in water	84
A.2	The saturation solubility of Nickel sulfate hexahydrate in water	86
B.1	Impurity ion mass values for of batch experiments conducted at 25°C based on a total solution mass of 656.17g	87

B.2	Solution composition of batch experiments conducted at 25°C.	88
B.3	Impurity ion mass values for of batch experiments conducted at 60°C based on a total solution mass of 280.853g	89
B.4	Solution composition of solubility tests conducted at 25°C, 50°C and 75°C.	89
B.5	Exact solubilities of solubility tests conducted at 25°C, 50°C and 75°C and exact values used in figure 4.21.	90

List of Abbreviations

BEV	Battery Electric Vehicles
XRD	X- Ray Diffraction
SEM	Scanning Electron Microscopy
ICP-MS	Inductively Coupled Plasma Mass Spectrometer

List of Symbols

A	preexponential factor	(-)
a	activity	(-)
a	area of the growth unit on the crystal surface	m^2
B	rate of secondary nucleation rate	1/s
C	concentration	mol/kg
G	linear crystal growth rate	(-)
G	overall excess free energy	J
G_{crit}	homogeneous critical free energy	J
G'_{crit}	heterogeneous critical free energy	J
G_{hyd}	Gibbs free energy of hydration	J
G_{mix}	Gibbs free energy of mixing	J
G_s	surface excess free energy	J
G_v	volume excess free energy	J
H_{mix}	enthalpy of mixing	J
H_{hyd}	enthalpy of hydration	J
I	ionic strength	mol per kg
J	rate of nucleation	1/s
k_N	secondary nucleation constant	(-)
k_g	growth rate constant	(-)
L	characteristic length	m
l	average distance between impurities	Å
M_T	magma density of the present solids	kg/m
M_1	mass put into solution	kg
M_2	mass taken out solution	kg
m_i	the molar concentration	mol per kg
$m_{NiSO_4*6H_2O,s}$	Nickel sulfate hexahydrate seed mass	g
$m_{NiSO_4*6H_2O,tot}$	initially dissolved mass of Nickel sulfate hexahydrate	g
m_{H_2O-PD}	mass of deionized water	g
$m_{NiSO_4*6H_2O-PD}$	mass of Nickel sulfate hexahydrate	g
\bar{R}	molar gas constant	J/(K*mol)
R	ratio of hydrated molar mass to anhydrous molar mass	(-)

R_G	growth rate	(-)
r	nucleus size	m
r_c	critical nucleus size	m
S	degree of supersaturation	(-)
S_{hyd}	entropy of hydration	J/K
S_{mix}	entropy of mixing	J/K
T	temperature	°C or K
t_{ind}	induction time	s
t_r	time required to achieve molecular clusters	s
t_n	nucleation time	s
t_g	time required for the nuclei to grow	s
t_l	latent time	s
v	molecular volume	m^3
v_0	step advancement velocity of a linear step	m/s
v_r	step advancement velocity of a curved step	m/s
z_i	charge of ion i	z
α_1	volume shape factor	(-)
β_1	surface shape factor	(-)
ϵ	agitator speed	RPM
γ	interfacial tension	newton/meter
γ_l	linear edge free energy of the step	J
λ	average distance between active sites	Å
$\mu_{crystal}$	chemical potential of the bulk of the crystal	J/mol
μ_s	chemical potential of the solute in solution	J/mol
μ_c	activity coefficient	(-)
Φ	wetting angle factor	(-)
ϕ	seeding ratio	%
ρ_c	crystal density	(-)
σ	relative supersaturation	(-)
θ	wetting angle	°
θ_*	active site coverage on the crystal surface	(-)
Y	ratio of $NiSO_4 \cdot 6H_2O$ to H_2O	(-)

Chapter 1

Introduction and Objective

In the past decades, batteries have improved steadily in what they are capable of powering. Steady innovations and improvements have increased their range from powering small electronics to powering vehicles. The first battery powered electric vehicles (BEV) were seen in the late 90's and were limited in their capacity and performance. Since then, BEVs have made great process, in large part because of the advancements to battery technology. Nickel sulfate is one of the components modern battery manufacturers use in the cathode of high performance Lithium-ion batteries. The cathode may seem like a minor part of a battery, but it can account for 28% of the total cost of a high Nickel content battery (Berckmans et al., 2017). The cathode specifically has seen a lot of attention and innovation in the last 15 years, as opposed to the anode which has largely been unchanged since the late 90s. ¹ The reason Nickel is useful in a Lithium-ion battery cathode is its ability to conduct electricity, energy density, comparatively low cost as opposed to Cobalt and Manganese, and overall lifetime. The Nickel industry is expected to see a demand increase as both Lithium-ion BEVs are becoming more common and high-nickel, low-cobalt cathodes² are being more utilized. (Berckmans et al., 2017; Nitta et al., 2015)

Most Nickel produced today is used as a component of stainless steel, industrial catalysts, and metal surface treatment, where extremely high purity is not a priority. This presents the main challenge facing the Nickel market: finding an economically viable method to produce high purity Nickel sulfate as the process of converting low grade nickel into battery grade Nickel sulfate is extremely expensive and inefficient. Battery grade Nickel Sulfate varies slightly based on different spec-lists of allowed ppm-contents of every element on the periodic table that battery manufacturers use.

¹The anode of Lithium-ion batteries is composed of graphite. A prediction based on research is that in 10 years, a silicone based anode and a Nickel based cathode will be the industry standard. (Berckmans et al., 2017)

²Such as the NCM (*Lithium Nickel Cobalt Manganese*) and NCA (*Lithium Nickel Cobalt Aluminum*) cathodes.

(Berckmans et al., 2017; Nitta et al., 2015)

Glencore Nikkelverk AS, a Kristiansand based company producing high quality nickel, copper, cobalt and sulfuric acid. The primary industrial methods that they use to separate and purify their products starts with metal ores being dissolved into aqueous solution via a process called leaching. After some processing, the aqueous solution is electrolyzed, meaning a large amount of electricity is applied to force a non-spontaneous reaction to take place. In this case being the reduction of the positive metal ions in solution to deposit on the cathode of the electrolysis cell³ as a pure metal. Electrolysis for this specific purpose is known as electrowinning. The pure metal is then sold to the customer for them to convert into nickel sulfate. (Berckmans et al., 2017)

In preparation for the forecasted rise in demand of Nickel sulfate, Glencore Nikkelverk AS is investigating alternative production routes for Nickel via a side stream for Nickel sulfate crystallization. The proposed side stream would deposit Nickel sulfate out of a feed of Nickel Sulfate and Nickel Chloride with some impurities such as Magnesium (Mg), Sodium (Na). This side stream would separate the product from the feed by crystallization as opposed to electrolysis. Crystallized Nickel sulfate would then be sold to the customer ideally without the need for further processing, this is beneficial for several reasons, here are a few:

- The demand for Nickel sulfate is expected to rise much faster than the supply, which means the selling price will most likely rise as well (Berckmans et al., 2017).
- Glencore Nikkelverk AS has access to internal sources of heating and cooling from other parts of the plant via heat exchangers, which may be utilized in the crystallization process. (Bøckmann, 2018)
- Glencore Nikkelverk AS would be able to widen their product range which may attract new customers.

Should Glencore Nikkelverk AS decide to produce battery grade Nickel sulfate, then information about purification methods becomes valuable. While they have resources already available, they would still require investment into new process units like crystallizers, evaporators, filtrators, solvent extractors, re-crystallizers and

³Unrelated to the Lithium-ion battery cathode mentioned previously

other treatment steps. (Bøckmann, 2018)

The investigations discussed in this thesis are primarily centered around analyzing precipitated salts from a feed stock containing various concentrations of the Sodium ion, Na^+ , the Chloride ion, Cl^- , and the Magnesium ion Mg^{2+} . The goal is to:

- Investigate the tendencies of Na^+ , Cl^- and Mg^{2+} to adsorb onto the surface of a growing Nickel sulfate crystal.
- Investigate how the presence of one impurity affects the behaviour of the two other impurities.
- Investigate the solubility of Nickel sulfate in the presence of impurities and pH changes.
- Investigate industrial crystallization conditions such as a crystallization temperature around $60^\circ C$ and a presence of sulfuric acid.
- Investigate partial dissociation as a method of reducing Na^+ , Cl^- and Mg^{2+} content from precipitated Nickel sulfate salts.

Chapter 2

Theory

A crystalline solid is a solid material, arranged in an ordered lattice that extends in all directions. This is the opposite of randomly arranged solids known as amorphous solids. The lattice structure is characterized as repeating unit cells with specific spatial and angular properties. Crystal lattice arrangements often contain low amounts of impurities due to their rigid structure (Mullin, 2001).

The process by which crystals are formed is known as *crystallization* which can happen in various ways, the most common being precipitation from solution. The two main mechanisms of crystallization is crystal nucleation and crystal growth. Crystal nucleation is when nuclei of a crystal phase appear in a supersaturated solution or a supercooled liquid. Crystal growth occurs when a crystal nuclei increases to a stable size which does not redissolve into the solution. From an industrial perspective, crystallization is used as a method of separation and/or purification of a variety of materials (Myerson, 2002).

2.1 The Crystalline State

Solids that are crystalline (ordered) differ in many ways from solids that are amorphous (disordered). One such way is the variance in physical properties¹ according to what direction they are measured in. Amorphous solids exhibit the same physical properties in every direction they are measured in. This quality is defined as the material being *isotropic*. Most crystals are *anisotropic*, their physical properties can change depending on which direction is used for measurement. This property allows for precision measurement and identification of unknown structures and/or compositions from tiny amounts of crystal. One such measurement technique is X-ray Diffraction (XRD). The highly ordered internal structure of crystals also result

¹Physical properties such as: mechanical, electrical, magnetic and optical

in a characteristic outward appearance. Such as smooth faces, sharp edges, distinct color, etc. (Mullin, 2001).

2.1.1 Dissociation and electrolyte ions

Ionic crystals are a type of crystal that may be defined as charged ions (cation and anion) in a fixed lattice structure, held in place by electrostatic forces called an ionic bond. The cation is positively charged and the anion is negatively charged, forming an electrically neutral compounds.

All salts are ionic compounds, and most salts are water soluble and *dissociate* into the constituent electrolytes when placed into water. Such a solution is also electronically neutral. An electrolyte is a substance which contain free ions and thus conduct electricity. The saturation solubility of salts is determined by lattice forces in the crystal and the solvent-solute interactions, which leads to patterns like: most sulfate-salts are soluble in water (Mullin, 2001).

Strong and weak electrolytes do not refer to the solubility of the parent compound, but rather to how they exist when dissolved. Weak electrolytes exist as charged molecules instead of pure ions, such as acetic acid, which dissolves into CH_3COO^- and H^+ . A strong electrolyte exists entirely or nearly entirely as ions. An example of a compound which dissociates to strong electrolytes is sulfuric acid (H_2SO_4) and hydrochloric acid (HCl), which exist as H^+ , SO_4^{2-} (or HSO_4^-) and H^+ , Cl^- in aqueous solution (Mullin, 2001).

Ionic Strength

The *ionic strength* of a solution is a measurement method of the concentration of ions of a solution. Electrolyte solutions composed of different dissolved salts of different concentrations will affect properties such as the solubility of the different salts. The molar ionic strength of a solution can be represented by equation 2.1 (Mullin, 2001).

$$I = \frac{1}{2} \sum_{i=1}^n m_i z_i^2 \quad (2.1)$$

Where

I = ionic strength

m_i = the molar concentration of ion i (mol/kg of solution)

z_i = charge of ion i

For a solution of a single charged salt, such as $NaCl$, the ionic strength is the same as the concentration. For a doubly charged salt such as $NiSO_4$, however the ionic charge is four times as large as the equivalent concentration of $NaCl$. The ionic strength can also be expressed in terms of mole fraction or volume.

Common and diverse ion effect on crystallization

"The addition of an electrolyte to a saturated solution of a sparingly soluble salt with a common ion depresses the solubility of the latter and leads to its precipitation" The addition of a common ion in a solution of a dissolved salt will tend to increase the solubility. The reason for this is as a result of Le Chatelier's principle, which states: The position of a chemical equilibrium will always shift in the direction that tends to counteract the effect of an applied change. An addition of a M^{n+} , in equation 2.2 will shift the equilibrium towards the product, which means the solubility of M^{n+} increases. If an ion which is common to those of the main salt is dissolved, the change in ionic strength may have a salting in effect, increasing the solubility of the main salt (Mullin, 2001).

2.1.2 Polymorphism

Many crystalline materials are capable of crystallizing into different but chemically identical crystalline forms, such a material is said to be *polymorphous*. The factors which determine whether a particular polymorph is expected to crystallize are most commonly solvent selection, crystallization temperature, certain impurities which inhibit or favour growth patterns and level of supersaturation. Due to the slight variation in intramolecular forces, polymorphs may differ in ways such as solubilities, diffraction patterns and melting points (Mullin, 2001).

2.2 Solubility

A *solution* is a type of homogeneous mixture containing two or more substances. In this type of mixture, the substance referred to as the solute is dissolved into the substance referred to as the solvent. Particles in solution cannot be seen by the naked eye, the solute cannot be separated from the solvent by mechanical separation or filtration, and solutions are stable, they do not separate over time. Solutions where water is the solvent are referred to as aqueous solutions. The ability of the solute

to dissolve into the solvent is called *solubility*. Most solutes display an increasing solubility with temperature. Solubility can be defined as the amount of dissolved material at the point where a dynamic equilibrium state is achieved between the rate of dissociation and the rate of precipitation (Mullin, 2001).

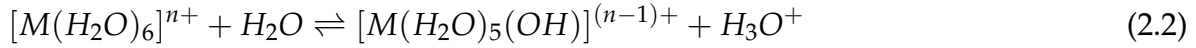
If one liquid completely dissolves into another, the two are said to be *miscible*. This is true for substances such as ethanol and water, or sulfuric acid and water. If two liquids never mix, they are *immiscible*, this is true for non-polar and polar liquids such as oil and water.

Solvent polarity is a factor to consider when determining if a solute will dissolve in a solvent. Polar solvents have areas of higher electron density (molecular dipoles) which can orient the appropriately charged portion of the solvent particle towards the solute in a process called *solvation*, given that the solute has dipoles or dissociates as electrolytes such as a salt. This generates stability due to static tension, and create macro molecules known as solvation shells around each particle of solute (Mullin, 2001).

2.2.1 Metal aquo complex

Metallic ions in aqueous solution do not exist in an isolated state, but is instead solvated molecular structures. This forms solvation shells known as *metal aquo complexes* and are relevant for understanding the structure of electrolyte solutions caused by the dissociation of inorganic salts. The primary solvation shell is the layer of water molecules directly bonded to the metal ion. The secondary solvation shell is the water molecules that are associated to the metal aquo complex through hydrogen bonding with the water molecules in the primary solvation shell. Water molecules (ligands) who bind themselves to the metal ion directly donate a lone pair of electrons to the unfilled orbitals of the metal ion. In theory, any molecule or ion with a lone pair of electrons can bind itself to a metal ion. The solutions of metal aquo complexes are acidic owing to the ionization of water as shown in equation 2.2 where a metal ion species (M^{n+}) is used as an example. The aquo complex used as an example in equation 2.2 is an octohedron configuration, 6 water molecules bound to the central metal ion, this configuration is common for transition metals in periods three and four of the periodic table. The decrease in pH of the solution is due to the generation of H_3O^+ ions. Thus, metal aquo complexes behave as weak acids. This

process is known as hydrolysis, meaning decomposition by water. Metal aquo complexes are also referred to as hydrolysis products (Jibbouri, 2002; Mullin, 2001).



The acidity of metal aquo complexes vary, but in general the higher the valency of the ion, the more acidic it is. This may vary in transition metals that have multiple ions such as Iron with Fe^{2+} and Fe^{3+} . Once a metal aquo complex is hydrolyzed, such as $[Ni(H_2O)_5(OH)]^+$, it is known as a metal hydroxo ion.

2.2.2 Gibbs Free Energy of mixing

For all solutions, it is always entropically favorable to mix into solution rather than to stay separated as solute and solvent. For most substances, however, there is an energetic cost to mixing which is to say the overall excess free energy of mixing, ΔG_{mix} , increases with increasing concentration of the solute. This assumes a non-ideal solution, where the thermodynamic properties cannot be approximated to that of a particles of ideal gas, i.e the enthalpy of mixing is greater than zero. As the concentration increases, the enthalpy of mixing increases as well. At some point, the increase in change of enthalpy of mixing outweighs the entropy of mixing decrease and no more solute can be dissolved. Dissociation no longer happens spontaneously because the overall excess free energy of mixing is no longer negative, this relationship is shown in equation 2.3. At this point the solution is *saturated*. The point where this happens depends on several other factors such as pressure and pH (Liebermann and Fried, 1972; Perrot, 1998; Roland et al., 2013).

$$\Delta G_{mix} = \Delta H_{mix} - T\Delta S_{mix} \quad (2.3)$$

Where,

ΔG_{mix} = overall excess free energy of mixing

ΔH_{mix} = enthalpy of mixing

ΔS_{mix} = entropy of mixing

Due to the negligible pressure change of association and dissociation, the system is assumed to be at constant pressure (closed). If this is assumed, the change in the enthalpy of mixing, ΔH_{mix} , can be defined as heat absorbed or released by a reaction. Whether or not heat is released or absorbed is defined by if bonds are formed or broken. Forming bonds is an exothermic reaction ($\Delta H < 0$), it releases heat along with the product of the reaction. Crystallization of salts is exothermic ($\Delta H < 0$) because the ionic bonds formed are stronger than the bonds between solute and solvent. Breaking bonds is endothermic, heat is absorbed by the surroundings. Dissociation means breaking bonds in solid compounds, which bind themselves to solvent molecules instead. Dissociation is most often endothermic ($\Delta H > 0$) because the solute-solute bond is typically stronger than the solute-solvent bond (Roland et al., 2013).

2.2.3 Expressions of solution composition

There are several ways to express solution composition, mass of solute per mass of solvent, mass fraction, mass of solute per mass of solution, etc. This is further complicated when introducing solvated ions forms such as hydrated ions. When a hydrated solid solute dissolves, both the mass of the solute in solution and solvent increase (given that the solvent is water). This results in different solubilities between a solute and its hydrate(s). Some expressions of solution composition is shown in the following equations (Mullin, 2001).

$$C_1 = \frac{C_2}{1 - C_2} \quad (2.4)$$

$$C_2 = \frac{C_1}{1 + C_1} \quad (2.5)$$

$$C_3 = \frac{RC_1}{1 + C_1} \quad (2.6)$$

$$C_4 = \frac{C_3}{1 - C_3} \quad (2.7)$$

Where,

C_1 = g of anhydrous substance/g of water

C_2 = g of anhydrous mass/g of solution

C_3 = g of hydrated mass/g of solution

C_4 = g of hydrated mass/g of "free H₂O"²

R = Ratio of hydrated molar mass to anhydrous mass

2.2.4 Supersaturation

There are four states the saturation with respect to a solute in a solution can be: undersaturated, saturated, meta stable and labile, where the metastable and labile states are considered supersaturated. A solution is supersaturated if there is a higher amount of solute dissolved in a solvent than the theoretical saturation solubility at a given temperature. Any supersaturated solution is unstable in nature, given enough time, the solution will precipitate solid solute particles until the concentration is decreased to the saturated solubility concentration. The time in which a supersaturated solution may precipitate varies with the degree of supersaturation in solution and also from substance to substance. At sufficiently high degrees of supersaturation, some solutions may crystallize spontaneously which is characterized as the solution being *labile*. Other supersaturated solutions can take anywhere from seconds to years to spontaneously precipitate, these solutions are *metastable*. Solutions which are not supersaturated may be saturated or undersaturated, where the concentration is too low to deposit crystals (Myerson, 2002; Mullin, 2001).

As displayed in figure 2.1 there are multiple methods to achieve supersaturation. Assuming a solution is close to saturation, such as in position A, supersaturation can be attained by reducing the temperature of the solution, as shown by arrow ABC, or increasing the concentration, as shown by line ADE. Increasing the concentration without dissolving more solute is typically done by removing solvent, such as by evaporation where boiling is the most common method. Once the solution reaches the labile zone, starting at any point on the supersaturation line, such as points C or E, crystal deposits can be detected in solution. Between the metastable zone and

²"free H₂O": referring to water not originating from crystal hydration, but rather from solvent.

labile zone lies the supersaturation line which is less well defined than the saturation line, because the exact concentration required for spontaneous crystallization can depend on a variety of factor such as rate and intensity of agitation, presence of impurities, cracks in the reactor lining, etc and can therefore be difficult to determine. The *metastable zone* lies between the saturation and supersaturation line, solutions in this zone are supersaturated, but do not spontaneously crystallize, the exact width of the metastable zone is difficult to determine because of the variance and unpredictability in the supersaturation line. Solutions whose concentrations are under or directly on the saturation line are in the *stable zone* will not crystallize (Mullin, 2001).

The methods discussed so far in order to reach supersaturation have been in the context of binary systems (solute and solvent). Supersaturation can also be attained by altering the solvent composition. Adding impurities which change pH or add ions can have a significant effect on the saturation solubility of the solute. When talking about solutions where electrolytes are involved, adding impurities can have a *salting out* or *salting in* effect, referring to decreasing or increasing solubility, respectively. While this may be an effective way to reduce or increase the solubility of an ionic solute, such as a salt, it may also increase the concentration of impurities in the precipitated crystals, which can be undesirable if high purity is desirable. Supersaturation can also be generated by chemical reaction, where the product of the reaction is less soluble than the reactants (Mullin, 2001).

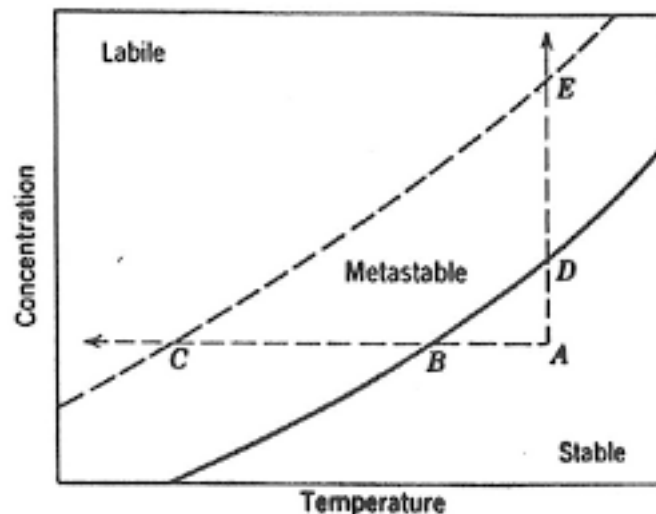


FIGURE 2.1: Solubility-Supersolubility diagram showing pathways to crystallization (Andreassen, 2015)

"Supersaturation is defined as the driving force for nucleation and growth of one-component crystals in liquid solutions" (Myerson, 2002).

Supersaturation can be described using the difference in chemical potential between the potential of the solute in solution, μ_s , and the potential of a solute in the bulk of the crystal phase, $\mu_{crystal}$. The relationship is described in equation 2.8.

$$\Delta\mu = \mu_s - \mu_c \quad (2.8)$$

If $\Delta\mu$ is positive, then a supersaturated solution is described, which indicates that the requirements for nucleation and crystal growth being met. If $\Delta\mu$ is 0 it indicates a saturated solution, and if $\Delta\mu$ is negative it indicates an undersaturated solution. Supersaturation can also be expressed in dimensionless form as:

$$\frac{\Delta\mu}{\bar{R}T} = \ln \frac{a}{a^*} = \ln \frac{C\gamma_c}{C^*\gamma_c^*} = \ln S \quad (2.9)$$

Where,

a = activity

C = concentration

μ_c = activity coefficient

\bar{R} = molar gas constant

S = degree of supersaturation

T = Temperature

* = denotes the property at saturated conditions

For low concentrations, the activity coefficient, μ_c , can generally be assumed to equal to 1, which introduces an approximation of supersaturation based solely on concentration.

$$S \approx \frac{C}{C^*} \quad (2.10)$$

Solutions which are non-ideal, the activity coefficients are not one, thus the supersaturation can't be expressed in terms of concentration unless low concentrations are assumed, limiting thermodynamic properties. *Relative* supersaturation, denoted by σ , be defined as:

$$\sigma = \frac{C - C^*}{C^*} = S - 1 \quad (2.11)$$

The birth and deposition of solid solute occurs in solutions which are supersaturated. As the temperature rises, the solubility does too, assuming such a relationship is often correct but there are known exceptions such as Sodium Sulfate (Na_2SO_4) where at approximately $32.4^\circ C^3$, water molecules previously in the metal aquo complex are unsolvated due to a phase change, and the solubility becomes almost independent from temperature as shown in figure 2.2 (Okorafor, 1999).

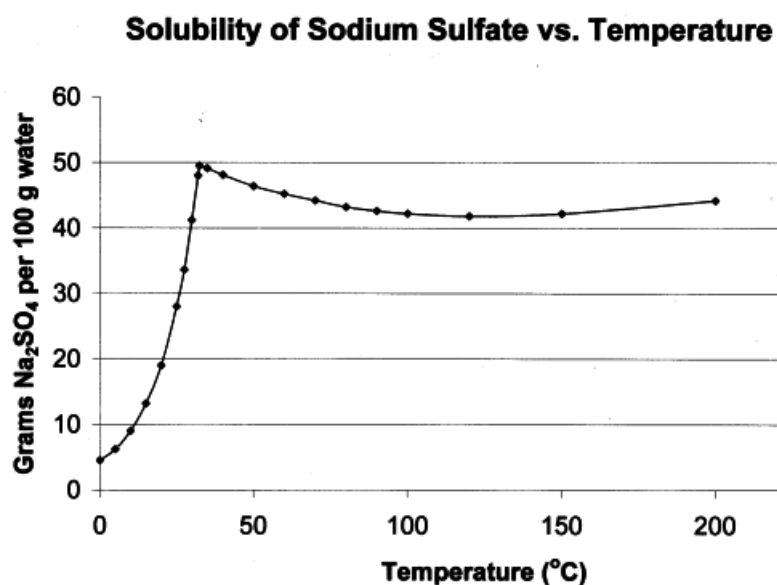


FIGURE 2.2: Saturation solubility diagram of Sodium Sulfate (Na_2SO_4) (Lohninger, 2011)

³This chemical phenomena is useful in the calibration and testing of temperature gauges due to its reliability.

2.3 Impurities

Impurities are substances that are unwanted or deliberately added to a process environment that are different from the substance being crystallized. Impurities deliberately added to a solution are known as an additive. Impurities which are not deliberately added can be poisons/inhibitors if they slow down the growth rate of a crystal or promoters if they accelerate the growth rate. The solvent used for growth or any other compound added to the solution can be considered an impurity. Reasons for adding impurities to a supersaturated solution can be to simulate industrial conditions, or to deliberately affect processed materials in a certain way. One such way is to decrease solubility or the overall free energy change associated with the formation of a critical nucleus needed for stable crystal growth as discussed in section 2.4 and section 2.5. Unwanted impurities can be unavoidable if the way of removing them can damage or poison process itself or removal requires uneconomical amounts of energy or time. Removal of 100% of impurities is nearly impossible because it would reduce the entropy of a system to 0, which would require an infinite amount of work as predicted by the second law of thermodynamics. Even if impurities can't be detected analytically, does not mean they do not exist. "Pure" substances like ultra pure water is allowed some very small levels of impurities (Jibbouri, 2002; Mullin, 2001).

2.4 Crystal Nucleation

Nucleation can be defined as the first step in the self-assembly of a phase change. Classical nucleation theory, stemming on the work of Gibbs (1948), Volmer (1939), and Becker and Döring (1935), is based on condensation of a supersaturated vapour which is summarized as: there must be a presence of droplet nuclei on the condensing surface before the liquid phase appears (Mullin, 2001). This view is extended to crystal nucleation. In terms of solid precipitation from solution (such as crystallization), where said phase change is heterogeneous (liquid-solid), this process can be described as the birth of a nuclei or birth of a crystal particle which can only happen spontaneously in supersaturated solution. Nucleation usually takes place in a local region of slightly higher degree of supersaturation such as near a source of cooling or on the liquid-air surface. Crystal nuclei are too small to be observed and are required to be present in solution for crystal growth to be detected. A solution being supersaturated is not enough for crystal growth to immediately occur. The different kinds of nucleation, primary and secondary, shown in figure 2.3 is differentiated by

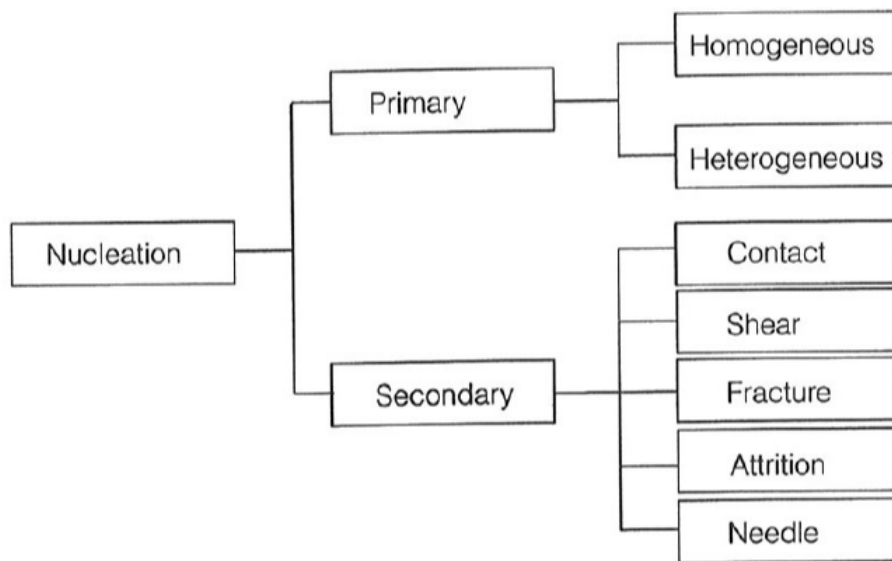


FIGURE 2.3: Nucleation types (Andreassen, 2015)

the aid of crystal particles already in solution in the latter (Mullin, 2001).

2.4.1 Primary homogeneous nucleation

Primary homogeneous nucleation is defined as the formation of nuclei without aid of surfaces or presence of foreign solid particles. A crystal nuclei formed in this manner needs not only its constituent particles to coagulate, but also to resist re-dissolving and orient into the respective lattice structure of a crystal. The process which a small nuclei undergoes after formation will always follow the state which has the lowest free energy and this depends primarily on its size⁴, either its radius is large enough to sustain growth or it re-dissolves. The *critical radius* (r_c), also represented by the *critical energy*, (ΔG_{crit}) in equation 2.15, represents the smallest possible radius which may be stable and sustain growth, and is determined by maximizing ΔG as seen in equation 2.14. The critical radius (r_c) varies from substance to substance. The overall excess free energy, ΔG , between a solid solute particle and dissolved solute is equal to the sum of the surface excess free energy and the volume excess free energy, which is a negative amount in supersaturated solutions and a negative ΔG represents a spontaneous growth of stable nuclei. As the radius grows, the overall excess free energy difference between the solid and dissolved states grows more negative due

⁴The size of a nuclei is assumed to be the radius of a sphere r

to the exponential nature of r^2 in ΔG_s and r^3 in ΔG_v from equation 2.13, further increasing stability of the nuclei (Mullin, 2001).

$$\Delta G = \Delta G_s + \Delta G_v \quad (2.12)$$

$$\Delta G = \Delta G_s + 4\pi r^2 \gamma + \frac{4}{3}\pi r^3 \Delta G_v \quad (2.13)$$

$$\frac{d\Delta G}{dr} = 8\pi r \gamma + 4\pi^2 \Delta G_v r^2 = 0 \quad (2.14)$$

and

$$\Delta G_{crit} = \frac{16\pi\gamma^3}{3(\Delta G_v)^2} = \frac{4\pi\gamma r_c^2}{3} \quad (2.15)$$

Where,

ΔG = overall excess free energy

ΔG_s = surface excess free energy

ΔG_v = volume excess free energy

ΔG_{crit} = critical free energy

γ = interfacial tension

r = nucleus size

r_c = critical nucleus size

The rate of nucleation can be written through Arrhenius reaction velocity equation, assuming the process is thermally activated, as shown in equation 2.16. Combine equation 2.16 with equation 2.15 and a relationship for the volume excess free energy, ΔG_v , shown in equation 2.18, and you get equation 2.17 which expresses the rate of nucleation (J) in terms of its governing variables: Temperature, T ; degree of supersaturation, S ; and interfacial tension, γ (Mullin, 2001).

$$J = A \exp\left(\frac{-\Delta G}{kT}\right) \quad (2.16)$$

$$J = A \exp\left(\frac{-16\pi\gamma^3 v^2}{3k^3 T^3 (\ln S)^2}\right) \quad (2.17)$$

$$-\Delta G_v = \frac{kT \ln S}{v} \quad (2.18)$$

Where,

k = Boltzmann Constant

A = preexponential factor

J = number of nuclei formed per unit time per unit volume (rate of nucleation)

v = molecular volume

True primary homogeneous nucleation will hardly ever occur due to the unavoidable presence of impurities as mentioned in section 2.3.

2.4.2 Primary Heterogeneous Nucleation

Primary heterogeneous nucleation is characterized by nucleation with the nuclei on a surface. The surface could be the lining of a reactor, undissolved microscopic solids, atmospheric dust, etc. In most cases, a foreign undissolved solid in solution is generally known to reduce the overall free energy change associated with the formation of a critical nuclei under heterogeneous conditions. This relationship can be visualized as:

$$\Delta G'_{crit} = \Phi \Delta G_{crit} \quad (2.19)$$

Where, $\Delta G'_{crit}$ = overall free energy change associated with the formation of a critical nuclei under heterogeneous conditions.

Φ = a factor between -1 and 1 depending on wetting angle between nuclei and surface, determined by the following relationship:

$$\Phi = \frac{(2 + \cos\theta)(1 - \cos\theta)^2}{4} \quad (2.20)$$

Where, θ = wetting angle; when θ lies between 0 and 180°, $\Phi < 1$. When $\theta = 0$, $\Phi = 0$.

A lower overall free energy change associated with the formation of a critical nuclei under heterogeneous conditions indicates that a lower supersaturation is required than in homogeneous conditions. The rate of nucleation is also changed in heterogeneous conditions, reducing the preexponential factor, A .

2.4.3 Secondary Nucleation

A supersaturated solution nucleates much more readily when crystals of the solute is already present in the or added to the solution. This particular type of nucleation is known as *secondary* nucleation. Despite similarities to primary heterogeneous nucleation, there are profound differences between the mechanisms. The mechanisms responsible for secondary nucleation is not as agreed upon as primary nucleation. Several possible mechanisms have been proposed as an explanation for secondary nucleation, such as *initial* breeding, *needle* breeding, *polycrystalline* breeding. Which all focus on the parent crystal as a source of nuclei. The second category focuses on the origin of secondary nuclei as a result of collisions and attrition (Mullin, 2001; Myerson, 2002).

$$B = k_N \sigma^b \epsilon k M_T^j \quad (2.21)$$

Where,

B = rate of secondary nucleation rate

k_N = secondary nucleation rate constant

M_T = magma density of the present of solids

ϵ = agitator speed

σ = relative supersaturation

Collision energy is denoted by k , crystal-crystal, crystal-wall or crystal-impeller interactions are represented by j and dependency on supersaturation by b . Models like this one or other impact attrition models have also been proposed, a general

explanation is that crystal contacts are the cause of secondary nucleation in supersaturated solutions. Crystal-impeller impacts especially decrease the overall excess free energy for the formation of a nuclei, due to an energetic impact and possible split into secondary nuclei (Rousseau, 2009).

2.4.4 Seeding

Seeding is the addition of small particles of the material to be crystallized and is a commonly applied technique for the induction of crystallization used widely in the industry and in the laboratory. Seeding is highly popular not only for the ease of execution, but also because it allows for on-demand crystallization in systems which may either require an impractically high supersaturation in order to spontaneously crystallize or a long time required for spontaneous appearance of nuclei. Seeding can be both deliberate and unintentional, the latter of which may be hard to control in systems that are sensitive. Atmospheric dust in laboratories and industrial plants frequently contains particles of the crystalline product itself, which can prevent unstable phases, polymorphs or hydrates to crystallize (Mullin, 2001; Myerson, 2002).

Crystal seeds act as a controlling mechanism for particle size and their distribution in precipitated crystals. Seed materials do not necessarily need to consist of the material being crystallized in order to effectively seed a solution. Crystal seed size is believed to play a significant role on the effect of seeding. Large seeds split into a larger amount of secondary nuclei in agitated systems than smaller seeds due to a greater contact probability as well as collision energy. Small and large crystals behave differently in response to eddies and turbulence as a result of agitation which also has an impact on nucleation. Large crystal seeds more readily come in contact with the impeller itself and does not as easily follow currents due to a higher moment of inertia and physical size. Smaller crystal seeds move along with streamlines and currents within turbulence and may exhibit little to no difference in behaviour from a non-agitated solution, rarely colliding with the impeller or other crystals. (Mullin, 2001; Myerson, 2002).

2.4.5 Induction Period and Latent time

There is usually a period of time between the achievement of supersaturation or seeding and the appearance of crystals in solution. This period is referred to as the

induction period and is represented by equation 2.22.

$$t_{ind} = t_r + t_n + t_g (+t_l) \quad (2.22)$$

Where,

t_{ind} = induction time

t_r = time required for the system to achieve a quasi-steady state distribution of molecular clusters

t_n = nucleation time

t_g = time required for the nuclei to grow to a detectable size

t_l = latent time

In non-ideal systems, such as aqueous solutions of electrolytes, these quantities are nearly impossible to isolate. The induction time is generally dependent on degree of supersaturation, rate of agitation, presence of impurities, viscosity of solution, etc. The *latent time* is only observed in systems of low supersaturation and is defined as the onset of time before an initial change is observed in the solution such as massive nucleation. At high supersaturations, induction time may be so short that it is indistinguishable from latent time. Detection of crystallization can be measured visually, but a different result can be recorded if a more sensitive method is utilized such as laser scattering, conductivity measurement stemming from the removal of ions from solution or measurement of a temperature increase stemming from the heat of crystallization of solid crystals (ΔH_{crys}) (Mullin, 2001). This topic is expanded upon in section 2.5.1.

2.5 Crystal Growth

As soon as particles with size larger than the critical radius, r_c , they begin to grow into crystals of visible size. The mechanism in which this happens is referred to as *crystal growth*. Crystal growth can be considered as a combination of three steps, volume diffusion, surface reaction and heat transfer. Volume diffusion is the mass transport of the ions in solution by diffusion from the bulk of the solution to the crystal surface. The second step is the surface integration of growth units into the crystal lattice. The third step is the liberation of heat of crystallization as the solute changes

phase from liquid to solid.

Crystal growth is explained by several theories, the surface integration theory, diffusion-reaction theory, kinematic, adsorption layer theory and birth and spread theory are five examples. The surface integration theory is that growth shape and minimum surface energy has a correlation. This theory is largely unused. The diffusion-reaction theory is based on a growth rate which is proportional to the difference between concentration between the point of deposition and the bulk of the solution, similar to traditional mass transfer processes, matter is continuously deposited onto the crystal face. The adsorption layer theory is based on the assumption that there is a discontinuation in the deposition onto the crystal phase from layer to layer. Kinematic theory explain the generation of steps at some location on the crystal face, followed by an outward growth across the face. Birth and spread theory states that as nuclei adsorb to a surface, a monolayer is formed as a result, which spread across the surface (Jibbouri, 2002; Mullin, 2001). Linear crystal growth rate is defined as:

$$G = \frac{dL}{dt} = k_g \sigma^g \quad (2.23)$$

Where,

G = crystal growth rate

L = characteristic length (r for spherical particles)

k_g = growth rate constant (depends on temperature)

g = dependency on supersaturation

σ = relative supersaturation

The driving force in crystal growth is the degree of supersaturation. The degree of supersaturation controls whether or not a dissolved supersaturated solute can homogeneously form a stable solid interface or if heterogeneous nucleation is needed for growth. This affects how the crystals grow and their shape and size. The expression of overall linear growth rate in terms of weight of the crystals and size of crystal seeds is given in equation 2.24.

$$G = \frac{L}{t} \left[\left(\frac{M_2}{M_1} \right)^{1/3} - 1 \right] \quad (2.24)$$

Where,

M_1 and M_2 are mass of crystals in and mass of crystals taken out, respectfully.

The overall linear growth rate, G , and the growth rate, R_G , are related in equation 2.25

$$R_G = \frac{3\alpha_1}{\beta_1} \rho_c G \quad (2.25)$$

Where,

β_1 and α_1 are surface and volume shape factors, respectively.

When crystals grow, the factors which determine the rate of deposited solute on the growing crystal are diffusion through the electrical double layer and the surface reaction. If the parameters of these two steps are known, then calculation of crystal growth is easy to calculate. These are almost impossible to isolate, however, but they can be explained through the concept of the effectiveness factors. Effectiveness factors approximate the degree of diffusion and surface integration for the system. There are many effectiveness factors related to crystal growth, but in general they compare the actual linear growth rate to the growth rate that would be obtained if the bulk solution conditions were assumed to exist at the crystal interface. This is primarily affected by the degree of supersaturation and temperature at the crystal interface and bulk of the solution. The heat produced by crystal growth changes the solution temperature, altering the kinetics of crystal growth, which changes the effectiveness factor from what was evaluated in the bulk of the solution. (Garside, 1971)

2.5.1 Heat of crystallization

As stated by the second law of thermodynamics, any irreversible process must increase the entropy of the universe ($\Delta S > 0$). There is a common misconception that the process of crystallization is completely reversible. In any system brought from one state to another, such as a solute dissolving, there are intramolecular friction and collisions which cause energy dissipation to the surroundings that is unrecoverable should the process be reversed. Crystal growth and crystallization seemingly circumvent this due to the decrease in entropy of the system. This stems from association, lattice formation and phase separation, seemingly without any increase in universal entropy. As a crystal is formed, bonds are also formed which is an exothermic reaction, heat is released, increasing the temperature and entropy of the

system and the surroundings. This ensures the net entropy change in the universe is negative, resulting in a system undergoing change which does not deviate from the second law of thermodynamics. (De Boer et al., 1988; Callen and Welton, 1951)

Agglomeration and caking

Agglomeration describes the tendency of a particles in a liquid suspension to flocculate. When particles collide, and they are small enough, the van der waals forces of the particles may exceed that of the gravitational force, which prevents them from separating.

Caking is the tendency of crystalline material to bind together based on the moisture content on the crystal surface. Caking results in large clumps that need to be crushed in some manner. Caking varies from material to material. Elongated and of irregular shaped crystals are particularly prone to caking. A source of caking is the filtration process. If deposited crystals are not washed properly, traces of solvent may still be present on the surface of the crystals. This can cause insides of filter cakes to dry ineffectively, which affects its ability to flow freely or its ability to be distributed evenly. (Mullin, 2001)

2.5.2 Effects of impurities on crystal growth

The effects of impurities on crystal growth can be divided into two sides, the thermodynamic effects on the solution and the kinetic effects on the crystal.

Kinetic effect

The kinetic effect of impurities on crystal growth is focused around changing crystal growth habit. Modern impurity theories are based on the concept that impurity species adsorb at kinks, gaps, steps and terraces on the growing surface. The growing face is slowed down or in some cases stopped by the adsorption of impurities. The size, shape and purity of crystals are influenced by impurities. Impurities alter kinetic properties such as rate of nucleation, crystal growth, and dissociation. "The influence of impurities on the crystallization kinetics, is due to the adsorption of the hydrolysis product on the growth layer of the crystal surface which slows growth." (Jibbouri, 2002)

The *step advancement velocity* is slowed down by impurity adsorption on kink sites or step lines. The advancement of the monolayer is then forced to move around those sites. This mechanism is illustrated in figure 2.4. A curved step between two impurity adsorption sites of radius, r , will stop growing if r is smaller than the critical nuclei size r_c , this relationship can be explained by equation 2.26. (Mullin, 2001; Kubota and Mullin, 1995)

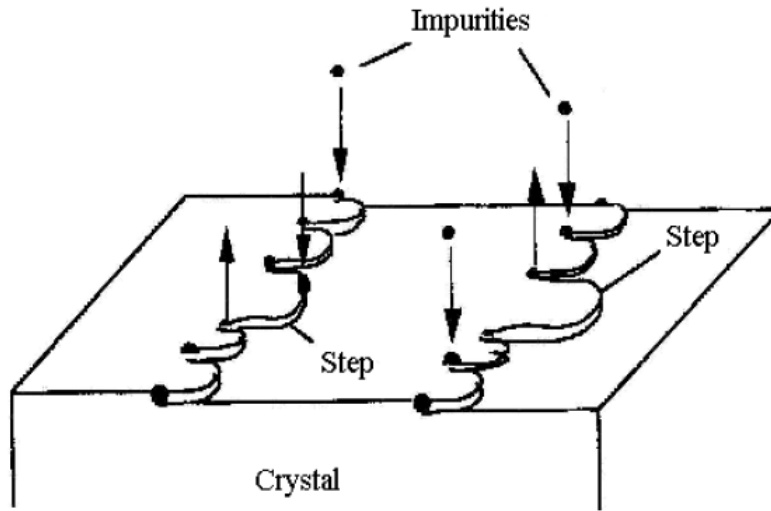


FIGURE 2.4: Visualized impurity adsorption and retardation of movement of the monolayer. (Kubota, Yokota, and Mullin, 1996).

$$\frac{v_r}{v_0} = 1 - \frac{r_c}{l} \quad (2.26)$$

Where,

v_0 = step advancement velocity of a linear step (no impurities)

v_r = step advancement velocity of a curved step

l = the average distance between impurities

The maximum step velocity is v_0 and the minimum step velocity is on a curved face where $r=l/2$. At this point, if all growth centers on a surface are blocked by an impurity, the growth rate is reduced to zero. The active site coverage of impurities θ_* is related to the step advancement velocity in equation 2.27.

$$\frac{v_r}{v_0} = 1 - \left(\frac{\gamma l a}{k T \sigma \lambda} \right) \theta \quad (2.27)$$

Where,

λ = the average distance between active sites on the crystal surface

θ_* = active site coverage on the crystal surface

γ_l = linear edge free energy of the step

σ = relative supersaturation

a = area of the growth unit on the crystal surface

k = Boltzmann constant

The impurity effectiveness factor is defined as the effectiveness of an impurity under a given supersaturation and temperature. The effectiveness of an impurity to prevent crystal growth is defined as the impurity effectiveness factor α , a strong impurity has $\alpha > 1$, which means the average step velocity will quickly approach zero. An impurity of $\alpha = 1$ means the average step velocity approaches zero over time. An impurity with $\alpha < 1$ means the average step velocity will approach a value greater than 0, but reduced compared to v_0 . This relationship is shown in equation (Mullin, 2001; Kubota and Mullin, 1995; Jibbouri, 2002).

$$\alpha = \left(\frac{\gamma a}{k_B T \sigma \lambda} \right) \quad (2.28)$$

As the supersaturation of any solution increases, the impurity effectiveness factor α decreases.

Thermodynamic effect

The other side of the explanation of the effects of impurities on crystal growth is using thermodynamics. Thermodynamics can be used to predict the solubility of salts in aqueous solution by using the Pitzer equation which estimates an activity coefficient at any temperature used in equation 2.9. The change of characteristic crystal form with impurities present is due to a difference in adsorption energy on the faces of the crystal, which cause them to adsorb to faces selectively. Impurities will adsorb on surfaces with the maximum free energy of adsorption. The surface potential distribution of a growing crystal is the dominant factor of crystal growth. (Mullin, 2001; Kubota and Mullin, 1995; Buckley, 1930)

The presence of free bases and acids change the behaviour and concentration of ions in solution. It may be explained as a change of solution structure, specifically the structure of hydronium ions, H_3O^+ . Most cations and hydroxide ions, OH^- , are hydrated. The factors which determine how likely an ion is to hydrate is ionic radius [Å] and enthalpy of hydration. The ion with the most negative hydration enthalpy and lowest ionic radius is H^+ , therefore it is never seen isolated in aqueous solution, but rather as H_3O^+ . Na^+ , for example, has a much smaller chance of being hydrated due to its low enthalpy of hydration and larger radius, therefore it has a tendency to drift towards the crystal surface rather than to stay hydrated in solution. Anions like OH^- stabilize the solution, keeping Na^+ from reaching the crystal surface. Anions have a much larger ionic radius than cations, and generally less negative enthalpy of hydration and are therefore less likely to hydrate from water molecules. Physical properties of common ions are displayed in table 5.1. (Mohameed and Ulrich, 1996; Mullin, 2001; Jibbouri, 2002)

2.5.3 Electrical double layer

"At the interface of a charged solid and a liquid there is always a separation of electrical charge. The surface of the solid has an excess of one charge and the balancing is found in the adjacent surface region of the liquid" (Jibbouri, 2002). The surface charge can be caused by several mechanisms. Mechanisms such as dissociation of inorganic groups in the surface of the particle and adsorption or desorption of ions in solution. The surface charge causes an electrical field, which attracts counter ions. This layer forms an interface which is known as the *electrical double layer* around the surface. Any counter-ion that is attracted to the surface needs to pass through the electrical double layer, which adds resistance to the crystal growth process. This is part of the explanation for why crystal growth rates are lower than dissociation rates. The largest changes in the electrical double layer of a growing crystal stems from the adsorption of cations and anions. Any electrical potential on the crystal surface may lead to a change in the growth rate. (Jibbouri, 2002)

The electrical double layer is divided into three layers, the surface charge, the Stern layer and the diffuse layer. The Stern layer consists of hydrated ions which are tightly bound and is located just above the surface. Ions which are adsorbed to the crystal surface are indistinguishable from the crystal itself, such as Ni^{2+} and SO_4^{2-} on Nickel sulfate hexahydrate. The outer layer is the diffuse layer which consists of a loose formation of oppositely charged ions which are attracted to the surface but also repelled

by the Stern layer.

Zeta-potential

Particles in a polar solution such as water have a surface charge, which is the net charge of all the ions close to the surface. Interactions of the particle in a polar solution is not controlled by the surface charge, but rather by the average electrostatic potential in the *slipping plane* known as the *Zeta potential* (ζ , measured in [V]). The slipping plane is the surface of polar fluid surrounding any charged particle. The fluid surrounding this particle is assumed stationary. All of the material inside the slipping plane is considered part of the same kinetic unit. Meaning, when the particle moves, so does a certain quantity of solution inside the slipping plane. The Zeta potential is changed when ions are dissolved off or adsorbed onto the surface.

The zeta potential is an indicator of how stable a solution is. High zeta potential means the solution is very stable and less likely to crystallize. Solutions with low zeta potential will agglomerate due to attractive forces outweighing repulsive forces.

Chapter 3

Experimental setup

3.1 Experimental overview and parameters

The experiments conducted in this project can be divided into four parts. 25°C batch crystallization, 60°C batch crystallization, partial filtration and solubility. During the course of the experiments there were several aspects of the experimental procedure which were kept constant and others which were varied.

3.1.1 Saturation solubility and phase diagram of Nickel sulfate

The saturation solubility of Nickel sulfate, NiSO_4 , and its hexahydrate is shown in tables A.1 and A.2 respectively. The values in these tables were calculated using saturation mass percentage of Nickel sulfate in aqueous solution at different temperatures (Haynes, 2014; Mullin, 2001).

3.1.2 Impurity selection and concentration

The specific impurities used were suggested by Glencore Nikkelverk AS based on their feed contents, these were Sodium ion (Na^+), Chloride ion (Cl^-) and Magnesium ion (Mg^{2+}). The impurity concentration that was used in the experiments is not representative of the composition of the feed at Glencore Nikkelverk AS. Instead the experiments serve as a generalized approach to the effects of the specific impurities on the solubility of Nickel sulfate, concentration in crystallized crystals, and their effect on other impurities (if present) (Bøckmann, 2018). The concentrations in solution was decided to be 3, 5 and 10 grams per solution kg for each impurity and the combination of all three. The unit of concentration measurement [g/kg] was chosen because a mass based concentration is easier to measure accurately than a volume based concentration [g/L]. Another reason for the choice of a mass based concentration is because the volume of a solution can be hard to predict because electrolytes

do not affect the volume in an additive way in a highly non-ideal solution.

De-clumping and dry-milling

As the crystallized Nickel sulfate crystals are filtered, washed and dried, they clump and cake together in masses reminiscent of hard-packed snow. In this state, the Nickel sulfate hexahydrate, $NiSO_4 \cdot 6H_2O$, is unusable. The two methods of breaking these clumps of crystal up were dry-milling and declumping. Declumping is the process of breaking apart clusters of crystal mass to the point where, ideally, there are only whole crystals left. To break these clumps up, a mortar and pestle was used gently. Great care went into not breaking up the crystals themselves. Heaps of about 5g were placed in the base of the mortar. The pestle was then slowly maneuvered in a circular motion across the top and through the base of the crystal heap. Despite being careful, crystals would sometimes break apart at the slightest pressure of the mortar and pestle.

Dry-milling is used when the crystals were needed as a powder, this was only done during sample preparation of X-ray diffraction. A mortar and pestle was used for both processes. The difference between declumping and dry-milling is an important distinction to make because during the partial filtration experiments, the uneven distribution of impurity concentration in the bulk of the crystal would not be effectively dissolved if the physical structure of the crystal was broken.

3.1.3 Temperature

Industrial crystallization is typically carried out around 60°C. Ideally, every variable except the impurity concentration in solution would remain the same as what is used in the industry, this includes crystallization temperature. Temperature control in crystallization experiments is not only of importance on the solution to be supersaturated, but also on filtration equipment. If a hot saturated solution is filtered through a cold Büchner funnel, it might partially crystallize on contact due to the rapid temperature decrease which may have an effect on the kinetics and impurity uptake. This introduces the first experimental limitation. Due to difficulties in temperature control of the filtration equipment, specifically the Büchner funnel, 25°C was selected which is approximately room temperature in the lab where the experiments took place, requiring no temperature control. A side investigation was also done at 60°C despite the difficulties to investigate potential differences, this is

discussed further in section 3.3.

3.1.4 Saturation level and solution volume

The desired solution composition is one which would not crystallize spontaneously upon being cooled to 25°C, but would still crystallize upon seeding, in other words the ideal solution is metastable at 25°C. A supersaturation ratio of $S=1.133$ was selected, which corresponds to a saturation temperature of 35°C. Using the setup in figure 3.2, the limiting factor when determining the optimal volume to use for crystallization was total submersion of the thermometer and pH meter, thus the minimum volume was found to be 450 mL.

3.1.5 Seeding ratio and particle diameter of seeds

The initiation of crystallization is important to control. If across several experiments, nucleation and crystal growth are initiated differently, the kinetics may differ, resulting in different growth rates, size distribution and impurity uptake. The initiation of crystallization was decided to be seeding for all experiments. This is an obvious choice to make because seeding is simple, effective and widely used in crystallization in both the laboratory and the industry. The seeding ratio is defined as the ratio of seed mass to the total crystal mass of Nickel sulfate:

$$\phi = \frac{m_{NiSO_4 \cdot 6H_2O,s}}{m_{NiSO_4 \cdot 6H_2O,s} + m_{NiSO_4 \cdot 6H_2O,tot}} \quad (3.1)$$

Where,

ϕ = seeding ratio (expressed as %)

$m_{NiSO_4 \cdot 6H_2O,s}$ = Nickel sulfate hexahydrate seed mass

$m_{NiSO_4 \cdot 6H_2O,tot}$ = Initially dissolved mass of Nickel sulfate hexahydrate

A seeding ratio of 0.25% was constant throughout the duration of the investigation. The seeds were prepared by declumping $NiSO_4 \cdot 6H_2O$ crystals using a mortar and pestle. Declumping is to break up clumps and crystals which are caked and agglomerated to maximize surface area. The particle diameter and size of seeds after this process is not easy to estimate based on the odd and irregular shapes of

$NiSO_4 \cdot 6H_2O$ crystals, however, rough estimates were made regardless. The crystal size ranges anywhere from 0.5-3 mm and are shaped roughly. This is a consequence of declumping and can be seen in figure 3.1.

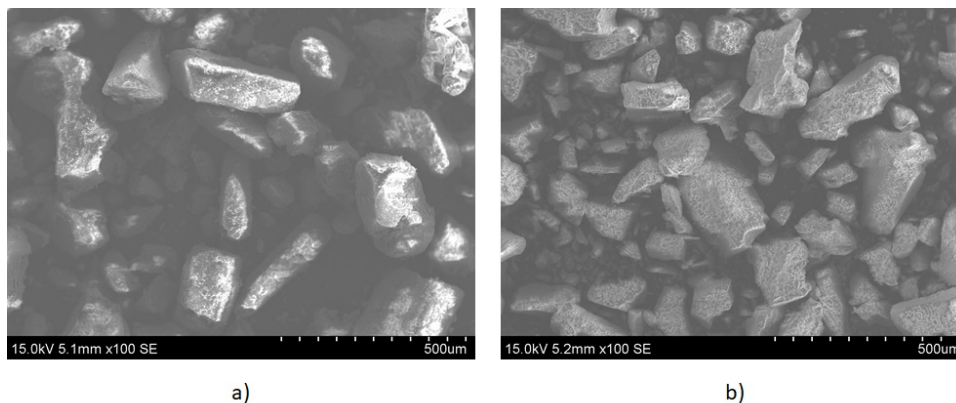


FIGURE 3.1: SEM pictures a) and b) show declumped Nickel sulfate hexahydrate seeds containing no impurities.

3.1.6 Chemicals

The chemicals used in this project are shown in table 3.1. $NiSO_4 \cdot 6H_2O$ was used in every experiment. Nickel chloride was used to add Chloride ions (Cl^-) to solution. Sodium sulfate was used to add Sodium ions (Na^+) to the solution. Magnesium sulfate was used to add Magnesium ions (Mg^{2+}) to the solution. Sulfuric acid was used as a process impurity in industrial batch crystallization experiment and the solubility experiment. Nitric acid and ultra-pure water was used as a solvent during sample preparation for Inductively coupled plasma mass spectrometry (ICP-MS). Deionized water was used as a solvent for every experiment. Ethanol was used to wash wet crystals after separation from solution.

3.2 Batch Reactor and filtration setup

Solution preparation was done using a closed 1L glass Erlenmeyer flask on an IKA RH digital CH/T Hotplate set to $60^\circ C$ and magnetic stirrer set to 600 RPM for 1 hour.

TABLE 3.1: Chemicals used in this project

Chemical	Purity	Manufacturer
Nickel sulfate hexahydrate ($NiSO_4 \cdot 6H_2O$)	98%	Sigma-Aldrich
Nickel chloride ($NiCl_2$)	98%	Sigma-Aldrich
Sodium sulfate (Na_2SO_4)	98%	Emsure
Magnesium sulfate ($MgSO_4$)	97%	Sigma-Aldrich
Sulfuric acid (H_2SO_4)	95-98%	Sigma-Aldrich
Nitric Acid (HNO_3)	65%	Emsure
Water	deionized	NTNU
Water	ultra-pure	Simplicity UV
Ethanol	96%	VWR

The experiments were then performed batch-by-batch in a 1L jacketed glass reactor as shown in figure 3.2. Stirring was performed using a three-bladed metal impeller connected to a sealed and stoppered reactor lid, additionally equipped with two baffles to improve heat transfer efficiency and disrupt laminar flow patterns. Temperature and pH monitoring was a Mettler-Toledo SevenCompact benchtop connected to a Mettler-Toledo Inlab Expert pro electrode which recorded the temperature and pH of the solution every 20 seconds. Temperature control was done using a Julabo F33-ME Refrigerated/Heating Circulator with regular water as the cooling medium. Weighing was done using a Ohaus AX224 Adventurer Analytical scale. This setup is similar to the one shown in figure 3.6. The procedure for this experiment is briefly summarized in the following list. The experimental procedure is described in detail in Appendix C.1. The solution compositions used in these experiments are shown in Appendix B.2.

1. Prepare an aqueous solution of Nickel Sulfate which saturates at 35°C.
2. Add any impurities.
3. Insert the solution in batch reactor with agitation at 600 RPM.
4. Allow the system to reach equilibrium at 60°C.
5. Cool solution to 25°C.
6. Insert seeds.
7. Filter crystals out of solution using vacuum filtration.
8. Wash filter cake with 150 mL of ethanol.

9. Dry crystals at 50°C for 24 hours.
10. Declump the crystals using a mortar and pestle.
11. Analyze sample using XRD, ICP-MS or SEM.

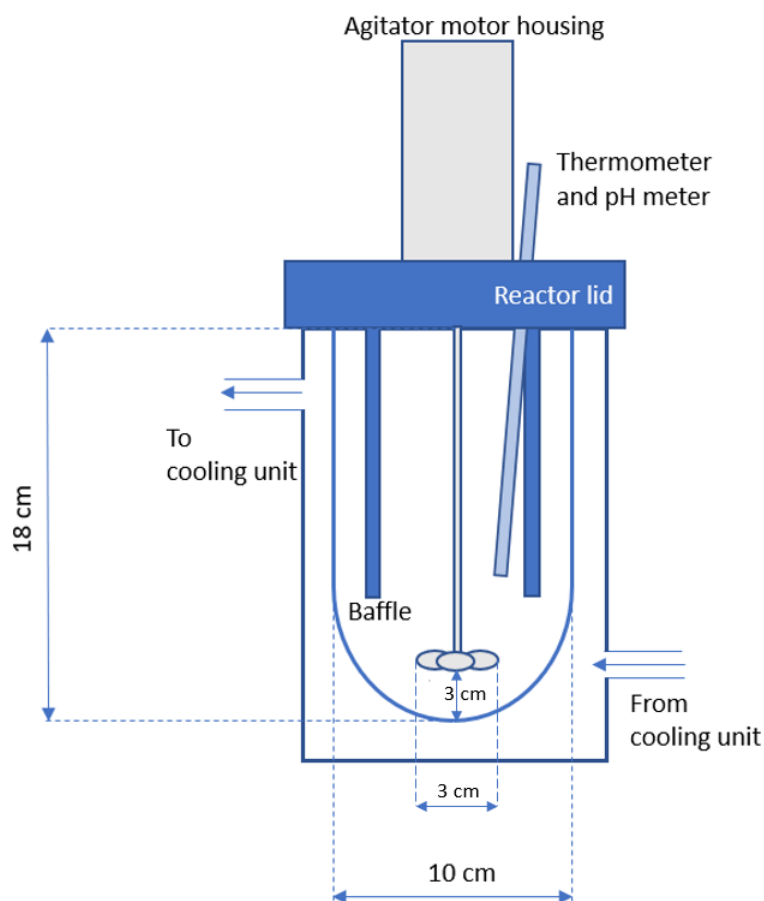


FIGURE 3.2: Batch crystallizer used in experiments (not to scale)

Separation of the crystals from the solution was done using a vacuum filtration setup as shown in 3.3. The partial vacuum caused by the removal of air will force the separation of crystal and solution. The Büchner funnel used is 150 mm in diameter and made of porcelain. The filter paper used in this setup was Schleicher & Schuell 589 Rundfilter Ø 150 mm filter paper. An improperly sealed filtration setup can result in solute slipping past the filter. Therefore, wetting the filter paper slightly will seal the flask and achieve partial vacuum prior to the crystals being filtered, ensuring no loss of solute. While using a stronger vacuum would increase filtration speed, it may

also rupture the filter paper, which may lead to massive loss of crystal. Use too weak vacuum, and it will slow down the filtration speed or be unable to completely seal the flask, which may also lead to loss of crystal.

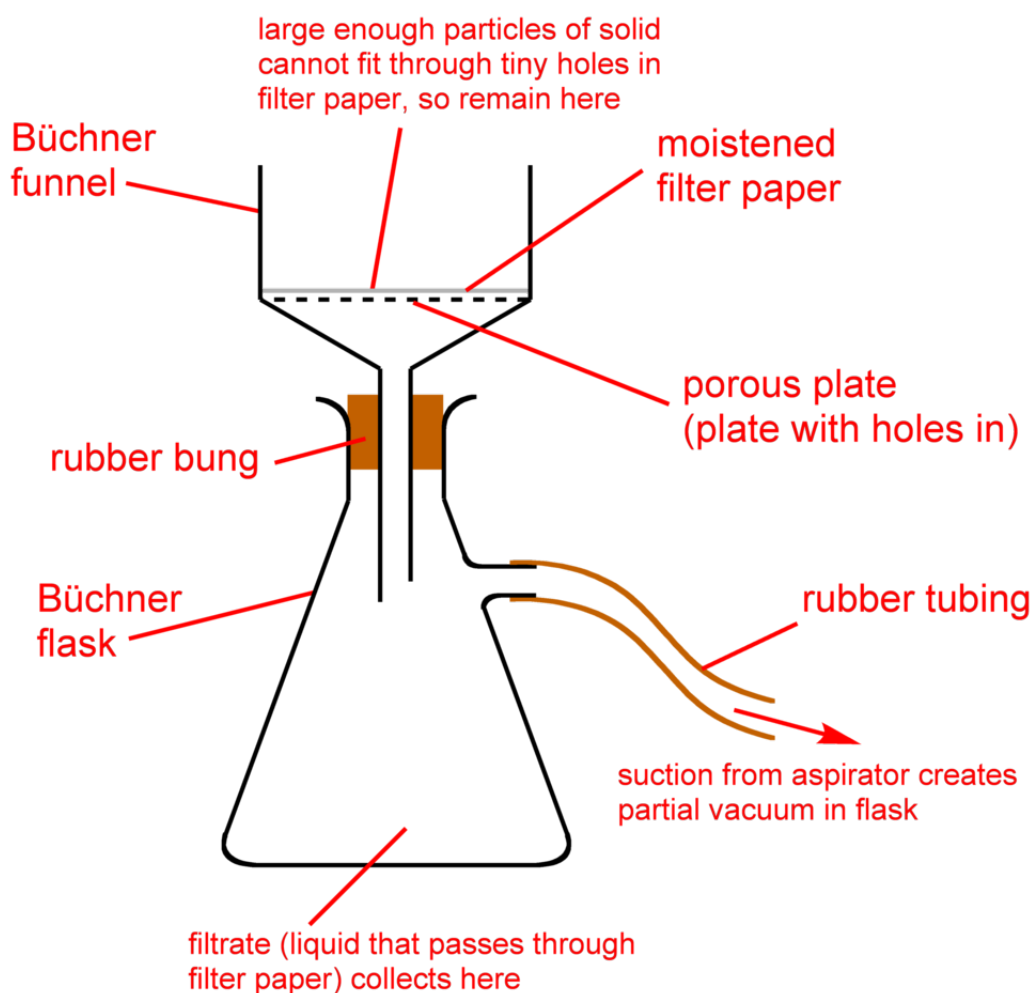


FIGURE 3.3: Vacuum filtration setup (chem.libretexts.org, 2017)

Rough estimates for the induction time were also done. Once the crystal seeds were inserted into the supersaturated solution, a temperature increase indicates that crystal growth has started. As mentioned above, the temperature readings were only logged every 20 seconds, so there is a considerable margin for error.

3.3 60°C batch crystallization experiment

60°C was used as the crystallization temperatures in this experiment to study the differences in uptake in the precipitated crystals. Experiments were only done for

solutions containing Na, Cl and Mg. Despite difficulties in temperature control of the Büchner funnel, measures were put in place to reduce the temperature difference between the hot solution to be filtered and the Büchner funnel. The Büchner funnel was placed in a 60°C heating cabinet for a minimum of 1 day prior to being used for filtration. There was no more temperature control beyond this point. Immediately before filtration, the Büchner funnel is taken out of the heating cabinet, placed on top of the Büchner flask, readying the vacuum filtration setup for use. In the process, however, the Büchner funnel radiates some of its heat to the surroundings, which decreases its temperature by an unknown amount. The justification for conducting this experiment despite the discrepancy in temperature control is the fact that temperature control of filtration equipment is not as strict in the industry as it may be in a laboratory setting. A temperature difference of up to 30°C between solution and funnel is accepted and often unavoidable (Bøckmann, 2018).

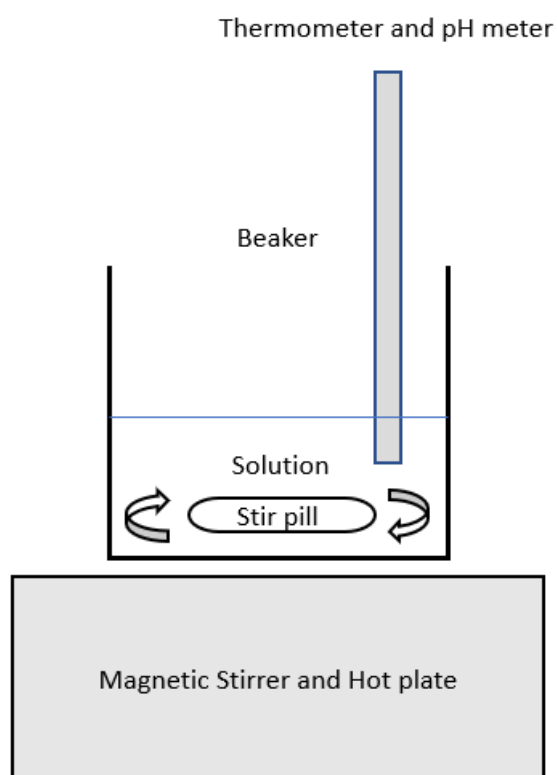


FIGURE 3.4: Sketch of High temperature Crystallization (not to scale)

The batch reactor setup was left unused because of difficulties in evaporation. Even if left unstoppered, the openings in the top of the reactor seal were so small that evaporation was highly ineffective and time consuming. Therefore, an open 600 mL glass beaker on a hot plate with magnetic stirring was used instead. Using this setup, the submersion of the thermometer/pH meter is not a limiting factor on the total volume of the solution. Thus, there is no need to restrict the volume to 450 mL, a smaller solution volume of 175 mL was chosen instead with a saturation temperature of 70 °C. An additional 75g of water was also added to be evaporated over the course of the experiment. The industrial batch crystallization experiments were only done using all impurities at the same time as the underlying purpose of these experiments was to mimic industrial conditions. The experiment may be replicated in the detailed steps described in Appendix C.2 and the solution compositions of the experiments are shown in Appendix B.4. The experiment is briefly summarized in the following list. The setup is illustrated in figure 3.4.

1. Prepare an aqueous solution of Nickel Sulfate which saturates at 70°C.
2. Add any impurities and an extra 75g of deionized water and 5g/kg sulfuric acid.
3. Insert the solution in an open beaker on a hotplate with magnetic stirring.
4. Allow the system to stay at 80°C until about half of the excess water is evaporated.
5. Cool solution to 60°C.
6. Insert seeds when the solution volume reaches 175 mL.
7. Filter crystals out of solution using vacuum filtration.
8. Wash filter cake with 100 mL of ethanol.
9. Dry crystals at 50°C for 24 hours.
10. Declump or dry mill the crystals using a mortar and pestle.
11. Analyze sample using SEM, XRD or ICP-MS

3.4 Partial filtration setup

In early impurity content experiments, a significant spread of concentration were detected in crystals from the same sample. Based on these inconsistencies the following hypothesis was proposed: The varying concentration of impurities in precipitated crystals from a solution containing a flat concentration of impurities may be a result of uneven distribution of concentration of impurities throughout the bulk of the crystal mass. A method to test this hypothesis is briefly described in the following list.

1. Prepare a small amount of Nickel sulfate and an even smaller amount of water.
2. Gently mix the two together using magnetic stirring for 60 minutes
3. Using vacuum filtration with a Millipore 0.22 μ m, $\varnothing=47$ mm filter, separate the partially dissolved crystals from the slurry.
4. Wash the crystals with ethanol to disperse excess solution present on the surface of the wet, partially dissolved crystals.
5. Dry the crystals for 24 hours in a 50°C heating cabinet
6. Analyze new concentration

The goal of this method was to physically remove the outer layer of each crystal by filtration. This was done by mixing precipitated crystal with small amounts of water. Therefore, a finely tuned ratio, as shown in equation 3.2, of $NiSO_4 * 6H_2O$ to water was crucial:

$$Y = \frac{m_{NiSO_4 * 6H_2O - PD}}{m_{H_2O - PD}} \quad (3.2)$$

Where,

Y= Ratio of $NiSO_4 * 6H_2O$ to H_2O

$m_{NiSO_4 * 6H_2O - PD}$ = Mass of $NiSO_4 * 6H_2O$

$m_{H_2O - PD}$ = Mass of deionized water

If too much water is used, the entire sample will dissolve, resulting in no separation after filtration. If too little water is used, some of the crystal is left dry and entirely undissolved. Therefore, Y is ideal when a portion of the crystal is dissolved, yet no crystal is left dry. $Y=2$ was found to fulfill these criteria. After this process is complete, using a ratio of 2 at 25°C , about 43% of the initial crystal mass is dissolved. The experimental procedure is described in detail in Appendix C.3, the setup is illustrated in figure 3.5:

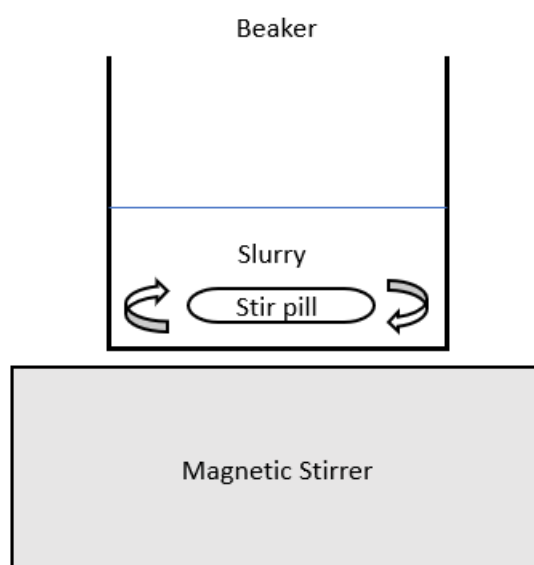


FIGURE 3.5: Sketch of partial filtration setup (not to scale)

3.4.1 Expectations from partial dissociation

From this process, one out of three results can be expected when comparing the concentration of impurities of partially dissolved crystals to undissolved crystals: the new concentration could increase, decrease or remain the same. These possibilities are discussed in the following list.

1. **Increased concentration:** This result would signify that the mass of the crystals that was dissolved and separated contained a lower concentration of impurities than the mass of the crystal which was left undissolved, thus resulting in an increase of concentration of impurities, which would imply that the higher concentration of impurities lies on the inside structures of the $\text{NiSO}_4 \cdot 6\text{H}_2\text{O}$ crystals.

2. **Decreased concentration:** This result would imply that the mass of the crystals that was dissolved and separated contained a higher concentration of impurities than the mass of the crystal which was left undissolved, which decreases the concentration of impurities, which would imply that the higher concentration of impurities lies on the outside structures of the $NiSO_4 \cdot 6H_2O$ crystals.
3. **No change in concentration:** This result would imply that the concentration of impurities is evenly distributed in the bulk of the crystal mass, which implies that partial filtration does not affect the concentration of impurities in $NiSO_4 \cdot 6H_2O$ crystals, rendering it an ineffective method of controlling the presence of impurities in precipitated Nickel sulfate.

3.5 Solubility setup

One of the side investigations included the solubility of aqueous Nickel sulfate in the presence of a flat amount of sulfuric acid (H_2SO_4) at different temperatures. Solubility data and phase diagrams for specific multicomponent systems, such as the Nickel sulfate-water-sulfuric acid system, are often unavailable due to the vast number of possible systems and proportions. A magnetic stirrer and hotplate was used. Therefore, there was no volume restriction, and 250 mL was chosen. Temperature control of the filtration equipment is important during solubility tests for the same reasons as the high temperature crystallization experiments discussed in section 3.3. The Büchner funnel was placed in a heating cabinet. The heating cabinet is set to the same temperature as the one being investigated for a minimum of 1 day prior to being used for filtration. There was no more temperature control beyond this point. Immediately before filtration, the Büchner funnel is taken out of the heating cabinet, placed on top of the Büchner flask, readying the vacuum filtration setup for use. In the process, however, the Büchner funnel radiates some of its heat to the surroundings, which decreases its temperature by an unknown amount. The justification for this experiment despite poor temperature control is the same as stated in section 3.3. The setup used is illustrated in figure 3.6. The experiment can be replicated through by following the steps in Appendix C.4:

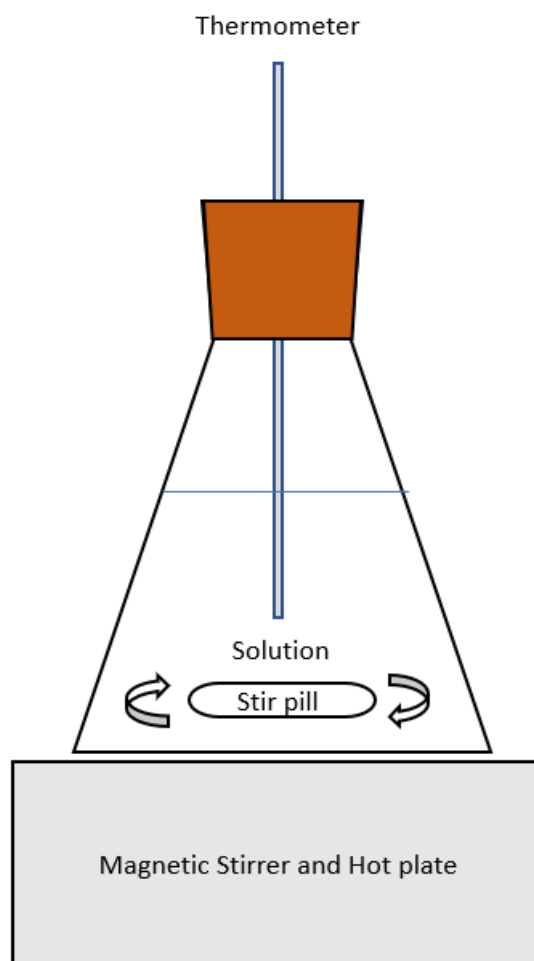


FIGURE 3.6: Sketch of the solubility setup (not to scale)

3.6 Analytical procedures

3.6.1 X-ray diffraction (XRD)

X-ray diffraction is a method to identify crystalline materials by observing diffracted x-rays which are reflected off the surface of the material. Crystalline materials are most common but it can be used on amorphous materials as well. Different compounds diffract x-rays in distinct ways, allowing identification of unknown materials. XRD can also be used to characterize unit cell dimensions and crystal structures of compounds because of its ability to identify atomic spacing in a crystal lattice.

XRD was used to identify the hydration levels of Nickel sulfate in the sample, and to identify if there were separate compounds present in the sample. For instance

in tests containing multiple impurities, XRD would be able to detect if other compounds were present together with the precipitated Nickel sulfate. The output XRD patterns from each test can be compared to the XRD "fingerprint" of other materials. Based on the compounds used in each experiment, the possibilities other than Nickel sulfate are $NaCl$, $MgCl_2$, Na_2SO_4 , $MgSO_4$ or $NiCl_2$. As mentioned in section A.0.1, $NiSO_4 \cdot 6H_2O$ is insoluble in ethanol, this also means that ethanol is an antisolvent to Nickel sulfate. An antisolvent is a solvent that decreases the solubility of the solute. This has a profound salting out effect on Nickel sulfate, causing it to precipitate immediately. Compounds like Na_2SO_4 are also insoluble in ethanol, which introduces a hypothesis that suggests that washing the Nickel sulfate with ethanol may crystallize any sodium ions on the crystal surface as Na_2SO_4 . Sample preparation for XRD is fairly straightforward, place a small amount of finely ground sample into a special holder, which is then analyzed. The XRD machine used is a D8 Advance DaVinci, ("DaVinci1") with LynxEyeTM super-speed detector and 60-position sample changer. The XRD patterns from the experiments are shown in Appendix D.

3.6.2 Inductively coupled plasma mass spectrometry (ICP-MS)

Is a method of identifying precise contents of unknown materials. This is done by ionizing a material with inductively coupled plasma (ICP), and then using a mass spectrometer to identify those ions based on mass and charge.

The ICP-MS instrument used is an Agilent 8800 ICP Triple Quad (ICP-QQQ) high resolution ICP-MS with a Thermo-Fischer Element 2 high resolution ICP-MS, which boasts the highest accuracy, precision and detection resolution ($\mu g/L$) of any other setup in the ICP-MS market (Lierhagen, 2018). The sample preparation process for water soluble salts was to dissolve about 50 mg amount of crystal in a 15mL solution of 0.1M nitric acid and ultra-pure water. These were analyzed for content for each element. Certain quantities were known in each sample, such as amount of Nickel and sulfur, and other quantities were unknown such as the deliberately added impurities. Four parallel samples were analyzed per $NiSO_4 \cdot 6H_2O$ test at 25°C, 60°C and partially dissolved tests. The known contents, mass and volume of each sample was recorded on a spreadsheet which was delivered to the ICP-MS engineers along with each sample.

Due to the extent of the detection resolution of the ICP-MS instrument, it is also very sensitive to change. Incredibly small contaminations can be registered and differ

the ICP-MS reading from the calculated value based on the mass of crystal in each sample. For every ICP-MS test, some discrepancy is expected between the amount that each sample was calculated to contain and the reading which the ICP-MS instrument found the sample to contain. The reasons for such a discrepancy is most likely a contamination which can stem from an almost unlimited number of things such as from atmospheric dust during sample preparation, contamination from the material inside of the test beaker itself, contamination from the ICP-MS instrument itself, etc. To gauge the error of the instrument for each element, four parallels of standard quantities of each impurity element was analyzed. The substances used in these tests were Sodium sulfate, Nickel chloride, and Magnesium sulfate. This known quantity was compared to the quantity which the ICP-MS instrument found the sample to contain. The error between the two quantities were averaged and standard deviation calculated. This error is accounted for when calculating the error of the measurements.

3.6.3 Scanning Electron Microscopy (SEM)

Some characteristics of the final products were investigated using *Scanning Electron Microscopy* (SEM). Characteristics like size and shape of the deposited crystals. About 50 mg of declumped crystal sample was coated on an adhesive carbon tape on a brass holder which was placed in position under the microscope in a partial vacuum. A Hitachi 3400N SEM was used to take each picture at a magnification of 100x which was found to be the optimal range to display the surface characteristics such as roughness, as well as the size and shape of the crystals. The photographs shown in later chapters were taken in areas of high density in each sample, though there was also a focus on not being selective or having any biases when choosing objects to photograph. No quantitative analysis was done on the size, crystal growth and size distribution of the crystals.

Chapter 4

Results from experiments

4.1 Impurity uptake from experiments

The concentration of every element as obtained from ICP-MS were given in [$\mu\text{g}/\text{L}$] based on the contents of the test tubes which were analyzed. To gauge the uptake levels of Nickel sulfate hexahydrate, $\text{NiSO}_4 \cdot 6\text{H}_2\text{O}$, the impurity concentrations were measured relative to the concentration of Ni^{2+} in each test. As mentioned in section 3.6.2, the concentration Ni^{2+} is a known quantity and represents the remaining mass of the salt irrespective of hydration level. Figures 4.1 to 4.19 show the impurity uptake in precipitated crystals from solution containing different impurity concentrations and compositions. The experimental data for the results presented in this chapter is found in Appendix B.

4.1.1 Plot setup

The figures 4.1 to 4.19 are split into two plots which are labeled a) and b). Both plots a) and b) display the same information about the same solutions but the impurity ion concentration of the solution (the information on the x-axis) is formulated using different units. Plot a) shows the concentrations in the same units in both the x- and y- axes: impurity ion mass per Ni^{2+} mass in the crystals on the y-axis and impurity ion mass per Ni^{2+} mass in the solution on the x-axis. Plot b) displays the same information on the y-axis as plot a), but displays the concentration of the solution differently on the x-axis; impurity ion mass per kilogram of solution.

The reason why the same information is shown in two different ways is because they display the information from two sides. Plot a) shows information consistently from x-axis to y-axis, but it isn't as easily digested because the concentration is displayed using units that are specific to the system and not commonly used outside of impurity uptake investigations. Plot b) is not consistent from x to y-axis, different units

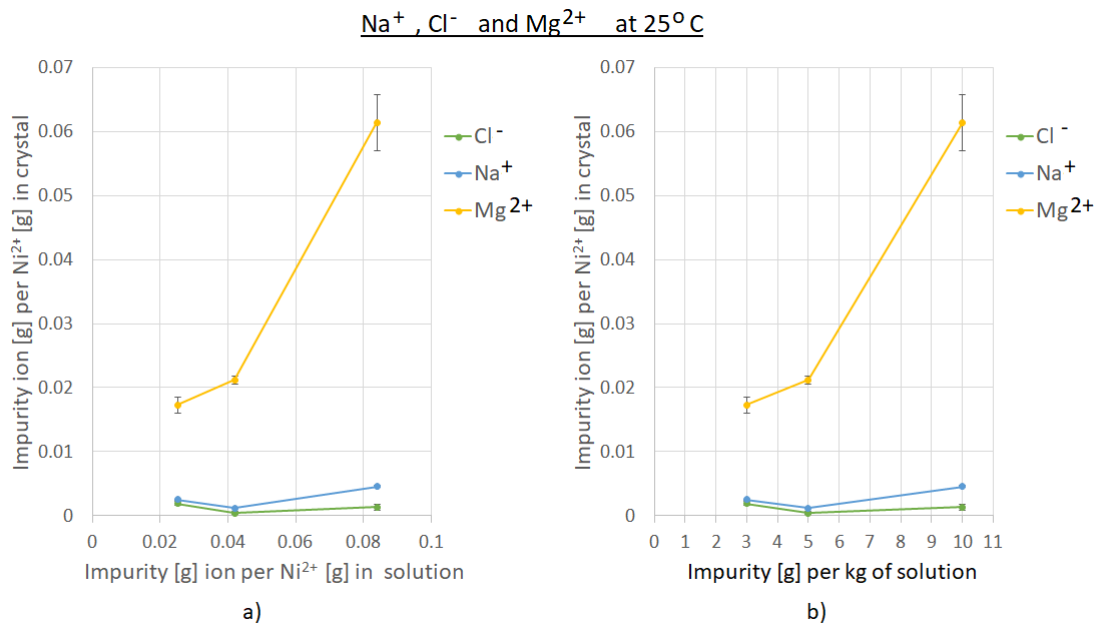


FIGURE 4.1: Plots a) and b) display the concentrations of crystallized $NiSO_4 \cdot 6H_2O$ salts *before* partial dissociation) from solutions containing 3, 5 and 10 g/kg of solution of Na^+ , Cl^- , and Mg^{2+} at 25°C. Plot a) and b) display the same information, but use different units on the x-axis.

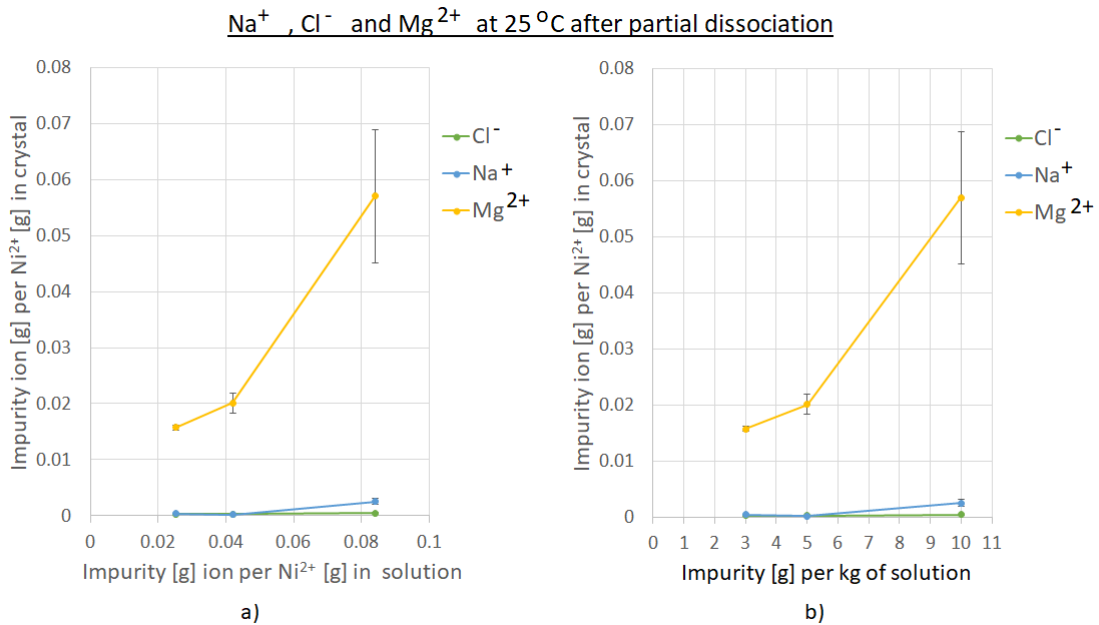


FIGURE 4.2: Plots a) and b) display the concentrations of crystallized $NiSO_4 \cdot 6H_2O$ crystals *after* partial dissociation. The crystals are precipitated at 25°C from solutions containing 3, 5 and 10 g/kg of solution of Na^+ , Cl^- , and Mg^{2+} . Plot a) and b) display the same information, but use different units on the x-axis.

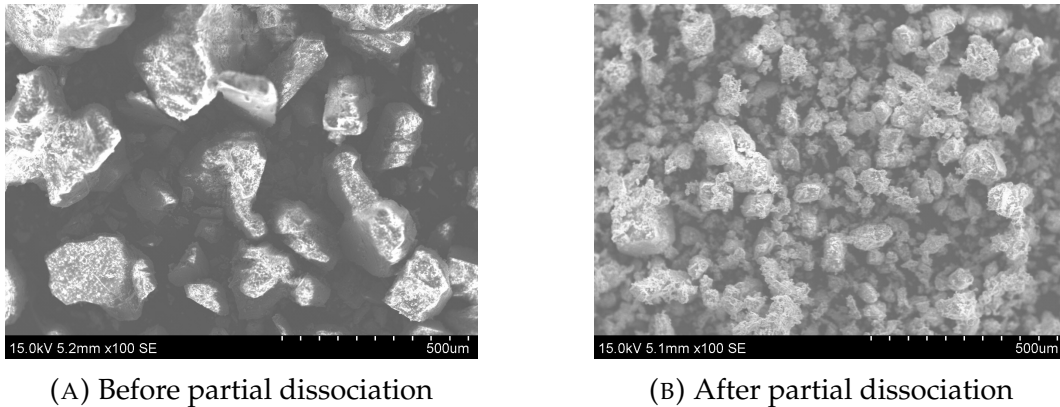


FIGURE 4.3: Final crystals from experiment with 3 grams per kg of Na^+ , Cl^- and Mg^{2+} at $25^\circ C$ before and after partial dissociation. Scale bar of $500 \mu m$ shown as reference

of concentration is used, but it is easily digested because it uses the same units of concentration for the solution as in the experimental procedure.

The slope of plot a) in every figure can be used to investigate the change in uptake rate in the crystals. The manner in which the ion concentration in the crystal increases as the ion concentration in the solution increases is not always obvious without calculation. In figure 4.1, the uptake of Mg^{2+} in the crystal went from 68% at 3g/kg to 73% at 10g/kg. As the concentration of the solution increases, the concentration of the crystal accelerates faster. This information is displayed in table 4.2 along with every other test.

Error bars

Each point on each plot in figures 4.1 to 4.19 is the average of four parallel ICP-MS tests. The error bars on each data point displays the standard deviation of those four values in order to convey the presence of spread in the data. The error bars also include a flat percentage based on the error of the standard ICP-MS tests. Every data point has an error, but some are too small to be seen because of little spread in the data. Generally, the spread of the data grows as the numbers themselves grow. This is to be expected and makes sense as percentages of larger numbers are much larger than percentages of smaller numbers.

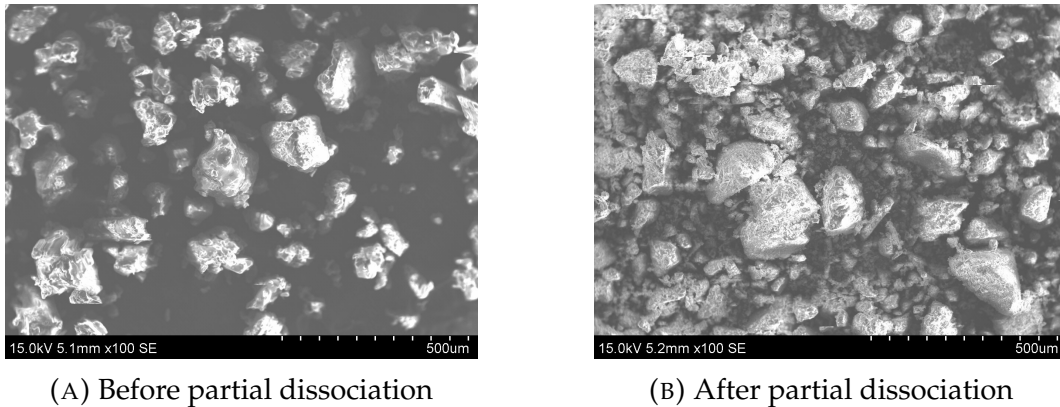


FIGURE 4.4: Final crystals from experiment with 5 grams per kg of Na^+ , Cl^- and Mg^{2+} at $25^\circ C$ before and after partial dissociation. Scale bar of $500 \mu m$ shown as reference

4.1.2 SEM photographs

SEM photographs for tests with Na^+ , Cl^- and Mg^{2+} for both $25^\circ C$ and $60^\circ C$ can be seen in this chapter, SEM photographs for all other tests are in Appendix E. The purpose of the SEM photographs is to identify general trends in crystal habit and behaviour, as a result of impurities or partial dissociation. There is a noticeable roughness to the surfaces of crystals which were crystallized at $25^\circ C$, this is evident in SEM photographs 4.3a and 4.5a. Tests at $60^\circ C$ display a more soft and rounded surface as seen in SEM photographs 4.7a and 4.8a.

4.2 Impurity content in samples containing multiple impurities

In figures 4.1, 4.2, 4.6, and 4.10, the contents of each test are split up to the individual impurity to emphasize their behaviour relative to the other impurities. Each component is investigated on their own in sections 4.3, 4.4 and 4.5. Figure 4.1 shows the impurity content of $NiSO_4 \cdot 6H_2O$ that is crystallized at $25^\circ C$, containing 3, 5 and 10 grams of added Na^+ , Cl^- , and Mg^{2+} per kg of solution mass. These plots show the impurity content *before* partial dissociation.

Both plots in figure 4.1 provide valuable information: by using the slope of Plot a) in each data point, it can be seen that the concentration of Mg^{2+} is almost as high in the deposited crystals as in the solution, which may seem high, but this is a misleading result. Relative to the rest of the crystal mass, this impurity uptake only represents a weight percentage of 0.4% at 3g/kg and 1.4% at 10g/kg as seen in table 4.4. Plot b)

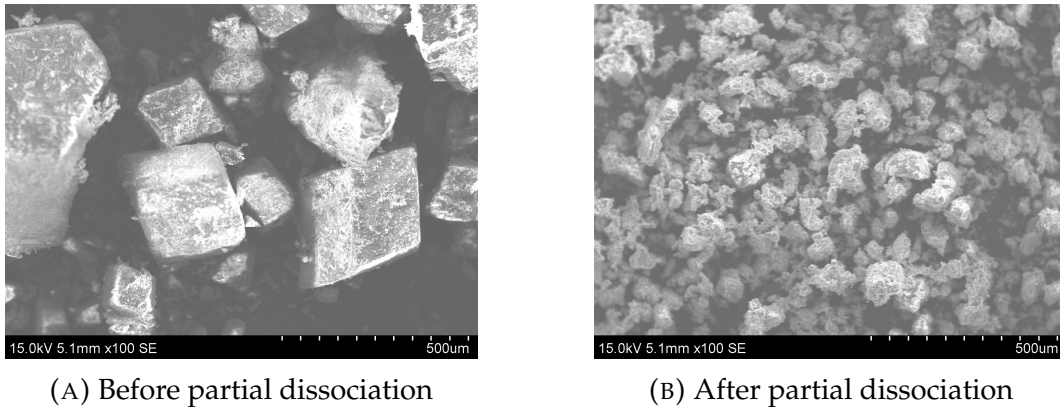


FIGURE 4.5: Final crystals from experiment with 10 grams per kg of Na^+ , Cl^- and Mg^{2+} at $25^\circ C$ before and after partial dissociation. Scale bar of $500 \mu m$ shown as reference

gives a more practical outlook on how the solution concentration affects the uptake of impurities in precipitated crystals because it shows the concentration in the same units as used in the experimental procedure. Both plots reiterate the fact that each impurity has the same initial solution concentration.

The concentration of Na^+ and Cl^- is much lower in the crystals than in the solution. This suggests that they are not favored to adsorb to a growing crystal, but rather stay in the supersaturated solution. The concentration of Mg^{2+} is much higher which suggests that it is more favored to adsorb to the growing $NiSO_4 \cdot 6H_2O$ crystal in a supersaturated solution.

Figure 4.2 shows the impurity content after partial dissociation of $NiSO_4 \cdot 6H_2O$ that is crystallized from a solution at $25^\circ C$, containing 3, 5 and 10 grams of added Na^+ , Cl^- , and Mg^{2+} per kg of solution mass. The plots show the impurity content of the same $NiSO_4 \cdot 6H_2O$ from figure 4.1 except after partial dissociation. The partial dissociation process reduced the concentration of Na^+ by an average of 62%, Cl^- by an average of 71% and Mg^{2+} by an average of 7%. This data can be seen in tables 5.2 and 5.3.

Figure 4.6 shows the impurity content of $NiSO_4 \cdot 6H_2O$ that is crystallized at $60^\circ C$, containing 3, 5 and 10 grams of added Na^+ , Cl^- , and Mg^{2+} per kg of solution mass. These plots show the impurity content *before* partial dissociation. The content of impurities at $60^\circ C$ can be compared to that at $25^\circ C$. Slightly higher weight percentage for all impurities as seen in tables 4.4 and 4.5. Though this may be a consequence of rapid crystallization during dissociation through a colder Büchner funnel. Most prominent is the increase in Na^+ uptake from $25^\circ C$ to $60^\circ C$. The concentration of

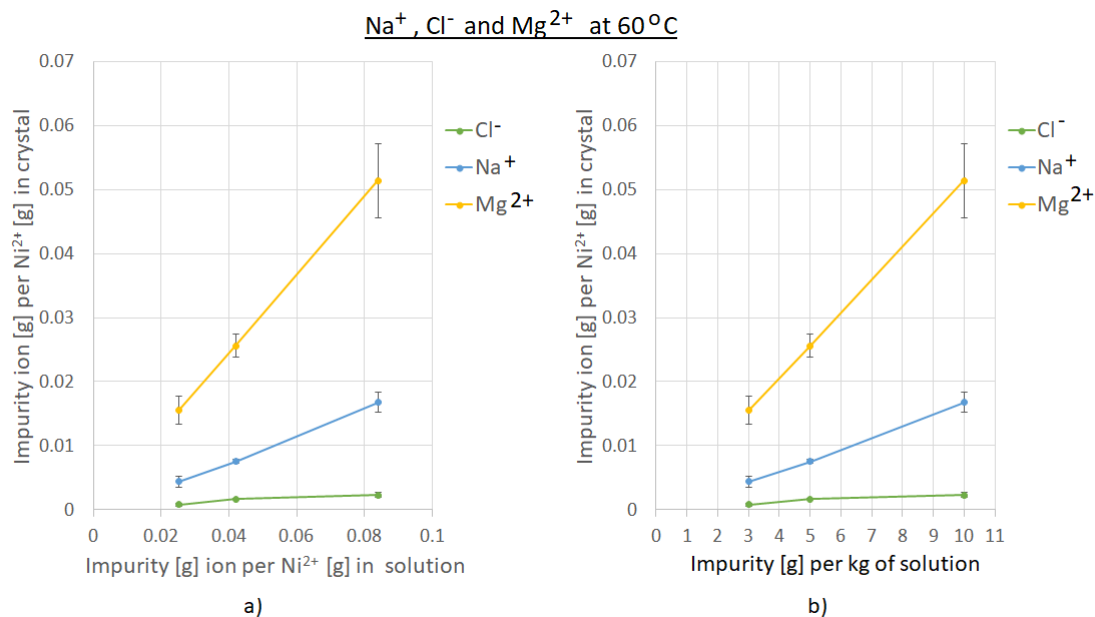
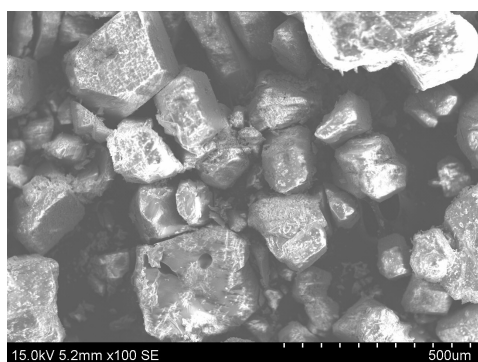
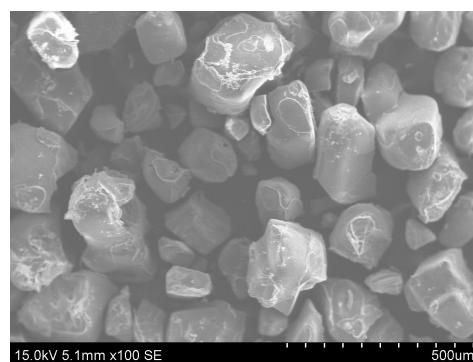


FIGURE 4.6: Plots a) and b) display the concentrations of crystallized $NiSO_4 \cdot 6H_2O$ (before partial dissociation) from solutions containing 3, 5 and 10 g/kg of solution of Na^+ , Cl^- , and Mg^{2+} . These crystals were precipitated at 60°C. Plot a) and b) display the same information, but use different units on the x-axis.



(A) Before partial dissociation

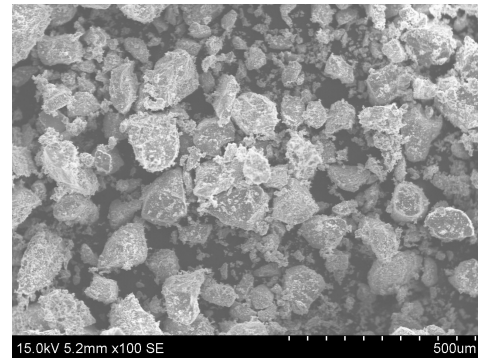


(B) After partial dissociation

FIGURE 4.7: Final crystals from experiment with 3 grams per kg of Na^+ , Cl^- and Mg^{2+} at 60°C before and after partial dissociation. Scale bar of 500 μm shown as reference

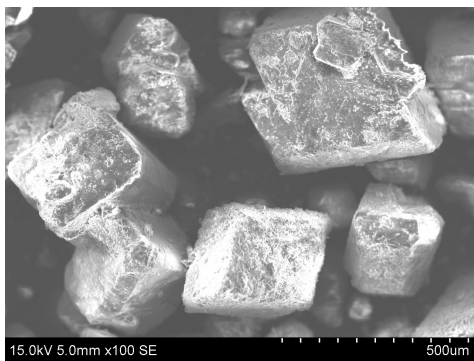


(A) Before partial dissociation

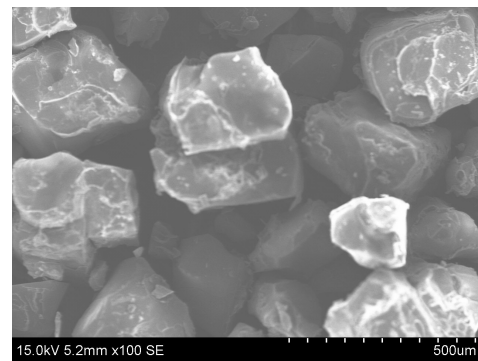


(B) After partial dissociation

FIGURE 4.8: Final crystals from experiment with 5 grams per kg of Na^+ , Cl^- and Mg^{2+} at $60^\circ C$ before and after partial dissociation. Scale bar of $500 \mu m$ shown as reference



(A) Before partial dissociation



(B) After partial dissociation

FIGURE 4.9: Final crystals from experiment with 10 grams per kg of Na^+ , Cl^- and Mg^{2+} at $60^\circ C$ before and after partial dissociation. Scale bar of $500 \mu m$ shown as reference

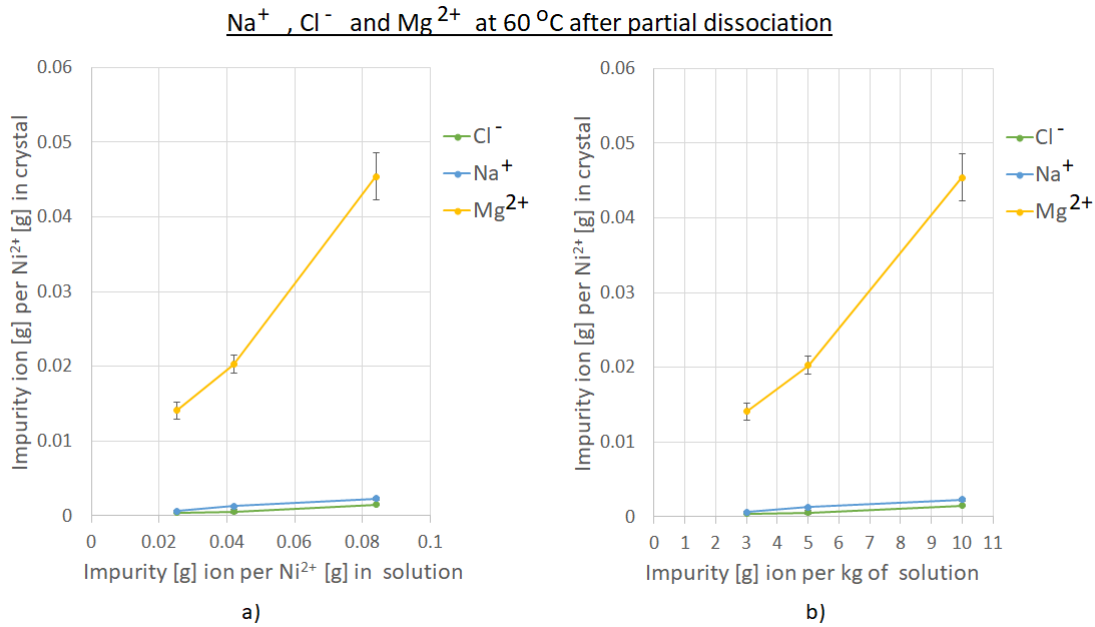


FIGURE 4.10: Plots a) and b) display the concentrations of crystallized $NiSO_4 * 6H_2O$ crystals *after* partial dissociation. The crystals are precipitated at 60°C from solutions containing 3, 5 and 10 g/kg of solution of Na^+ , Cl^- , and Mg^{2+} . Plot a) and b) display the same information, but use different units on the x-axis.

Na^+ increased by an average of 247% before partial dissociation. This may be a large increase, but in relation to the rest of the crystal mass, it only represents a fraction of the crystal mass. This goes for Cl^- as well, even though there is a much smaller increase in average uptake of about 30% from 25°C to 60°C before partial dissociation, the relative mass is very low. Mg^{2+} has a much higher concentration in the crystals at 60°C compared to Na^+ and Cl^- , similar to 25°C. There is, however, a decrease in average uptake from 25° to 60°C at -7%. This seems to suggest that Mg^{2+} is slightly less favored to be attracted to the growing crystal surface in a supersaturated solution in higher temperatures.

Figure 4.10 shows the impurity content of $NiSO_4 * 6H_2O$ that is crystallized at 60°C, containing 3, 5 and 10 grams of added Na^+ , Cl^- , and Mg^{2+} per kg of solution mass. These plots show the impurity content of the $NiSO_4 * 6H_2O$ from figure 4.6 after partial dissociation. Partial dissociation reduces all impurity uptakes at 60°C in a similar fashion as 25°C. The impurity content in each test at 60°C is shown in table 4.5.

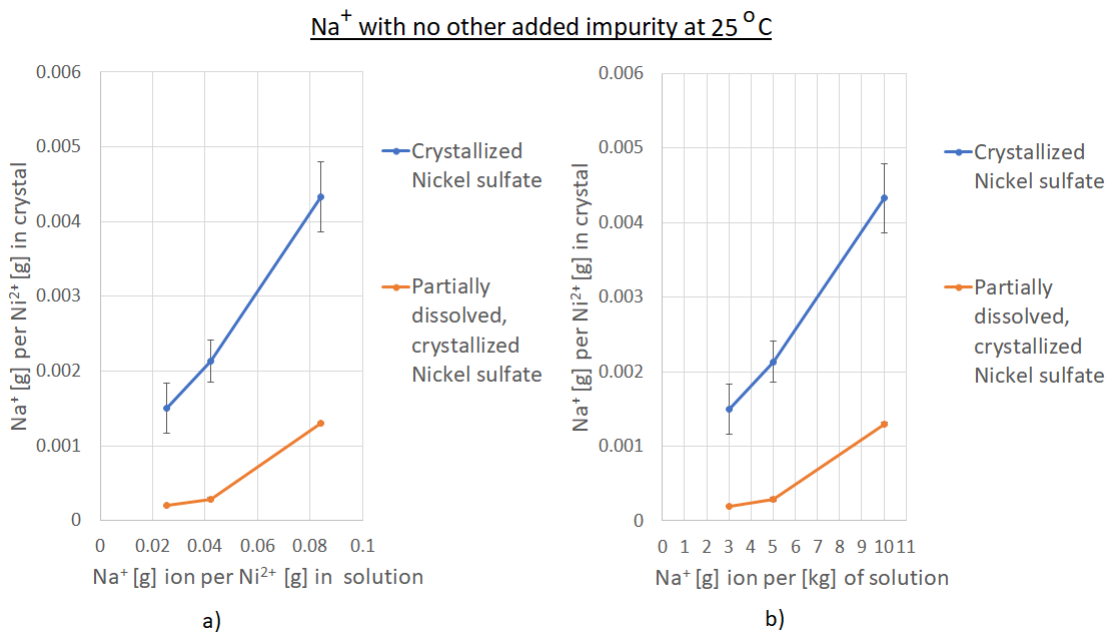


FIGURE 4.11: Na^+ [g] per Ni^{2+} [g] in crystallized $\text{NiSO}_4 \cdot 6\text{H}_2\text{O}$ plotted against Na^+ concentration of the solution before crystallization at 25 °C in the presence of no other deliberately added impurities. Plot a) and b) display the same information, but use different units on the x-axis.

4.3 Na^+ as a crystallization impurity on Nickel sulfate

4.3.1 Na^+ at 25 °C without any other deliberately added impurities

Figure 4.11 displays the concentration of Na^+ in crystallized $\text{NiSO}_4 \cdot 6\text{H}_2\text{O}$ from aqueous solution containing 3, 5 and 10 grams of Na^+ in the presence of no other deliberately added impurity at 25 °C. Figure 4.11 shows a clear decrease in concentration after partial dissociation at all concentration levels. As seen in plot a), the concentration of Na^+ is much lower in the crystal than in the solution, which suggests it is favored to stay dissolved in a supersaturated solution. There is some spread in the values of undissolved Nickel sulfate, which indicates that there is an uneven distribution of concentration in the crystal bulk of the solution, this is significantly reduced after partial dissociation which suggests the portion of the crystal bulk which was dissolved and filtered away contained the bulk of the variation of Na^+ concentration. This also indicates that the concentration of Na^+ left after partial dissociation is evenly distributed. The weight percentage of Na^+ before and after partial dissolution in this series of experiments can be seen in table 4.3.

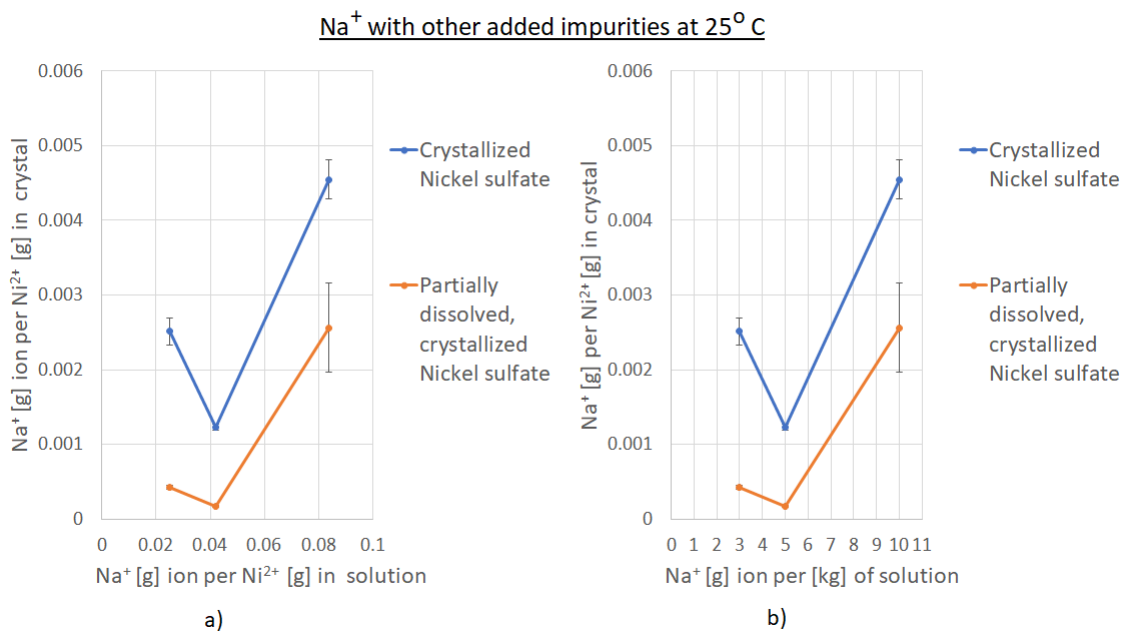


FIGURE 4.12: Na^+ [g] per Ni^{2+} [g] in crystallized $NiSO_4 \cdot 6H_2O$ plotted against Na^+ concentration of the solution before crystallization at 25°C in the presence of Cl^- and Mg^{2+} as other deliberately added impurities. Plot a) and b) display the same information, but use different units on the x-axis.

4.3.2 Na^+ at 25°C with Cl^- , and Mg^{2+} in equal proportions

Figure 4.12 displays the concentration of Na^+ in crystallized $NiSO_4 \cdot 6H_2O$ from aqueous solution containing 3, 5 and 10 grams of Na^+ in the presence of Cl^- and Mg^{2+} as deliberately added impurities at 25°C. This figure shows the same information as figure 4.1 and 4.2, but with the focus on Na^+ , undissolved and partially dissociated. Figure 4.12 shows a clear decrease in concentration after partial dissociation at all concentration levels. As seen in plot a), the concentration of Na^+ is much lower in the crystal than in the solution, which suggests it is favored to stay dissolved in a supersaturated solution. The weight percentage of Na^+ before and after partial dissolution in this series of experiments can be seen in table 4.4.

The drop in concentration of Na^+ from 3 g/kg to 5 g/kg is illogical. What would make the concentration of Na^+ in the crystal decrease despite an increase in the concentration of the solution? One explanation is that this is an error and should be ignored, the drop in concentration of Na^+ may seem very large by looking at figure 4.12, but it only represents a change of 0.029% weight percent. If it is assumed

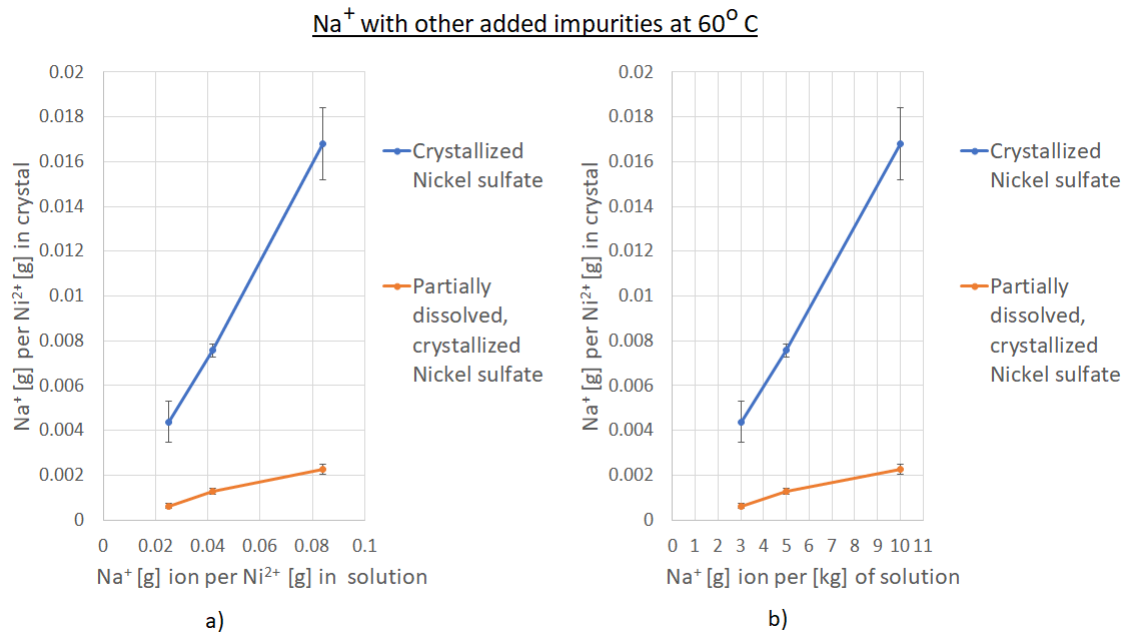


FIGURE 4.13: Na^+ [g] per Ni^{2+} [g] in crystallized $NiSO_4 \cdot 6H_2O$ plotted against Na^+ concentration of the solution before crystallization at 60°C in the presence of Cl^- and Mg^{2+} as other deliberately added impurities. Plot a) and b) display the same information, but use different units on the x-axis.

that this is not an error it may be a product of resistance from the electrical double layer and more competition from the other cations, most notably Ni^{2+} and to a lesser extent Mg^{2+} , when adsorbing to the growing crystal surface. From 5 g/kg to 10 g/kg, the concentration increases again though, along with the concentrations of the other impurities in the sample. The most logical explanation for the drop in concentration from 3 g/kg to 5g/kg is either a measurement error of the instrument or a contamination. There is also a significant spread in the data as seen by the error bars, which indicates an uneven distribution of impurity concentration in the undissolved crystal bulk. The large spread in the partially dissolved sample at 10g/kg in figure 4.12 suggests this sample may not have been partially dissolved as thoroughly as the samples at 3 and 5 g/kg, which have no spread, indicating an evenly distributed concentration of Na^+ .

4.3.3 Na^+ as a crystallization impurity at 60°C in the presence of Mg^{2+} and Cl^- in equal proportions

Figure 4.13 displays the concentration of Na^+ in crystallized $\text{NiSO}_4 \cdot 6\text{H}_2\text{O}$ from aqueous solution containing 3, 5 and 10 grams of Na^+ in the presence of Cl^- and Mg^{2+} as deliberately added impurities at 60°C . This figure shows the same information as figure 4.6 and 4.10, but with the focus on Na^+ , undissolved and partially dissociated. Figure 4.13 shows a Cl^- ear decrease in concentration after partial dissociation at all concentration levels. As seen in plot a), the concentration of Na^+ is much lower in the crystal than in the solution, which suggests it is favored to stay dissolved in a supersaturated solution. There is a minor spread in the values of undissolved $\text{NiSO}_4 \cdot 6\text{H}_2\text{O}$, which indicates that there is an uneven distribution of concentration of Na^+ in the undissolved crystal bulk. The concentration and spread of Na^+ is significantly reduced after partial dissociation. This suggests that the concentration of Na^+ which was left in the crystal after partial dissociation is evenly distributed. The weight percentage of Na^+ before and after partial dissolution in this series of experiments can be seen in table 4.5.

At this temperature, there is no drop in concentration between 3g/kg and 5g/kg as in figure 4.12, further reinforcing the assumption of it being an error. The most logical expectation is to see an increase in concentration in the crystal as the concentration of the solution is increased.

4.4 Cl^- as a crystallization impurity on Nickel sulfate

4.4.1 Cl^- at 25°C

Figure 4.14 displays the concentration of Cl^- in crystallized $\text{NiSO}_4 \cdot 6\text{H}_2\text{O}$ from aqueous solution containing 3, 5 and 10 grams of Cl^- in the presence of no other deliberately added impurity at 25°C . Figure 4.14 shows a Cl^- ear decrease in concentration after partial dissociation at all concentration levels. As seen in plot a), the concentration of Cl^- is much lower in the crystal than in the solution, which suggests it is favored to stay dissolved in a supersaturated solution. The weight percentage of Cl^- before and after partial dissolution in this series of experiments can be seen in table 4.3.

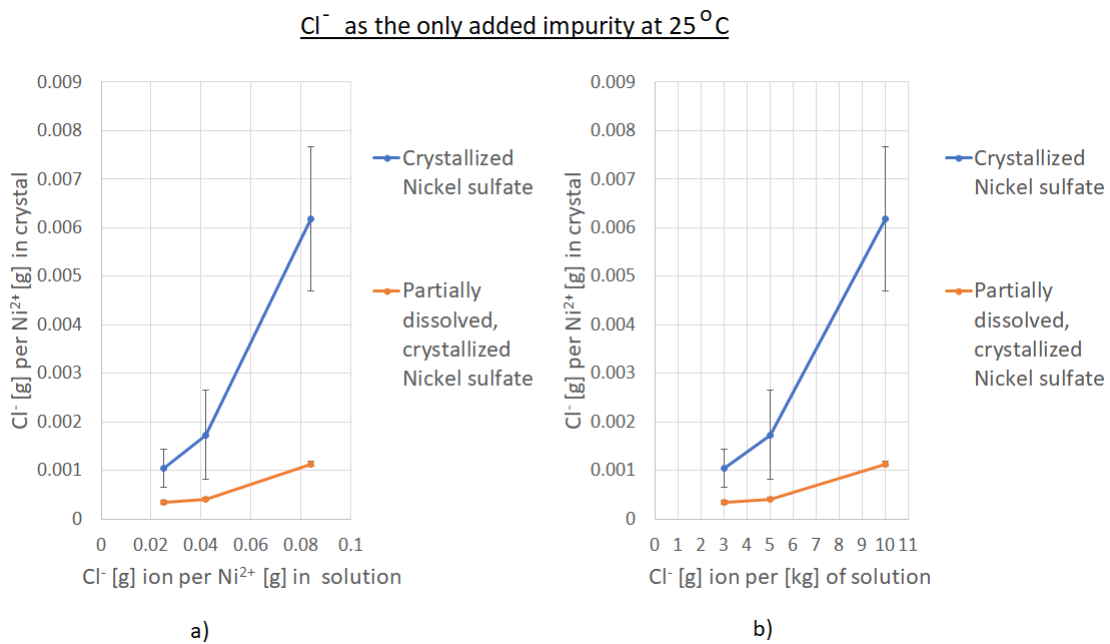


FIGURE 4.14: Cl^- [g] per Ni^{2+} [g] in crystallized $NiSO_4 \cdot 6H_2O$ plotted against Cl^- concentration of the solution before crystallization at 25°C in the presence of no other deliberately added impurities. Plot a) and b) display the same information, but use different units on the x-axis.

There is a noticeable spread in the concentration of undissolved $NiSO_4 \cdot 6H_2O$ in figure 4.14. Measurements like these led to the hypothesis of an uneven distribution of impurity content in the bulk of the crystal. This spread is significantly reduced after partial dissociation which suggests the portion of the crystal bulk which was dissolved and filtered away contained the bulk of the Cl^- concentration. This suggests that the portion left in the crystal after partial dissociation contained an evenly distributed concentration of Cl^- .

4.4.2 Cl^- at 25°C with equal proportions of Na^+ and Mg^{2+}

Figure 4.15 displays the concentration of Cl^- in crystallized $NiSO_4 \cdot 6H_2O$ from aqueous solution containing 3, 5 and 10 grams of Cl^- in the presence of Na^+ and Mg^{2+} as deliberately added impurities 25°C. This figure shows the same information as figure 4.1 and 4.2, but with the focus on Cl^- , undissolved and partially dissociated. Figure 4.15 shows a Cl^- decrease in concentration after partial dissociation at all concentration levels. As seen in plot a), the concentration of Cl^- is much lower in the crystal than in the solution, which suggests it is favored to stay dissolved in a

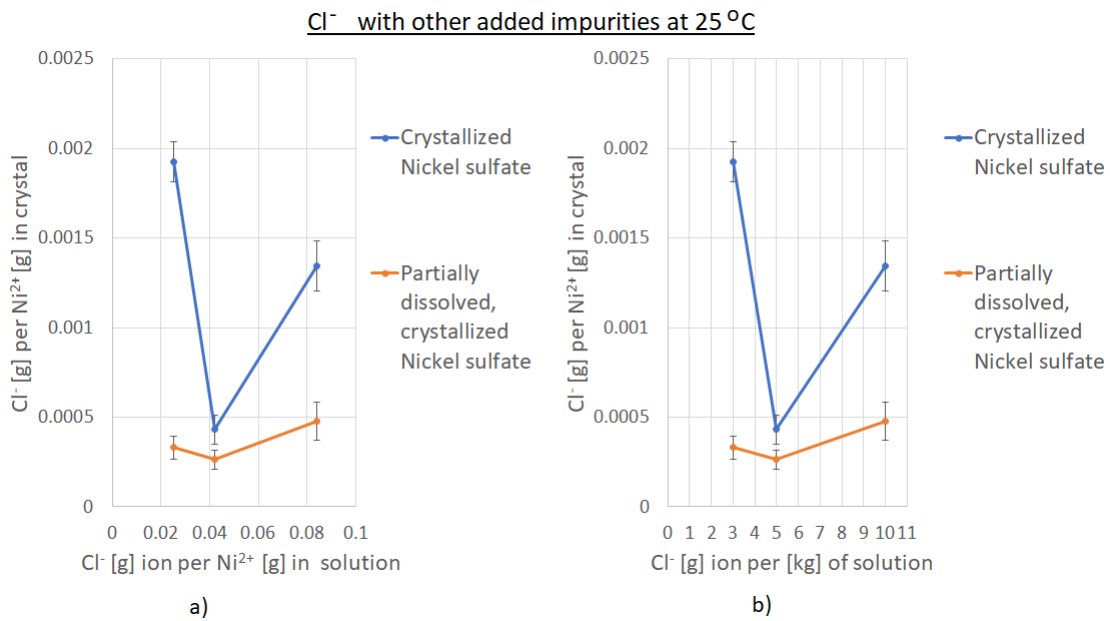


FIGURE 4.15: Cl⁻ [g] per Ni²⁺ [g] in crystallized NiSO₄ * 6H₂O plotted against Cl⁻ concentration of the solution before crystallization at 25°C in the presence of Na⁺ and Mg²⁺ as other deliberately added impurities. Plot a) and b) display the same information, but use different units on the x-axis.

supersaturated solution. The weight percentage of Cl⁻ before and after partial dissolution in this series of experiments can be seen in table 4.4.

The drop in concentration of Cl⁻ from 3 g/kg to 5 g/kg is illogical. What would make the concentration of Cl⁻ in the crystal decrease despite an increase in the concentration of the solution? One explanation is that this is an error and should be ignored, the drop in concentration of Cl⁻ may seem very large by looking at figure 4.15, but it only represents a change of 0.033% weight percent. If it is assumed that this is not an error it may be a product of resistance from the electrical double layer and more competition from the other anions, most notably SO₄²⁻, when adsorbing to the growing crystal surface. From 5 g/kg to 10 g/kg, the concentration increases again though it does not increase more than the value at 3g/kg. The most logical explanation for the drop in concentration from 3 g/kg to 5g/kg is either a measurement error of the instrument or a contamination.

There is some spread in the values of both undissolved NiSO₄ * 6H₂O and partially dissolved NiSO₄ * 6H₂O, which indicates that there is an uneven distribution of concentration in the crystal bulk of the solution. Though the concentration of Cl⁻ is significantly reduced after partial dissociation, the spread was rather unaffected. This

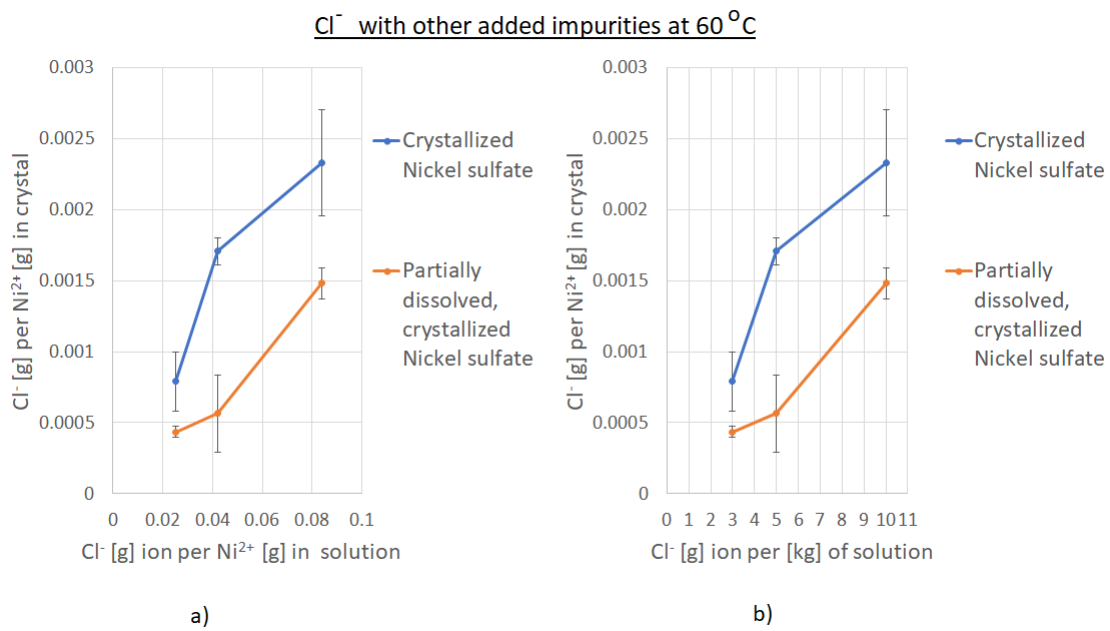


FIGURE 4.16: Cl^- [g] per Ni^{2+} [g] in crystallized $NiSO_4 \cdot 6H_2O$ plotted against Cl^- concentration of the solution before crystallization at 60°C in the presence of Na^+ and Mg^{2+} as other deliberately added impurities. Plot a) and b) display the same information, but use different units on the x-axis.

suggests that the concentration of Cl^- which is left in the crystal after partial dissociation was not evenly distributed.

4.4.3 Cl^- at 60°C with equal proportions of Na^+ and Mg^{2+}

Figure 4.16 displays the concentration of Cl^- in crystallized $NiSO_4 \cdot 6H_2O$ from aqueous solution containing 3, 5 and 10 grams of Cl^- in the presence of Na^+ and Mg^{2+} as deliberately added impurities at 60°C. This figure shows the same information as figure 4.6 and 4.10, but with the focus on Cl^- , undissolved and partially dissociated. Figure 4.16 shows a Cl^- decrease in concentration after partial dissociation at all concentration levels. As seen in plot a), the concentration of Cl^- is much lower in the crystal than in the solution, which suggests it is favored to stay dissolved in a supersaturated solution. There is some spread in the values of undissolved Nickel sulfate, which indicates that there is an uneven distribution of concentration in the crystal bulk of the solution, particularly for 10g/kg Cl^- . The spread is significantly reduced after partial dissociation which suggests that the portion of the crystal bulk which was dissolved and filtered away contained the bulk of the Cl^- concentration, and that the portion of the crystal bulk after partial dissociation

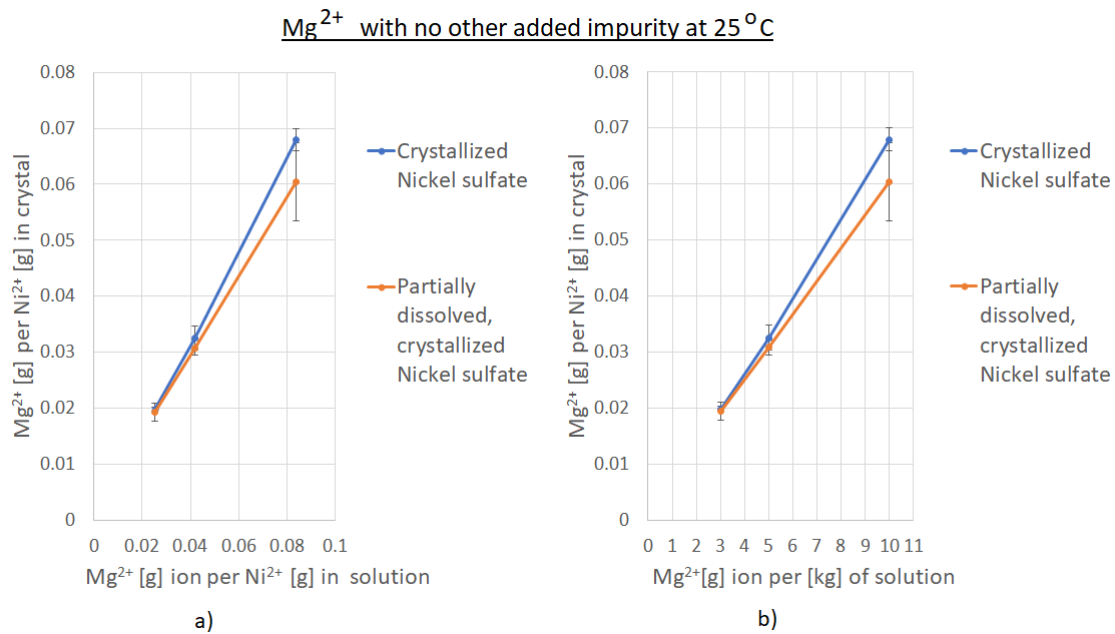


FIGURE 4.17: Concentration of solution before crystallization plotted against Na^+ [g] per Ni^{2+} [g] in crystallized $NiSO_4 \cdot 6H_2O$ at 25 °C with no other deliberately added impurity. Plot a) and b) display the same information, but use different units on the x-axis.

contains an evenly distributed concentration of Cl^- . The weight percentage of Na^+ before and after partial dissolution in this series of experiments can be seen in table 4.5.

4.5 Mg^{2+} as a crystallization impurity on Nickel sulfate

4.5.1 Mg^{2+} at 25 °C

Figure 4.17 displays the concentration of Mg^{2+} in crystallized $NiSO_4 \cdot 6H_2O$ from aqueous solution containing 3, 5 and 10 grams of Mg^{2+} in the presence no other deliberately added impurities at 25 °C. Figure 4.17 shows a Cl^- ear decrease in concentration after partial dissociation at all concentration levels. As seen in plot a), the concentration of Mg^{2+} in the crystal is nearly as high as and increases nearly linearly to the concentration in the solution, which suggests it is favored to move to the crystal surface in a supersaturated solution. The weight percentage of Mg^{2+} before and after partial dissociation in this series of experiments can be seen in table 4.3. There is some spread in the values of both undissolved and partially dissolved $NiSO_4 \cdot 6H_2O$, which indicates that there is an uneven distribution of concentration

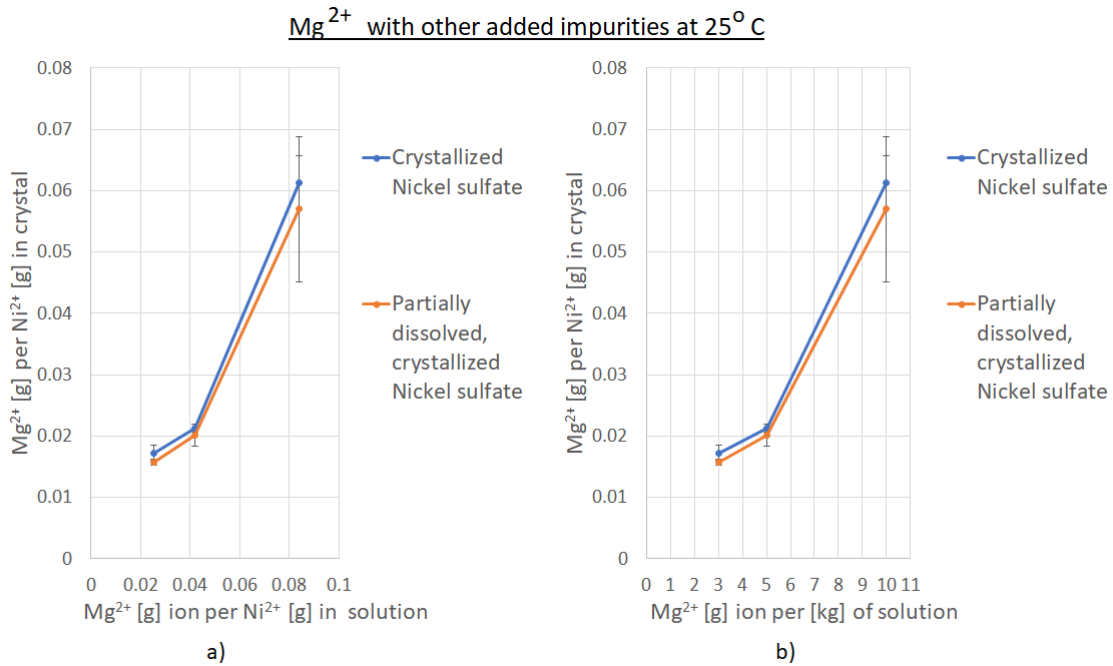


FIGURE 4.18: Concentration of solution before crystallization plotted against Na^+ [g] per Ni^{2+} [g] in crystallized $NiSO_4 \cdot 6H_2O$ at 25°C with no other deliberately added impurity. Plot a) and b) display the same information, but use different units on the x-axis.

in the crystal bulk. This variation is not reduced after partial dissociation which suggests the portion of the crystal bulk which was dissolved and filtered away contained nearly the same concentration of Mg^{2+} .

4.5.2 Mg^{2+} at 25°C with equal proportions of Na^+ and Cl^-

Figure 4.18 displays the concentration of Mg^{2+} in crystallized $NiSO_4 \cdot 6H_2O$ from aqueous solution containing 3, 5 and 10 grams of Mg^{2+} in the presence of Na^+ and Mg^{2+} as deliberately added impurities at 25°C. This figure shows the same information as figure 4.1 and 4.2, but with the focus on Mg^{2+} , undissolved and partially dissociated. Figure 4.18 shows a Cl^- ear decrease in concentration after partial dissociation at all concentration levels. As seen in plot a), the concentration of Mg^{2+} in the crystal is nearly as high as and increases nearly linearly to the concentration in the solution, which suggests it is favored to move to the crystal surface in a supersaturated solution. There is spread in the values of both undissolved and partially dissolved $NiSO_4 \cdot 6H_2O$, which indicates that there is an uneven distribution of concentration in the crystal bulk. This variation is not reduced after partial dissociation which suggests the portion of the crystal bulk which was dissolved and filtered away contained nearly the same concentration of Mg^{2+} . The weight percentage of Mg^{2+}

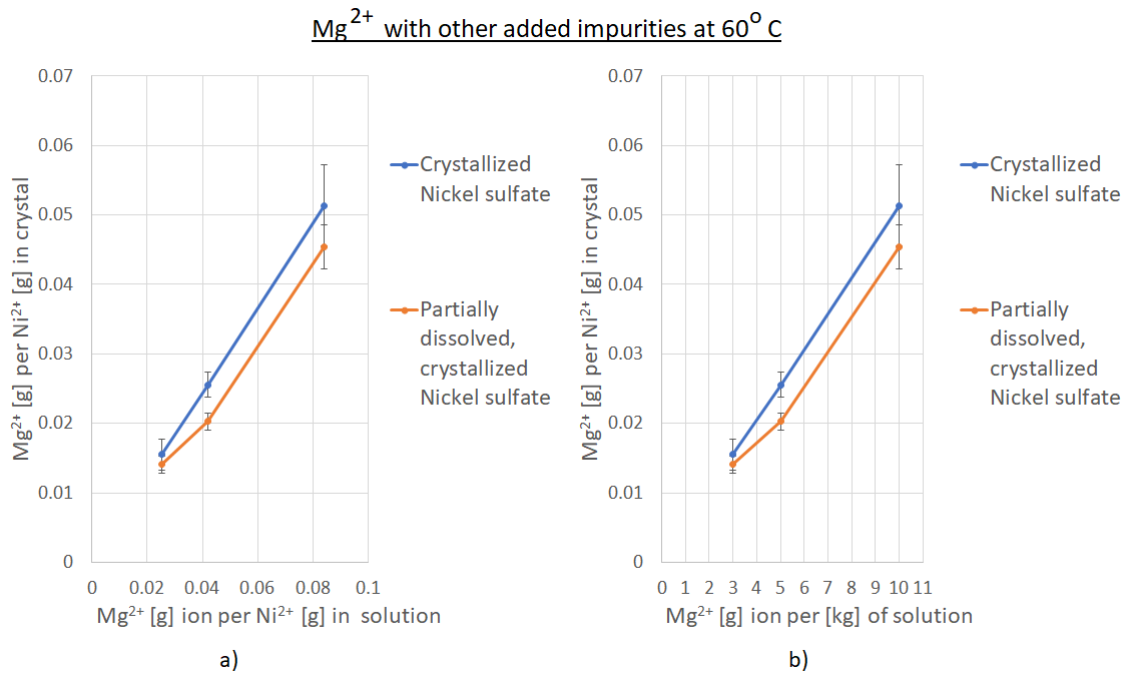


FIGURE 4.19: Concentration of solution before crystallization plotted against Na^+ [g] per Ni^{2+} [g] in crystallized $NiSO_4 \cdot 6H_2O$ at 25°C with no other deliberately added impurity. Plot a) and b) display the same information, but use different units on the x-axis.

before and after partial dissolution in this series of experiments can be seen in table 4.4.

4.5.3 Mg²⁺ at 60°C with equal proportions of Na⁺ and Cl⁻

Figure 4.19 displays the concentration of Mg^{2+} in crystallized $NiSO_4 \cdot 6H_2O$ from aqueous solution containing 3, 5 and 10 grams of Mg^{2+} in the presence of Na^+ and Mg^{2+} as deliberately added impurities at 60°C. This figure shows the same information as figure 4.6 and 4.10, but with the focus on Mg^{2+} , undissolved and partially dissociated. Figure 4.19 shows a clear decrease in concentration after partial dissociation at all concentration levels. As seen in plot a), the concentration of Mg^{2+} in the crystal is nearly as high as and increases nearly linearly to the concentration in the solution, which suggests it is favored to move to the crystal surface in a supersaturated solution. There is some spread in the values of both undissolved and partially dissolved $NiSO_4 \cdot 6H_2O$, which indicates that there is an uneven distribution of concentration in the crystal bulk. This variation is not reduced after partial dissociation which suggests the portion of the crystal bulk which was dissolved and

TABLE 4.1: Induction times for experiments at 25°C at intervals of 20 seconds

Solution concentration	Induction time [s]
No impurity	60
3g/kg Na^+	80
5g/kg Na^+	80
10g/kg Na^+	80
3g/kg Cl^-	80
5g/kg Cl^-	80
10g/kg Cl^-	80
3g/kg Mg^{2+}	100
5g/kg Mg^{2+}	140
10g/kg Mg^{2+}	260
3g/kg Na^+, Cl^-, Mg^{2+}	100
5g/kg Na^+, Cl^-, Mg^{2+}	140
10g/kg Na^+, Cl^-, Mg^{2+}	260

filtered away contained nearly the same concentration of Mg^{2+} . The weight percentage of Mg^{2+} before and after partial dissolution in this series of experiments can be seen in table 4.5. The concentration of Mg^{2+} at 60°C is significantly lower than a similar test at 25°C as seen in figure 4.18, which seems to suggest that Mg^{2+} is more active in lower temperatures.

4.6 Impurities and induction time estimations

The induction time of Nickel sulfate in the presence of impurities are shown in table 4.1. The Heat of crystallization at 60°C was not always detected at 60°C, so only tests at 25°C are recorded. Magnesium seems to greatly slow the crystal growth process to the point where the onset of crystallization is delayed by up to three minutes at higher concentrations.

4.7 Impurity uptake and crystal purity

The impurity uptake of every test is shown in tables 4.3, 4.4, and 4.5 as weight percentage. The tables also display the percentage crystal purity from each test. The

crystal purity is over 98% in every single experiment. The impurity content peak level is from 10g/kg of Na^+ , Cl^- and Mg^{2+} at 60°C at 1.573%.

4.7.1 Impurity uptake rate

Comparing the concentration of impurities in the solution to the crystals predicts the behaviour of impurities. Impurities with a low uptake rate like Cl^- and Na^+ have a low effect on the solubility and crystal growth of Nickel sulfate. Impurities with a high uptake rate such as Mg^{2+} also has a significant effect on the solubility and crystal growth of Nickel sulfate. impurity uptake rates from each experiment are shown in table 4.2.

4.8 XRD results

The XRD diagrams in Appendix D seem to indicate that the vast majority of each sample is $NiSO_4 * 6H_2O$. The impurity content of precipitated $NiSO_4 * 6H_2O$ salts is caused by the adsorption of impurity ions in solution. The mechanisms for how this happens is either lattice integration, where a foreign ion incorporates itself into the crystal matrix, or adsorption, where a foreign compound adheres on a growing face of a crystal. The uptake mechanism, physical absorption or chemical adsorption can be identified by XRD patterns. If other compounds were adhered to the crystal face of $NiSO_4 * 6H_2O$, then XRD would be able to detect it. The XRD pattern from a test containing 10g/kg of Na^+ , Cl^- and Mg^{2+} is compared to XRD patterns from compounds such as $NaCl$, Na_2SO_4 , $MgCl_2$, $MgSO_4$ or $NiCl_2$. The XRD diagrams on display in figure 4.20 shows the sample in black, with an overlay of the XRD pattern of Magnesium sulfate in blue.

4.9 Results from the solubility tests

Figure 4.21 indicates a decrease in solubility of Nickel sulfate in water in the presence of deliberately added sulfuric acid. The reason for the large decrease in solubility at 75°C is as a result of poor temperature control on the Büchner funnel. This caused the hot Nickel sulfate solution to crystallize on contact with it, which increases the amount of $NiSO_4 * 6H_2O$ forced out of solution. The temperature control of the

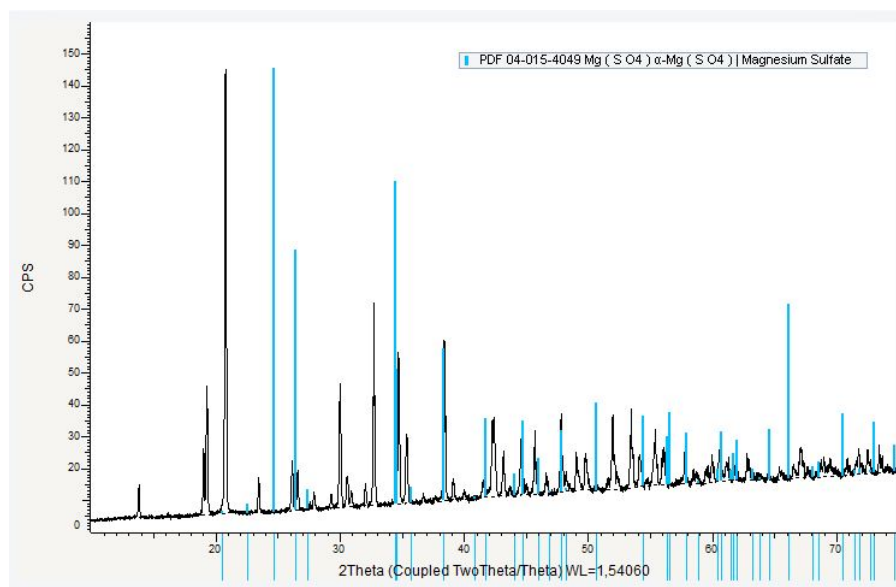


FIGURE 4.20: XRD pattern of $NiSO_4 \cdot 6H_2O$ crystallized from a supersaturated solution at $25^\circ C$ with deliberately added impurities of 10 g/kg of Na^+ , Cl^- , and Mg^{2+} overlaid with the XRD pattern of Magnesium sulfate

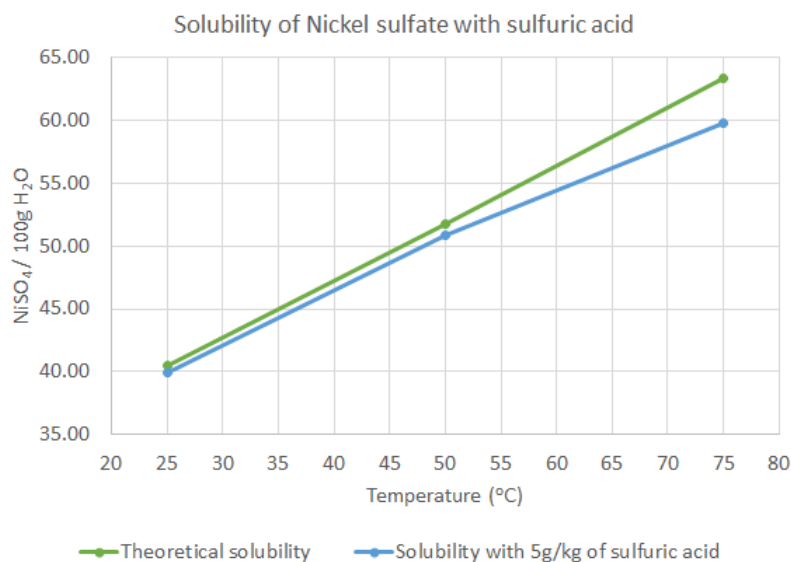


FIGURE 4.21: Solubility of aqueous Nickel sulfate with deliberately added 5g/kg of sulfuric acid (H_2SO_4) at 25, 50 and $75^\circ C$ plotted alongside theoretical solubility of Nickel sulfate with no impurities.

Büchner funnel can be described in sections 3.3 and 3.5. The exact solubility values can be found in figure B.5.

4.10 Crystal yields of crystallization experiments

Table 4.6 and figures 4.22 and 4.23 show how the solution conditions affect the solubility and resulting crystal yield of $NiSO_4 \cdot 6H_2O$. Several trends are easy to establish, Na^+ might decrease the solubility, Cl^- may increase the solubility, and Mg^{2+} may decrease the solubility dramatically. However, it is not that simple. Observations like these can be misleading. The ions are not added to the solution alone, rather as a salt, which means that a counter ion is added as well. An addition of Cl^- , for example, is accompanied by Ni^{2+} in the salt Nickel chloride, $NiCl_2$. An addition of Na^+ and Mg^{2+} is accompanied by SO_4^{2-} . Thus, the effects of both ions must be taken into account when considering solubility changes. The common ion effect states that an addition of a common ion to a main salt has a salting out effect on that salt. Such as an addition of Ni^{2+} or SO_4^{2-} to a solution of Nickel sulfate has a salting out effect on that salt. Diverse ions have the opposite effect, a salting in effect, increasing the solubility of the main salt. The combined effects of ion and counter ion is seen in figures 4.22 at 25°C and 4.23. The exact compositions which lead to the following crystal yields are shown in Appendix A.

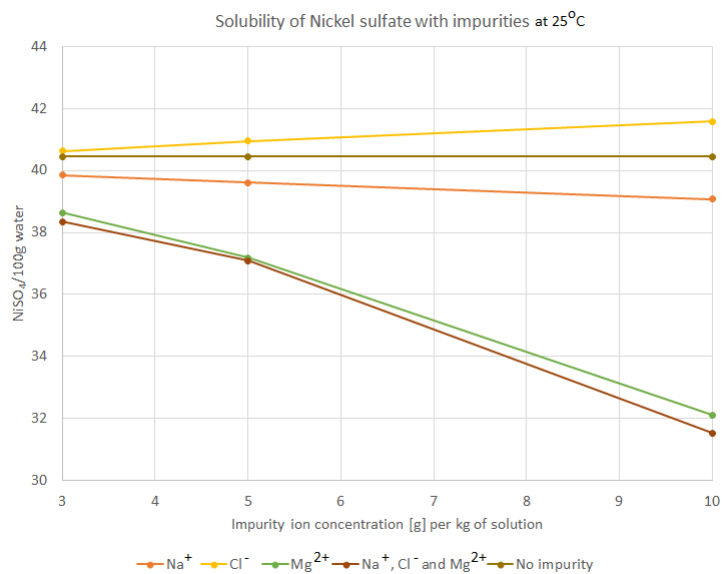


FIGURE 4.22: Solubility of aqueous Nickel sulfate at 25°C with various impurities at different concentration. The saturation solubility at 25°C is shown for reference.

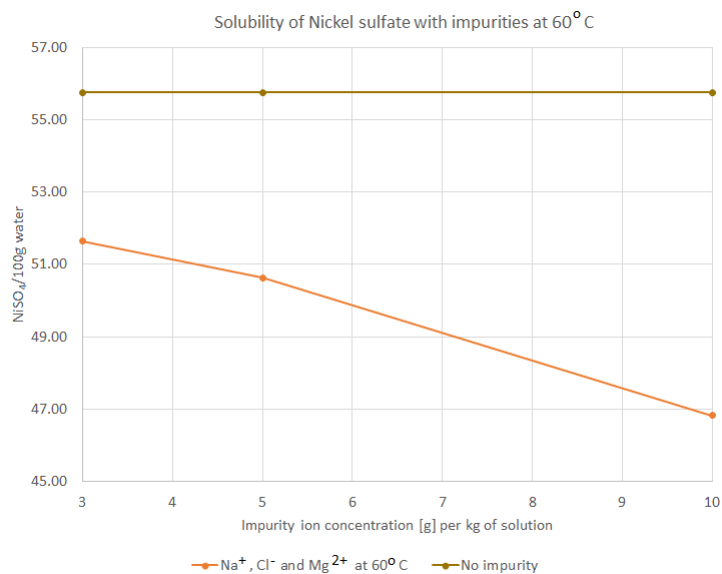


FIGURE 4.23: Solubility of aqueous Nickel sulfate at 60°C with various impurities at different concentration. The saturation solubility at 60°C is shown for reference.

TABLE 4.2: Percentage impurity uptake rate from concentration in solution to crystal (slope of plot a) in figures 4.1 to 4.19. If the solution concentration has "(PD)" following it, then the crystals are **partially dissociated**.

Solution concentration	[Na ⁺] [%]	[Cl ⁻] [%]	Mg ²⁺ [%]
3g/kg Na ⁺	5.97		
5g/kg Na ⁺	5.08		
10g/kg Na ⁺	5.16		
3g/kg Na ⁺ (PD)	0.78		
5g/kg Na ⁺ (PD)	0.69		
10g/kg Na ⁺ (PD)	1.55		
3g/kg Cl ⁻		4.16	
5g/kg Cl ⁻		4.13	
10g/kg Cl ⁻		7.37	
3g/kg Cl ⁻ (PD)		1.38	
5g/kg Cl ⁻ (PD)		0.97	
10g/kg Cl ⁻ (PD)		1.35	
3g/kg Mg ²⁺			78.79
5g/kg Mg ²⁺			77.49
10g/kg Mg ²⁺			81.01
3g/kg Mg ²⁺ (PD)			76.93
5g/kg Mg ²⁺ (PD)			73.45
10g/kg Mg ²⁺ (PD)			72.00
3g/kg Na ⁺ , Cl ⁻ , Mg ²⁺	9.99	7.64	68.81
5g/kg Na ⁺ , Cl ⁻ , Mg ²⁺	2.93	1.03	50.61
10g/kg Na ⁺ , Cl ⁻ , Mg ²⁺	5.42	1.60	73.13
3g/kg Na ⁺ , Cl ⁻ , Mg ²⁺ (PD)	1.68	1.31	62.66
5g/kg Na ⁺ , Cl ⁻ , Mg ²⁺ (PD)	0.40	0.63	47.95
10g/kg Na ⁺ , Cl ⁻ , Mg ²⁺ (PD)	3.05	0.57	67.91
3g/kg Na ⁺ , Cl ⁻ , Mg ²⁺ at 60°C	17.39	3.13	61.63
5g/kg Na ⁺ , Cl ⁻ , Mg ²⁺ at 60°C	18.04	4.07	60.94
10g/kg Na ⁺ , Cl ⁻ , Mg ²⁺ at 60°C	20.00	2.78	61.19
3g/kg Na ⁺ , Cl ⁻ , Mg ²⁺ at 60°C (PD)	2.47	1.73	55.86
5g/kg Na ⁺ , Cl ⁻ , Mg ²⁺ at 60°C (PD)	3.06	1.35	48.35
10g/kg Na ⁺ , Cl ⁻ , Mg ²⁺ at 60°C (PD)	2.71	1.76	54.12

TABLE 4.3: Impurity uptake [weight percentage] in precipitated $NiSO_4 \cdot 6H_2O$ from solutions at 25°C with single, varying concentrations of Na^+ , Cl^- or Mg^{2+} . If the solution concentration has "(PD)" following it, then the crystals are **partially dissociated**.

Solution concentration	Na^+ [wt%]	Cl^- [wt%]	Mg^{2+} [wt%]	Total uptake [wt%]	Crystal purity [wt%]
3g/kg Na^+	0.034			0.034	99.966
5g/kg Na^+	0.048			0.048	99.952
10g/kg Na^+	0.097			0.097	99.903
3g/kg Na^+ (PD)	0.004			0.004	99.996
5g/kg Na^+ (PD)	0.006			0.006	99.994
10g/kg Na^+ (PD)	0.029			0.029	99.971
3g/kg Cl^-		0.023		0.023	99.977
5g/kg Cl^-		0.039		0.039	99.961
10g/kg Cl^-		0.138		0.138	99.862
3g/kg Cl^- (PD)		0.008		0.008	99.992
5g/kg Cl^- (PD)		0.009		0.009	99.991
10g/kg Cl^- (PD)		0.025		0.025	99.975
3g/kg Mg^{2+}			0.443	0.443	99.557
5g/kg Mg^{2+}			0.726	0.726	99.274
10g/kg Mg^{2+}			1.518	1.518	98.482
3g/kg Mg^{2+} (PD)			0.432	0.432	99.568
5g/kg Mg^{2+} (PD)			0.688	0.688	99.312
10g/kg Mg^{2+} (PD)			1.349	1.349	98.651

TABLE 4.4: Impurity uptake [weight percentage] in precipitated $NiSO_4 \cdot 6H_2O$ from solutions at 25°C with 3, 5 and 10 g/kg of solution of Na^+ , Cl^- and Mg^{2+} . If the solution concentration has "(PD)" following it, then the crystals are **partially dissociated**.

Solution concentration	Na^+ [wt%]	Cl^- [wt%]	Mg^{2+} [wt%]	Total uptake [wt%]	Crystal purity [wt%]
3g/kg Na^+ , Cl^- , Mg^{2+}	0.056	0.043	0.386	0.485	99.515
5g/kg Na^+ , Cl^- , Mg^{2+}	0.027	0.010	0.474	0.511	99.489
10g/kg Na^+ , Cl^- , Mg^{2+}	0.102	0.030	1.370	1.502	98.498
3g/kg Na^+ , Cl^- , Mg^{2+} (PD)	0.009	0.007	0.352	0.369	99.631
5g/kg Na^+ , Cl^- , Mg^{2+} (PD)	0.004	0.006	0.449	0.459	99.541
10g/kg Na^+ , Cl^- , Mg^{2+} (PD)	0.057	0.011	1.273	1.340	98.660

TABLE 4.5: Impurity uptake [weight percentage] in precipitated $NiSO_4 \cdot 6H_2O$ of experiments at 60°C with 3, 5 and 10 g/kg of solution of Na^+ , Cl^- and Mg^{2+} . If the solution concentration has "(PD)" following it, then the crystals are **partially dissociated**.

Solution concentration	Na^+	Cl^-	Mg^{2+}	Total uptake	Crystal purity
	[wt%]	[wt%]	[wt%]	[wt%]	[wt%]
3g/kg Na^+ , Cl^- , Mg^{2+}	0.098	0.018	0.346	0.462	99.538
5g/kg Na^+ , Cl^- , Mg^{2+}	0.169	0.038	0.571	0.778	99.222
10g/kg Na^+ , Cl^- , Mg^{2+}	0.375	0.052	1.147	1.573	98.427
3g/kg Na^+ , Cl^- , Mg^{2+} (PD)	0.014	0.010	0.314	0.338	99.662
5g/kg Na^+ , Cl^- , Mg^{2+} (PD)	0.029	0.013	0.453	0.494	99.506
10g/kg Na^+ , Cl^- , Mg^{2+} (PD)	0.051	0.033	1.014	1.098	98.902

TABLE 4.6: Crystal yields from crystallization experiments

Solution condition	$NiSO_4 \cdot 6H_2O$ in	$NiSO_4 \cdot 6H_2O$ out
	[g]	[g]
No added impurities	350.16	61.55
3g/kg Na^+ at 25°C	350.16	63.12
5g/kg Na^+ at 25°C	350.16	65.54
10g/kg Na^+ at 25°C	350.16	70.79
3g/kg Cl^- at 25°C	350.16	55.34
5g/kg Cl^- at 25°C	350.16	52.12
10g/kg Cl^- at 25°C	350.16	45.66
3g/kg Mg^{2+} at 25°C	350.16	75.03
5g/kg Mg^{2+} at 25°C	350.16	89.31
10g/kg Mg^{2+} at 25°C	350.16	135.98
3g/kg Na^+ , Cl^- , Mg^{2+} at 25°C	350.16	77.95
5g/kg Na^+ , Cl^- , Mg^{2+} at 25°C	350.16	90.44
10g/kg Na^+ , Cl^- , Mg^{2+} at 25°C	350.16	140.06
3g/kg Na^+ , Cl^- , Mg^{2+} at 60°C	179.83	48.08
5g/kg Na^+ , Cl^- , Mg^{2+} at 60°C	179.83	55.79
10g/kg Na^+ , Cl^- , Mg^{2+} at 60°C	179.83	86.40

Chapter 5

Discussion

5.1 Interpretation of Results

5.1.1 The Structure of the solution

When Nickel sulfate hexahydrate, $NiSO_4 \cdot 6H_2O$, and various added impurities are dissociated in water to become an aqueous electrolyte solution, several different species can be found: the cations, the anions and the water molecules. It is, however, useful to define how those ions exist in solution in order to understand the structure of how the solution exists. The solution consists of the following: the Nickel aquo complex ($[Ni(H_2O)_6]^{2+}$), the Sodium aquo complex ($[Na(H_2O)_6]^+$), the Magnesium aquo complex ($[Mg(H_2O)_6]^{2+}$), the hydronium ion: H_3O^+ , the hydroxide ion: OH^- , water (H_2O), the sulfate ion (SO_4^{2-}), and the Chloride ion (Cl^-).

Cations exist as metal aquo complexes, as described in section 2.2.1. Anions exist on their own without hydrolysis or solvation shells, the exception to this is hydrogen sulfate (HSO_4^-) which is the conjugate base of sulfuric acid, which will hydrolyze water to increase the pH of solution. OH^- and Cl^- are structure breakers, and SO_4^{2-} is a structure former. The interactions which are possible in the system include ion-ion, water-water and water-ion. Each of the above ions behave differently in aqueous solution as a result of physical properties shown in table 5.1.

5.1.2 Structure formers and structure breakers

The behaviour of electrolytes in aqueous solution can be determined by thermodynamics, specifically by studying the enthalpy of hydration, H_{hyd} , and entropy of hydration, S_{hyd} . These two quantities reveal a lot about how electrolytes behave in undersaturated and supersaturated states. H_{hyd} refers to the energy released as an ion is dissolved, and conversely to the strength of the water-ion bond. As can be

seen from table 5.1, ionic radius has a positive correlation to H_{hyd} . Ionic radius is strongly linked to the amount of valence electrons an ion, generally, the fewer valence electrons, the smaller the ionic radius, indicating a strong H_{hyd} . The greater the positive charge on a metal cation, the easier it is for a proton to dissociate for an attached water molecule. Thus, in general, interactions between the ion and water molecules gets stronger as the size of the ion and the number of electrons in the outer shell decreases. This is observed in table 5.1. Therefore, the presence of small ions in the solution has a greater tendency for interaction with water molecules than larger ions. The relation between H_{hyd} and metal-oxygen bond (of a water molecule) is shown in equation 5.1.

$$\Delta H_{hyd} = \frac{-69500z^2}{r_{M-O}} \quad (5.1)$$

Where

ΔH_{hyd} = enthalpy of hydration

z = charge of ion

r_{M-O} = metal-oxygen distance

S_{hyd} of each individual electrolyte is a quantity that stems from the number of accessible hydrated states at a given temperature. Accessible hydrated states of an ion refers to the accessible internal degrees of freedom associated with hydration. S_{hyd} of a system controls how ordered the structure of a solution is. For instance, the more negative S_{hyd} gets, the more ordering is in the forming of the metal aquo complex for metal cations. Metals with a more positive S_{hyd} suggest that the first and second solvation shells are somewhat undefined, whereas a very negative S_{hyd} suggests very ordered hydrated states. This data is contained in table 5.1 for the ions encountered in the solutions and some other commonly seen in the industry. If S_{hyd} of an electrolyte has a more negative value (more charged) then it is a *structure former*. If the entropy of an electrolyte is less negative (less charged) then it is a *structure breaker*. The ionic radius is also a deciding factor for the behaviour of electrolytes, where a smaller ionic radius indicates a larger tendency for the electrolyte to be a structure former, and a large ionic radius indicating a structure breaker. The ionic radius is particularly important in the behaviour of cations (Jibbouri, 2002).

Structure breakers and structure formers behave differently in solution. This can explain the reason for uneven uptake of impurities in $NiSO_4 \cdot 6H_2O$ as seen in tables 4.3, 4.4, and 4.5. In a supersaturated solution of Nickel sulfate, ions with a highly

TABLE 5.1: Physical properties of cations and anions at 298K (Jibbouri, 2002)

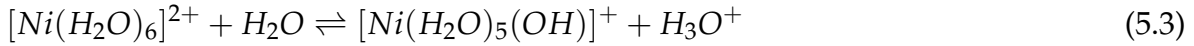
Ion	Ionic Radius	H_{hyd}	S_{hyd}	G_{hyd}
	Å	[H_{hyd}]	[$KJ.mol^{-1}K^{-1}$]	[$KJ.mol^{-1}$]
H_3O^+	(-)	-1129	-131	-1090
Na^+	0.95	-444	-110	-411
K^+	1.33	-360	-74	-338
Fe^{2+}	0.76	-2305	-383	-2191
Mg^{2+}	0.65	-1999	-311	-1906
Ni^{2+}	0.72	-2490	-396	-2372
Pb^{2+}	1.2	-1785	-228	-1717
Cl^-	1.81	-340	-76	-340
OH^-	1.4	-423	-149	-379
SO_4^{-2}	1.5	-1145	-263	(-)

negative S_{hyd} , like Ni^{2+} and Mg^{2+} , will move towards the crystal surface and adsorb because they are structure formers in relation to the other electrolytes. In supersaturated solutions structure breakers, like Na^+ and Cl^- tend to move away from the surface, which increases the stability of the solution, increasing the solubility of Nickel sulfate.

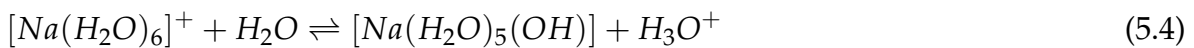
In unsaturated solution, structure formers like Mg^{2+} and Ni^{2+} will leave the crystal surface and spread into the solution, this gives the solution stability. Consequently, this also leads to hydrolysis reactions similar to 2.2, 5.2 and 5.3 which produces H_3O^+ ions. H_3O^+ ions destabilize the solution, meaning it decreases the saturation solubility of the Nickel sulfate. The destabilization of H_3O^+ ions is due to the low S_{hyd} which makes it a structure breaker. This decrease in solubility can be seen in table 4.6.



and



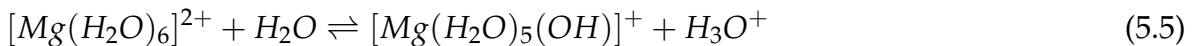
In an aqueous solution of Nickel sulfate, with Na^+ and SO_4^{2-} as impurities, the solubility of $NiSO_4 \cdot 6H_2O$ is affected by both species of ions. As seen in table 5.1, Na^+ has a less negative S_{hyd} ($-110 \text{ KJmol}^{-1}\text{K}^{-1}$), which means it is a structure breaker in comparison to Ni. Structure breakers are favored to move away from the crystal surface in supersaturated solution, which increases the stability of the solution. This explains the low uptake of Na^+ in precipitated $NiSO_4 \cdot 6H_2O$, and the lower concentration Na^+ in crystal than solution as seen in table 4.2. Moving away from the surface during supersaturation also means it has minimal effect on the crystal growth rate, size and size distribution of precipitated crystals. This can be seen in SEM photographs. As Na^+ ions are added to a Nickel sulfate solution, the solubility of $NiSO_4 \cdot 6H_2O$ increases. The reason why the solubility of Nickel sulfate increases in the presence of Na^+ is that it is unfavored to undergo hydrolysis (as seen in equation 5.4) because of its much larger radius (0.95\AA) and less negative H_{hyd} (-444 KJmol^{-1}) than Ni. The other reason for the increase in solubility is the diverse-ion effect, which has a salting-in effect on $NiSO_4 \cdot 6H_2O$ as a result of increased ionic strength of the solution. The sulfate ion has a much more negative S_{hyd} ($-263 \text{ KJmol}^{-1}\text{K}^{-1}$) than OH^- , making it a structure former. As SO_4^{2-} ions are added to the solution, the solubility of $NiSO_4 \cdot 6H_2O$ decreases. The combined effects of both Na^+ and SO_4^{2-} on the solubility is a net decrease as seen in table 4.6.



In an aqueous solution of Nickel sulfate, with Cl^- and Ni^{2+} as impurities, the solubility of $NiSO_4 \cdot 6H_2O$ is affected by both species of ions. As seen in table 5.1, Cl^- has a less negative S_{hyd} ($-76 \text{ KJmol}^{-1}\text{K}^{-1}$), which means it is a structure breaker in comparison to SO_4^{2-} . Structure breakers are favored to move away from the crystal surface in supersaturated solution, which increases the stability of the solution. This explains the low uptake of Cl^- in precipitated $NiSO_4 \cdot 6H_2O$, and the lower concentration Cl^- in crystal than solution as seen in table 4.2. Moving away from the surface during supersaturation also means it has minimal effect on the crystal growth rate, size and size distribution of precipitated crystals. This can be seen in SEM photographs. As Cl^- ions are added to a Nickel sulfate solution, the solubility

of $NiSO_4 \cdot 6H_2O$ increases. The presence of Cl^- causes a diverse-ion effect, the increase in ionic strength of the solution causes a salting-in effect which increases the solubility of $NiSO_4 \cdot 6H_2O$. The addition of more Ni^{2+} ions will decrease the solubility of Nickel sulfate as a result of the common ion effect. The combined effects of both Cl^- and an excess Ni^{2+} on the solubility is a net increase as seen in table 4.6.

In an aqueous solution of Nickel sulfate, with Mg^{2+} and SO_4^{2-} as impurities, the solubility of $NiSO_4 \cdot 6H_2O$ is affected by both species of ions. As seen in table 5.1, Mg^{2+} has a highly negative S_{hyd} ($-311 \text{ KJmol}^{-1}\text{K}^{-1}$), which means it should act as a structure breaker in relation to Ni, but since it has a slightly smaller ionic radius that it acts as a structure former. Structure formers are favored to move towards from the crystal surface in supersaturated solution, which decreases the stability of the solution. This explains the high uptake of Mg^{2+} in precipitated $NiSO_4 \cdot 6H_2O$, and the nearly equal concentration of Mg^{2+} in crystal than solution as seen in table 4.2. Being drawn to the surface during supersaturation also means it decreases the crystal growth rate, size and size distribution of precipitated crystals. This can be seen in SEM photographs. The slowed down growth rate can be observed by induction rate in table 4.1. As Mg^{2+} ions are added to a Nickel sulfate solution, the solubility of $NiSO_4 \cdot 6H_2O$ decreases. The reason why the solubility of Nickel sulfate decreases in the presence of Mg^{2+} is that both Mg^{2+} and Ni^{2+} compete to undergo hydrolysis (as seen in equation 5.5) because of its slightly smaller radius (0.65\AA) and slightly more positive H_{hyd} (-1999 KJmol^{-1}) than Ni. The sulfate ion has a much more negative S_{hyd} ($-263 \text{ KJmol}^{-1}\text{K}^{-1}$) than OH^- , making it a structure former. As SO_4^{2-} ions are added to the solution, the solubility of $NiSO_4 \cdot 6H_2O$ decreases. The combined effects of both Mg^{2+} and SO_4^{2-} result in a dramatic decrease on the solubility as seen in table 4.6.



In brief summary, in a solution of aqueous Nickel sulfate, the impurity electrolytes mentioned above behave in the following way:

- Na^+ is a structure breaker.
- Cl^- is a structure breaker.
- H_3O^+ is a structure breaker.

- OH^- is a structure breaker.
- Mg^{2+} is a structure former.
- excess Ni^{2+} is a structure former.
- excess SO_4^{2-} is a structure former.

The impurities Na^+ , Cl^- and Mg^{2+} do not have a linear/additive effect despite being in equal concentration. In an aqueous solution of Nickel sulfate, with Mg^{2+} , Na^+ , Cl^- and an excess of Ni^{2+} and SO_4^{2-} as impurities, the solubility of $NiSO_4 * 6H_2O$ is affected by all ion species, but some more than others. As seen in table 5.1 and discussed in the previous paragraphs, each electrolyte has an effect on the structure of a Nickel sulfate solution. The net effect of all impurities, as seen in table 4.6 is a massive decrease in overall solubility. The solubility of the solution, as well as the impurity uptakes, as seen in tables 4.4 and 4.5 and figures 4.22 and 4.23, is controlled by the presence of Mg.

5.1.3 XRD diagram discussion

As seen in the XRD diagrams D.1 to D.5 in Appendix D.1, none of the possible compounds which can co-crystallize on $NiSO_4 * 6H_2O$ are seen in the XRD diagram. The most likely compound to co-crystallize with $NiSO_4 * 6H_2O$ is Magnesium sulfate, due to the high content of Magnesium. As seen in figure 4.20, none of the main peaks coincide, which suggests the compound is not present. The crystal purity levels and XRD diagrams suggests that the vast majority of every sample is $NiSO_4 * 6H_2O$ despite coming from tainted solutions. It is possible, of course, that a separate compound is co-crystallized alongside $NiSO_4 * 6H_2O$, but this would only account for a maximum of 1.502% of the mass. 1.502% is the impurity content in one of the least pure tests, 10g/kg of all three impurities at 25°C. This is seen in table 4.4. Despite this, every major peak belongs to $NiSO_4 * 6H_2O$. No other XRD diagram was compared to other compounds. All XRD diagrams are in appendix D.

5.1.4 SEM photographs discussion

There are few general trends which can be seen from the SEM photographs. Tests at 60°C generally have softer, less jagged surfaces than tests at 25°C. This can most likely be attributed to the setups used. The crystallization experiments at 25°C were

done using a hard metal impeller, which most probably lead to more forceful crystal-impeller and crystal-crystal collisions during crystal growth. This most probably caused greater trauma to the crystals than the a plastic coated magnetic stirrer as was used at 60°C. Na^+ and Cl^- , as a result of their minimal uptake, have a minimal effect on the crystal size. Comparisons of SEM photographs of seeds, containing no impurities, (such as in figure 3.1 and precipitated crystals from solutions contaminated with Na^+ and Cl^- (such as in figures E.1 and E.4 reveal no changes. Crystals with Mg^{2+} content do not show any noticeable difference on the structure of the crystals either, this can be seen in SEM photos E.7a, E.8a and E.9a. With the higher uptake of Mg^{2+} , a change in crystal habit or size is expected, so the similar crystal size to other tests may be a result of breakage from too forceful declumping.

5.1.5 Effects of pH on the saturation solubility of ionic compounds

The solubility of $NiSO_4 \cdot 6H_2O$ is expected to change as a result of the added sulfuric acid and resulting pH decrease. The solubility experiments shown in figure 4.21 indicate a solubility decrease as a result of added sulfuric acid. This can be explained by the following methodology: the dissociation of an H^+ ion from a water molecule will have an effect on the structure of the solution. Lets consider a saturated solution of Nickel sulfate with deliberately added Mg^{2+} cations. The hydration of a Mg^{2+} ion, will increase the concentration of H_3O^+ in the solution. This is shown in the equilibrium hydrolysis reaction of the Magnesium aquo complex shown in equation 5.5 and. The increased concentration of H_3O^+ in solution will have an effect on the position of the equilibrium of the equation according to Le Chatelier's principle. Le Chatelier's principle states: the position of a chemical equilibrium will always shift in the direction that tends to counteract the effect of an applied change. Thus, an addition of H_3O^+ causes the equilibrium of the chemical reaction in equation 5.5 and 5.2 to shift towards the reactants (to the left). This means that the solubility of the Nickel sulfate will decrease because the addition of H_3O^+ ions discourage Nickel ions to undergo hydrolysis, i.e. a lower pH will decrease the solubility of Nickel sulfate. The solubility decrease of Nickel sulfate after an impurity is added is partly a result of the associated pH change. The pH can, of course, also decrease by adding an acid to the Nickel sulfate solution, as is the case in figure 4.21. (Jibbouri, 2002; Mullin, 2001).

The behaviour of hydronium ions are interesting because they function in two conflicting ways. Their presence decreases the solubility of $NiSO_4 \cdot 6H_2O$ due to the

shift in equilibrium in equation 5.3, which discourages the Ni^{2+} ion to undergo hydrolysis. But they are also structure breakers because of its less negative S_{hyd} in comparison to Ni^{2+} which means they stabilize the solution, increasing the solubility. Nonetheless, the net effect of adding hydronium ions to the solution of Nickel sulfate is a decrease in solubility as seen in figure 4.21. It must be mentioned, however, that this decrease in solubility is a result of adding sulfuric acid, which means it is also partly due to the addition of sulfate ions which is a structure former, which also decreases the solubility when added (Jibbouri, 2002).

5.1.6 Impurities' effect on each other

It does not seem like Na^+ , Cl^- and Mg^{2+} influence each others behaviour. A structure breaker may act like a structure former, only if it has a more negative S_{hyd} or smaller ionic radius than the other electrolytes. A structure former may behave like a structure breaker only if an electrolyte with a more negative S_{hyd} or smaller ionic radius is introduced to the system. As seen in table 5.1, Ni^{2+} already has the most negative entropy and H_{hyd} of the cations and SO_4^{2-} has the most negative H_{hyd} and entropy of the anions, therefore the Na^+ , Cl^- and Mg^{2+} do not affect the behaviour of the other impurities in any significant way. This is substantiated by the fact that the uptake of Na^+ , Cl^- and Mg^{2+} vary only slightly when all are combined or alone in solution.

An addition of hydroxide (OH^-) ions would increase the pH as a result of neutralization of H^3O^+ . As a consequence, the equilibrium of equation 2.2 to the right, which has the opposite effect, increasing the solubility of the main salt (Jibbouri, 2002).

5.2 Effectiveness of the partial filtration method

The purpose of the partial filtration method was to physically remove the outer portion of the crystal mass by partially dissolving the crystal, then filtrating it away, in order investigate its effectiveness at removing impurities. By referring to the results and the list in 3.4.1, the following observations can be made.

The concentration of Na^+ is reduced by the partial filtration in every test, as shown in figures 4.11 to 4.13, which suggests that Na^+ is concentrated in the outer portion of precipitated $NiSO_4 \cdot 6H_2O$ crystals in all tests and solution concentrations. The

TABLE 5.2: The average impurity content across all tests *before* partial filtration, the average impurity content of all tests after partial filtration and the difference from before to after

Solution concentration	Avg. impurity before [wt%]	Avg. impurity after [wt%]	Change [wt%]
Na^+	0.059	0.013	0.046
Na^+ w/ Cl^- , Mg^{2+} at 25°C	0.062	0.023	0.038
Na^+ w/ Cl^- , Mg^{2+} at 60°C	0.214	0.031	0.183
Cl	0.067	0.014	0.053
Cl w/ Na^+ , Mg^{2+} at 25°C	0.028	0.008	0.020
Cl w/ Na^+ , Mg^{2+} at 60°C	0.036	0.018	0.017
Mg	0.896	0.823	0.072
Mg w/ Na^+ , Cl^- at 25°C	0.743	0.691	0.052
Mg w/ Na^+ , Cl^- at 60°C	0.688	0.594	0.094

TABLE 5.3: The percentage of impurity uptake removed by partial filtration for each impurity and the average efficiency of partial filtration for each element across all tests.

Solution concentration	Removal efficiency [%]	Avg. efficiency [%]
Na^+	77.570	74.980
Na^+ w/ Cl^- , Mg^{2+} at 25°C	61.925	
Na^+ w/ Cl^- , Mg^{2+} at 60°C	85.445	
Cl^-	78.928	66.157
Cl^- w/ Na^+ , Mg^{2+} at 25°C	70.997	
Cl^- w/ Na^+ , Mg^{2+} at 60°C	48.545	
Mg^{2+}	8.087	9.596
Mg^{2+} w/ Na^+ , Cl^- at 25°C	6.998	
Mg^{2+} w/ Na^+ , Cl^- at 60°C	13.703	

concentration of Cl^- is reduced by the partial filtration in every test, as shown in figures 4.14 to 4.16, which suggests that Cl^- is concentrated in the outer portion of precipitated $NiSO_4 * 6H_2O$ crystals in all tests and solution concentrations. The concentration of Mg^{2+} is slightly reduced by the partial filtration in every test, as shown in figures 4.17 to 4.19, which suggests that the concentration of Mg^{2+} is more evenly precipitated throughout the bulk of precipitated $NiSO_4 * 6H_2O$ crystals, but slightly more concentrated in the outer portions. This is true for all tests and solution concentrations. The Na^+ content across all tests decreased an average of 74.985% after partial filtration. The Cl^- content decreased by an average of 66.157% across all tests after partial filtration. The concentration of Mg^{2+} is reduced as well, but to a much lesser degree. After partial filtration across all tests, the Mg^{2+} content decreased by an average of 9.5696%. Figures 5.2 and 5.3 display the efficiency rates of partial filtration across all tests for each experiment.

5.2.1 Possible explanations

There are three possible explanations as for why partial filtration is effective against Na^+ and Cl^- but not as effective against Mg.

The first possible explanation is it may have something to do with the structure of the solution. Ions which are attracted to the surface of a growing crystal, such as Mg^{2+} , will be more evenly distributed than ions which are not, this is logical because the crystal surface will attract those ions over the entire duration of the crystal growth process. This constant attraction results in a more even distribution. Na^+ and Cl^- , being structure breakers, are not favored to move to the surface of a growing Nickel sulfate crystal, which means there should be none of them in the crystal lattice. In every test, however, there is a presence of both ions, and in every test, the majority is filtered away by partial filtration. Therefore, Na^+ and Cl^- adsorb to the crystal surface towards the latter stages of the crystal growth process. If the assumption that the outer portions of the crystals are formed in the later stages of supersaturation, when it is on its decline before re-entering the undersaturated state, is true, that may indicate that Na^+ and Cl^- adsorb to the crystal surface at this stage of supersaturation. This is a plausible explanation because a lot of Mg^{2+} and Ni^{2+} will have crystallized already, which leaves less competition for adsorption.

The second possible explanation is that since concentrations of Na^+ and Cl^- are extremely low, which may indicate that even though they are structure breakers and

less favored to move to the crystal surface in a supersaturated solution, some Na^+ and Cl^- ions are forced towards the crystal surface as a product of movement of other ions and intense electrostatic repulsion and end up adsorbed to the crystal surface by chance, which happens to primarily happen on the outer shells of the bulk of the crystal. This makes some sense as a larger crystal is a larger target to get stuck to.

The third possible conclusion is that the concentrations of Na^+ and Cl^- on the outer portions of the crystal surface are a result of traces of solution still adhering to the crystal surface from crystallization and filtration despite washing in ethanol, and drying properly. This does seem unlikely.

Chapter 6

Summary and Conclusion

The investigation of three different impurities on the Nickel sulfate hexahydrate crystallization process formed the basis of this study; the Sodium ion, Na^+ , Chloride ion, Cl^- , and the Magnesium ion, Mg^{2+} . More precisely, Sodium sulfate, Na_2SO_4 , Nickel chloride, $NiCl_2$, and Magnesium sulfate, $MgSO_4$. This is an important distinction because the added counter ions affect Nickel sulfate as well, and together they each have pronounced effects on the crystallization of Nickel sulfate.

Na^+ and Cl^- are forced away from the growing crystal surface during supersaturation because compared to Ni^{2+} and SO_4^{2-} , respectfully, they are structure breakers. Being forced away from the crystal surface during supersaturation mean they have a minimal effect on the crystal growth rate, size, uptake into the lattice matrix and size distribution of precipitated $NiSO_4 \cdot 6H_2O$. Na^+ and Cl^- increase the solubility of Nickel sulfate because they increase the ionic strength of the solution which, through the diverse-ion effect, has a salting-in effect on Nickel sulfate.

Mg^{2+} is attracted to the surface of a growing crystal during supersaturation because along with Ni it is a surface former. Being attracted towards the crystal surface during supersaturation means it has a significant effect on the growth rate, size, uptake into the lattice matrix and size distribution of precipitated $NiSO_4 \cdot 6H_2O$. Mg^{2+} decreases the solubility of Nickel sulfate because being attracted to the crystal surface destabilizes the solution, and Mg^{2+} compete with Ni for hydrolysis of water molecules, which decreases the solubility as well.

It does not seem like Na^+ , Cl^- and Mg^{2+} influence each others behaviour. Ni^{2+} already has the most negative entropy and enthalpy of hydration of the cations and SO_4^{2-} has the most negative enthalpy and entropy of the anions, therefore the impurities do not affect the behaviour of the other impurities in any significant way. This is substantiated by the fact that the uptake of Na^+ , Cl^- and Mg^{2+} vary only slightly

when all are combined or when alone in solution.

Based on the results from ICP-MS shown in the figures and tables contained in chapter 4 and referring to the list in subsection 3.4.1, conclusions can be drawn to enhance our understanding of where Na^+ , Cl^- and Mg^{2+} are likely to be concentrated in the bulk of the $NiSO_4 \cdot 6H_2O$ crystal matrix. By extension, this aids our understanding of the behaviour of those impurities during Nickel sulfate crystallization. The results point to the conclusion that the partial dissociation method is efficient at reducing the concentration of Na^+ and Cl^- in precipitated $NiSO_4 \cdot 6H_2O$, which suggests that Na^+ and Cl^- have a consistently larger presence in the outer portions than in the inner portions of $NiSO_4 \cdot 6H_2O$. Partial dissociation is a less effective method for the removal of Mg, which suggests that the Mg^{2+} content is more evenly distributed in the bulk of the crystal mass, but slightly more concentrated in the outer portions. This conclusion is valid for a range of 3-10 g of Na^+ , Cl^- and Mg^{2+} per kilogram of solution in both 25°C and 60 °C solutions.

The XRD diagrams (shown in Appendix D) indicate that the samples are $NiSO_4 \cdot 6H_2O$. The most likely other compound to co-crystallize with $NiSO_4 \cdot 6H_2O$ is Magnesium sulfate, due to the high $MgSO_4$ content and the only other widely available anion being SO_4^{2-} . The sample used for comparison is 98.5% pure, and judging from various overlays on the XRD diagram, the presence of other compounds is difficult to observe, though it may well be the case.

The SEM photos show no consistent, noticeable differences between precipitated crystals from impurity contaminated solutions and crystals from no impurity. The largest difference is seen from 25°C and 60°C, though this is most probably a consequence of material of impeller used.

An change in pH of an aqueous Nickel sulfate solution affects the solubility because the concentration of hydronium ions has significant control of the hydrolysis reaction of Nickel and water molecules. An increase in pH decreases the solubility and vice versa.

Chapter 7

Recommendation for further work

This study comprises an investigation of the behaviour of Na^+ , Cl^- and Mg^{2+} in supersaturated aqueous solutions of Nickel sulfate. Impurities and pH has been shown to have a significant impact on the solubility of Nickel sulfate based on these behaviours. Partial dissociation has proven to be an effective method for purification of Nickel sulfate hexahydrate for Na^+ and Cl^- , and to a lesser extent, Mg^{2+} .

There are a number of aspects and areas of significance in Nickel sulfate crystallization from contaminated aqueous solution that are of high interest, yet unexplored by this investigation. First and foremost, is an investigation on more process impurities such as Calcium, Ca^{2+} , Potassium, K^+ , and Iron, Fe^{2+} or Fe^{3+} . This is of high interest because in a real industrial setting, there will be more than just three impurities in solution, which all have an effect on Nickel sulfate.

A thorough investigation on seeding and different supersaturation levels may be very interesting. Different seed materials and seeding ratios can have a significant effect on precipitated crystals and may prove to be valuable. Supersaturation levels can also affect the crystal habit and crystal growth of crystals.

Investigations of Nickel sulfate crystallization on a larger scale, perhaps using a continuous stirred-tank reactor or fluidized bed reactor (FBR) may replicate industrial conditions better than a small scale batch reactor. Such setups may also require similar filtration to that used in the industry which would provide valuable information.

Appendix A

Physical Properties of Nickel sulfate

A.0.1 Properties of Nickel sulfate hexahydrate ($NiSO_4 \cdot 6H_2O$)

Nickel sulfate hexahydrate is a green-blue, highly soluble in water, insoluble in ethanol, salt which, historically, has been uninteresting, and only been utilized as a byproduct for other reactions or as a source for Ni^{2+} ions for electroplating. Nickel sulfate is a carcinogen in humans, and highly toxic to the environment. The most common Nickel sulfate salt is the hexahydrate, which crystallizes between 30.7°C and 100°C, below 30.7°C the heptahydrate is crystallized. If Nickel sulfate hydrates are heated above 330°C, the water content of the crystals is destabilized and anhydrous Nickel Sulfate is formed. The crystal structure of Nickel sulfate hexahydrate is tetrahedral, the heptahydrate form is orthorhombic, and the anhydrous form is cubic. The lattice parameters of Nickel sulfate is shown in figure A.1 (Beevers and Lipson, 1932).

The saturation solubility of Nickel sulfate ($NiSO_4$) and its hexahydrate is shown in tables A.1 and A.2 respectively. The values in these tables were calculated using saturation mass percentage of Nickel sulfate in aqueous solution at different temperatures. (Haynes, 2014; Mullin, 2001).

	a (Å)	b (Å)	c (Å)	α	β	γ
Heptahydrate	11.86	12.08	6.81	90°	90°	90°
Hexahydrate	9.88	7.228	24.13	90°	98.38°	90°
Hexahydrate	9.878	7.214	24.065	90°	98.37°	90°

FIGURE A.1: Lattice parameters of Nickel sulfate (Hassanein, 2018; Beevers and Lipson, 1932)

TABLE A.1: The saturation solubility of anhydrous Nickel sulfate in water

[°C]	Mass percentage	$\text{NiSO}_4(\text{g})/\text{g}$ of solution	$\text{NiSO}_4(\text{g})/\text{g}$ of H_2O
0	21.4	0.214	0.272
10	24.4	0.244	0.323
20	27.4	0.274	0.377
25	28.8	0.288	0.404
30	30.3	0.303	0.435
35	31.4	0.314	0.458
40	32.0	0.320	0.471
50	34.1	0.341	0.517
60	35.8	0.358	0.558
70	37.7	0.377	0.605
75	38.8	0.388	0.634
80	39.9	0.399	0.664
90	42.3	0.423	0.733
100	44.8	0.448	0.812

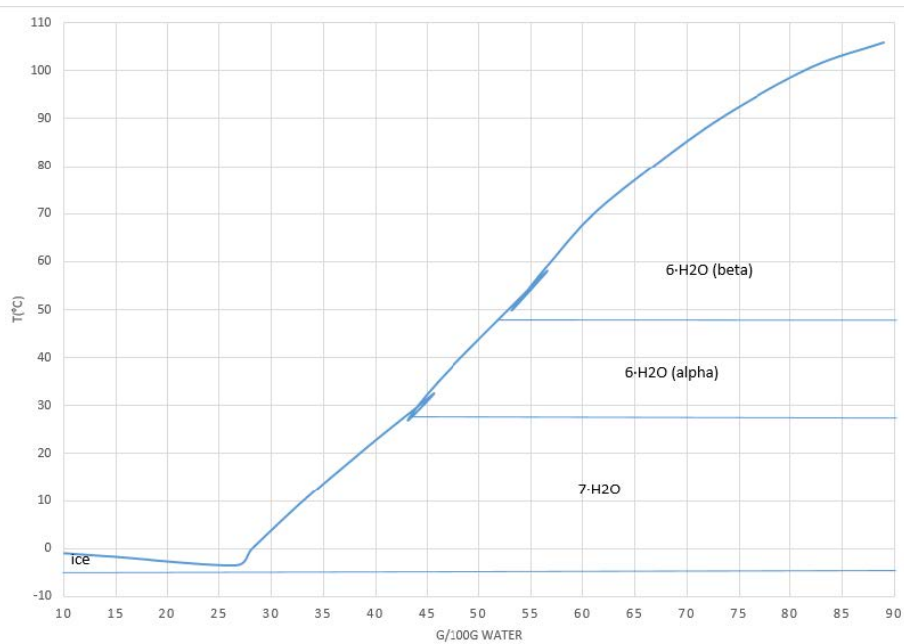


FIGURE A.2: Phase diagram of Nickel sulfate (Hassanein, 2018)

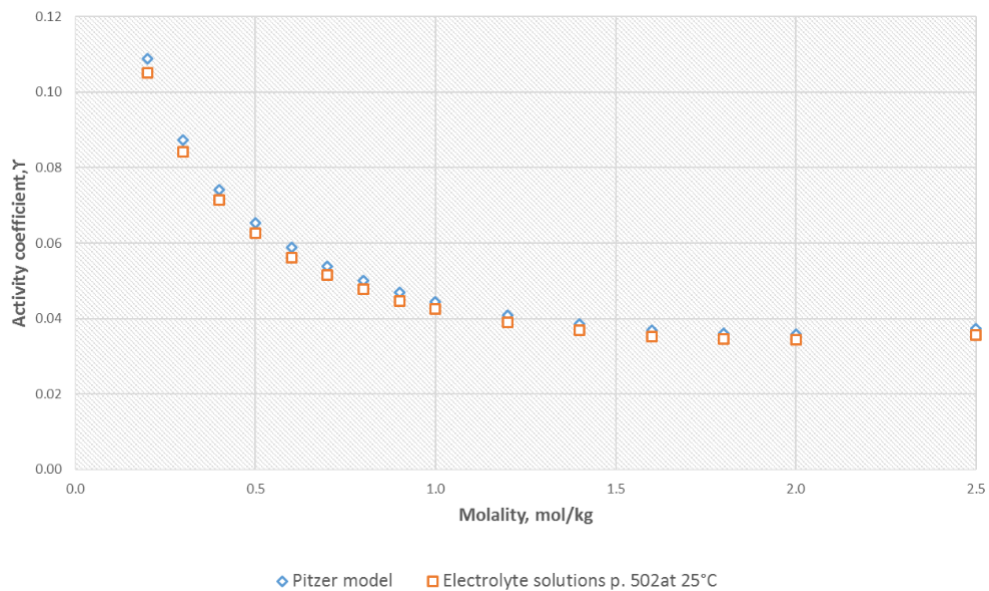


FIGURE A.3: Pitzer model of a pure Nickel sulfate aqueous solution to estimate activity coefficients at different temperatures. (Hassanein, 2018)

TABLE A.2: The saturation solubility of Nickel sulfate hexahydrate in water

[°C]	$\text{NiSO}_4 \cdot 6\text{H}_2\text{O}$ (g)/g of solution	$\text{NiSO}_4 \cdot 6\text{H}_2\text{O}$ (g)/g of "free H_2O "
0	0.363	0.571
10	0.414	0.708
20	0.465	0.870
25	0.489	0.958
30	0.515	1.060
35	0.533	1.143
40	0.544	1.191
50	0.579	1.376
60	0.608	1.551
70	0.640	1.780
75	0.659	1.933
80	0.678	2.103
90	0.718	2.552
100	0.761	3.183

Appendix B

Solution Compositions and induction times

The compositions used in every experiments is shown in the following tables.

B.1 25°C Batch Reactor Solution composition

The total mass of the solution before adding impurities is 656.17 grams, this value is used to calculate the impurity ion mass. Ion do not exist alone in the solid state, but rather as a salt. The table below shows the impurity ion mass to be added to solution for 3, 5 and 10 grams/kg of solution, and the equivalent salt mass. Table B.1 shows the equivalent values of ion mass to salt mass.

TABLE B.1: Impurity ion mass values for of batch experiments conducted at 25°C based on a total solution mass of 656.17g

Solution concentration	Impurity ion mass	Na_2SO_4	$NiCl_2$	$MgSO_4$
[g]	[g]	[g]	[g]	[g]
3g/kg of sol.	1.97	6.08	3.60	9.75
5g/kg of sol.	3.28	10.13	6.00	16.25
10g/kg of sol.	6.56	20.27	12.00	32.49

TABLE B.2: Solution composition of batch experiments conducted at 25°C.

Solution concentration	$NiSO_4 * 6H_2O$	H_2O	Na_2SO_4	$NiCl_2$	$MgSO_4$
	[g]	[g]	[g]	[g]	[g]
3g Na/kg sol.	350.16	306.01	6.08	(-)	(-)
5g Na/kg of sol.	350.16	306.01	10.13	(-)	(-)
10g Na/kg of sol.	350.16	306.01	20.27	(-)	(-)
3g Cl/kg of sol.	350.16	306.01	(-)	3.60	(-)
5g Cl/kg of sol.	350.16	306.01	(-)	6.00	(-)
10g Cl/kg of sol.	350.16	306.01	(-)	12.00	(-)
3g Mg/kg of sol.	350.16	306.01	(-)	(-)	9.75
5g Mg/kg of sol.	350.16	306.01	(-)	(-)	16.25
10g Mg/kg of sol.	350.16	306.01	(-)	(-)	32.49
3g Na, Cl, Mg/kg of sol.	350.16	306.01	6.08	3.60	9.75
5g Na, Cl, Mg/kg of sol.	350.16	306.01	10.13	6.00	16.25
10g Na, Cl, Mg/kg of sol.	350.16	306.01	20.27	12.00	32.49

TABLE B.3: Impurity ion mass values for of batch experiments conducted at 60°C based on a total solution mass of 280.853g

Solution concentration	Impurity ion mass	Na_2SO_4	$NiCl_2$	$MgSO_4$
[g]	[g]	[g]	[g]	[g]
3g/kg of sol.	0.84	2.60	1.54	4.17
5g/kg of sol.	1.40	4.33	2.57	6.95
10g/kg of sol.	2.81	8.66	5.13	13.90

TABLE B.4: Solution composition of solubility tests conducted at 25°C, 50°C and 75°C.

Temperature	$NiSO_4 * 6H_2O$ in	H_2O	H_2SO_4
	[g]	[g]	[g]
25°C	171.55	179.45	1.75
50°C	219.53	159.72	1.89
75°C	281.95	134.07	2.08

B.2 60°C batch reactor solution composition

The total mass of the solution before adding impurities is 280.853 grams, this value is used to calculate the impurity ion mass. Ion do not exist alone in the solid state, but rather as a salt. The table below shows the impurity ion mass to be added to solution for 3, 5 and 10 grams/kg of solution, and the equivalent salt mass. Table B.3 shows the equivalent values of ion mass to salt mass.

TABLE B.5: Exact solubilities of solubility tests conducted at 25°C, 50°C and 75°C and exact values used in figure 4.21.

Temperature	Theoretical solubility [g/100g water]	$NiSO_4 \cdot 6H_2O$ out [g]	Resulting solubility [g/100g water]
25°C	40.45	3.02	39.89
50°C	51.75	5.24	50.91
75°C	63.40	25.95	59.84

Appendix C

Detailed Experimental Procedures

C.1 25°C batch reactor experimental procedure

1. Weigh and prepare 350.16g of Nickel Sulfate Hexahydrate and 306.01g of deionized water, and any impurities, which will be used in the experiments. This ratio of Nickel sulfate at deionized water saturates at 35°C.
2. Combine the components and impurities in a heat-resistant glass container.
3. Close the system to prevent any evaporation or loss of material.
4. Heat to 60 °C using a hotplate and magnetic stirrer at 600 RPM.
5. Set the refrigerated/heating circulator connected to the Batch reactor to 60°C.
6. Allow 60 minutes for the Nickel sulfate hexahydrate and impurities to completely dissolve and for the batch reactor to reach steady state temperature.
7. Carefully pour the 60°C solution into the warm batch reactor.
8. Close the reactor lid and start agitation at 600 RPM.
9. Submerge temperature gauge in solution, with automatic temperature reading intervals of 20 seconds.
10. Set the target temperature on the refrigerated/heating circulator to 25°C.
11. Allow 120 minutes for the solution to cool to 25°C.
12. At 25°C, insert Nickel sulfate hexahydrate seeds.
13. A rise in temperature indicates crystallization has taken place.
14. Note approximate induction time.
15. When pH stabilizes, the crystal growth process has stopped.

16. Filter the crystals using a vacuum filtration setup as illustrated in figure 3.3.
17. Wash the wet crystals with ethanol to disperse solution still on the crystal surfaces.
18. The ethanol should harden and clump the filter cake to the point where it can be picked up in one piece without breaking.
19. Dry the deposited crystals in a 50°C heating cabinet for 24 hours.
20. Declump crystals using a mortar and pestle.
21. Analyze for impurity content.

C.2 60° batch experiment procedure

1. Weigh and prepare 179.83g Nickel sulfate hexahydrate, 101.03g deionized water (+75g of water to be evaporated), 1.4g sulfuric acid, and any impurities, which will be used in the experiment.
2. Combine the components and impurities in a heat-resistant 600 mL glass beaker on a hotplate with agitation of 600 RPM using magnetic stirring.
3. Heat the solution to 80°C.
4. Allow about 2 hours for excess water in the solution to evaporate and solute to dissolve.
5. Once 30-35 mL of the solution is evaporated, set the target temperature on the hotplate to 60°C.
6. Allow the remaining excess 40 mL to evaporate.
7. When the solution reaches 60°C and a total of 75 mL of water has evaporated, insert Nickel sulfate hexahydrate seeds.
8. A rise in temperature indicates crystallization has taken place.
9. Note approximate induction time.
10. When pH stabilizes, the crystal growth process has stopped.
11. Filter the crystals using a vacuum filtration setup as illustrated in figure 3.3.
12. Wash the wet crystals with ethanol to disperse solution still on the crystal surfaces.

13. Dry deposited crystals in a 50°C heating cabinet for 24 hours.
14. Declump crystals using a mortar and pestle.
15. Analyze for impurity content.

C.3 Partial dissociation experiment procedure

1. Prepare 5g of carefully declumped precipitated Nickel sulfate hexahydrate crystal and 2.5g of deionized water.
2. Place the crystals in a small breaker, contain the water in a syringe.
3. Using the syringe, distribute the water evenly into the beaker.
4. Gently mix the slurry for 60 minutes using a magnetic stirrer at 100 RPM. Figure 3.5 illustrates this setup.
5. Using vacuum filtration with a Millipore 0.22 μ m, \varnothing =47 mm filter, separate the partially dissolved crystals from the slurry.
6. Wash the crystals with ethanol to disperse excess solution present on the surface of the wet, partially dissolved crystals.
7. Dry the crystals in a heating cabinet for 24 hours.
8. Weigh new crystal mass at approximately 2.85g. This represents about 43% of the mass being dissolved by the process.
9. Declump crystals using a mortar and pestle.
10. Analyze new concentration of impurities.

C.4 Solubility experiment procedure

1. Prepare a solution of Nickel sulfate and water. The composition of said solution differs depending on the temperature being investigated. The exact compositions used for 25, 50 and 75°C are found in Appendix B.4.
2. Agitate at 600 RPM using a magnetic stirrer.
3. Add 5g/kg of sulfuric acid to the solution.
4. Heat solution to the target temperature.

5. Keep adding Nickel sulfate hexahydrate until it stops dissolving.
6. Allow the system 24 hours to reach and stay at equilibrium.
7. Filter using vacuum filtration as illustrated in figure 3.3.
8. Wash the crystals with ethanol to disperse solution from crystals.
9. Dry crystals in a 50°C heating cabinet for 24 hours.
10. Weigh dried crystals and compare with total weight dissolved and Nickel sulfate hexahydrate still in the solution to calculate solubility.

Appendix D

X-ray diffraction patterns

D.1 X-ray diffraction patterns compound identification

Figures D.1 to D.5 show XRD patterns of Nickel sulfate hexahydrate crystallized from a solution of 10 g/kg of Na^+ , Cl^- , and Mg^{2+} with overlays of other potential compounds that may have co-crystallized. Figures D.6 to D.17 show XRD patterns of every test at 25°C without partial filtration. XRD was not done on partially filtrated Nickel sulfate.

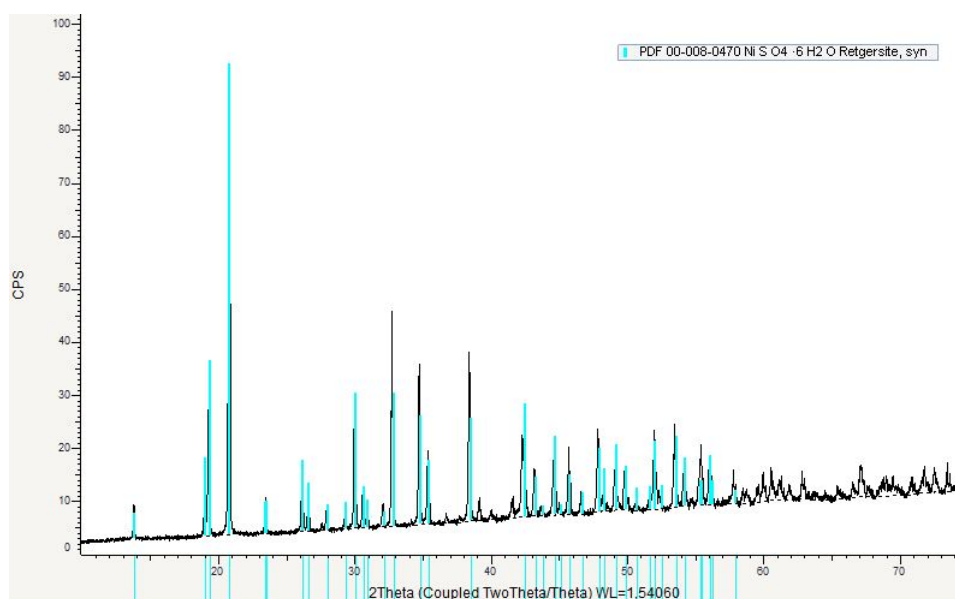


FIGURE D.1: XRD pattern of Nickel sulfate hexahydrate crystallized from a supersaturated solution at 25°C with deliberately added impurities of 10 g/kg of Na^+ , Cl^- , and Mg^{2+} overlaid with the XRD pattern of Nickel sulfate hexahydrate

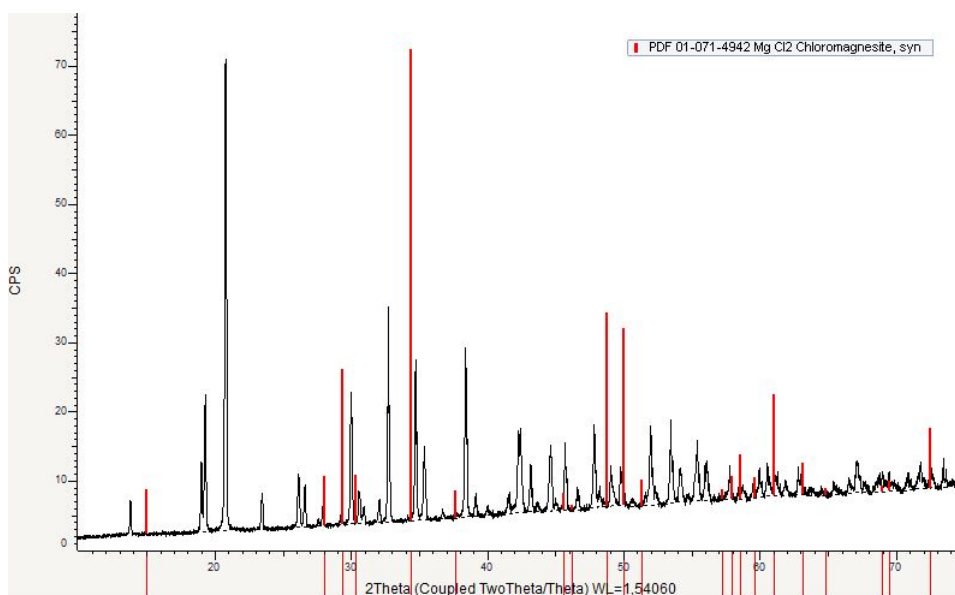


FIGURE D.2: XRD pattern of Nickel sulfate hexahydrate crystallized from a supersaturated solution at 25°C with deliberately added impurities of 10 g/kg of Na^+ , Cl^- , and Mg^{2+} overlaid with the XRD pattern of Magnesium chloride ($MgCl_2$)

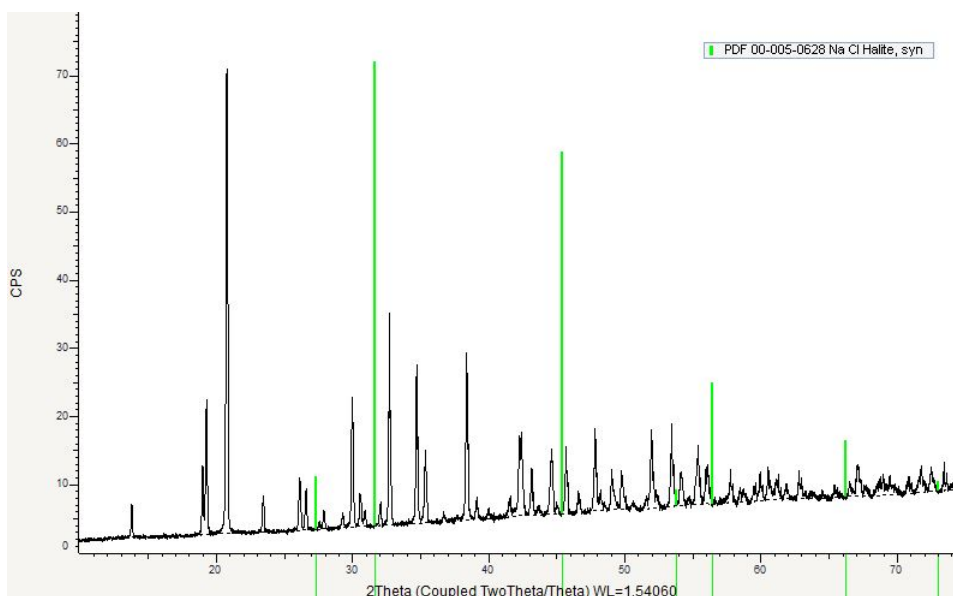


FIGURE D.3: XRD pattern of Nickel sulfate hexahydrate crystallized from a supersaturated solution at 25°C with deliberately added impurities of 10 g/kg of Na^+ , Cl^- , and Mg^{2+} overlaid with the XRD pattern of Sodium chloride ($NaCl$)

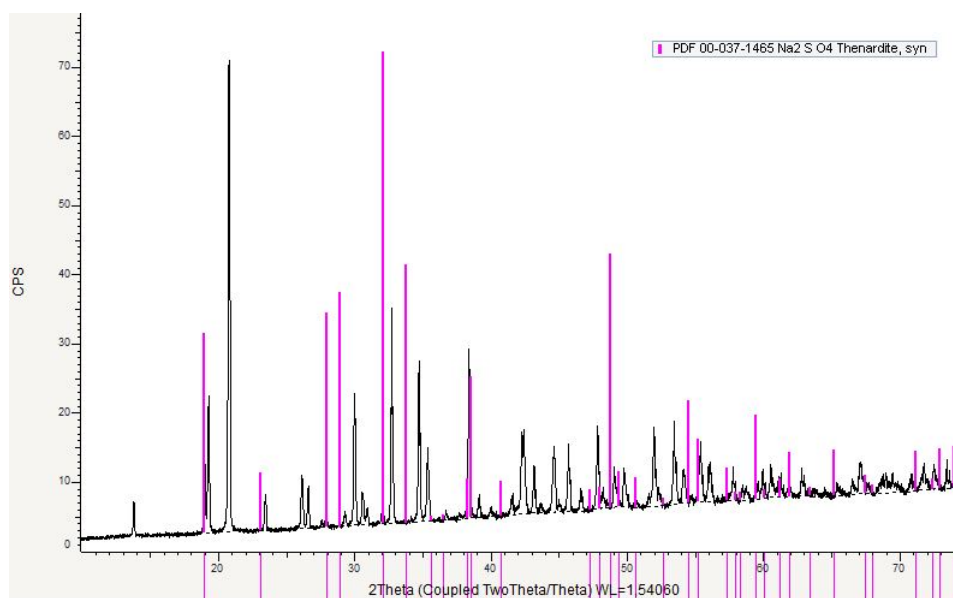


FIGURE D.4: XRD pattern of Nickel sulfate hexahydrate crystallized from a supersaturated solution at 25°C with deliberately added impurities of 10 g/kg of Na^+ , Cl^- , and Mg^{2+} overlaid with the XRD pattern of Sodium sulfate (Na_2SO_4)

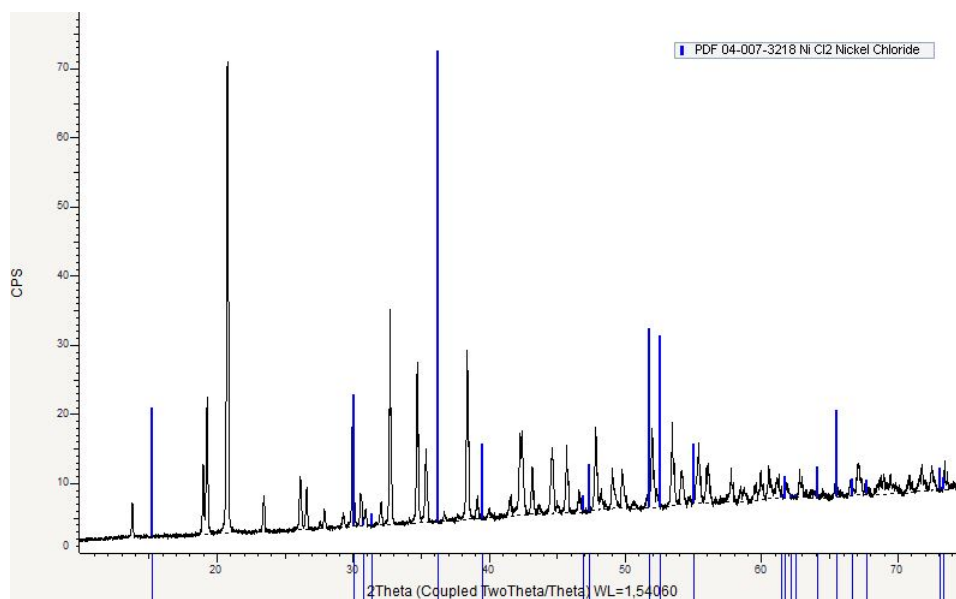


FIGURE D.5: XRD pattern of Nickel sulfate hexahydrate crystallized from a supersaturated solution at 25°C with deliberately added impurities of 10 g/kg of Na^+ , Cl^- , and Mg^{2+} overlaid with the XRD pattern of Nickel chloride ($NiCl_2$)

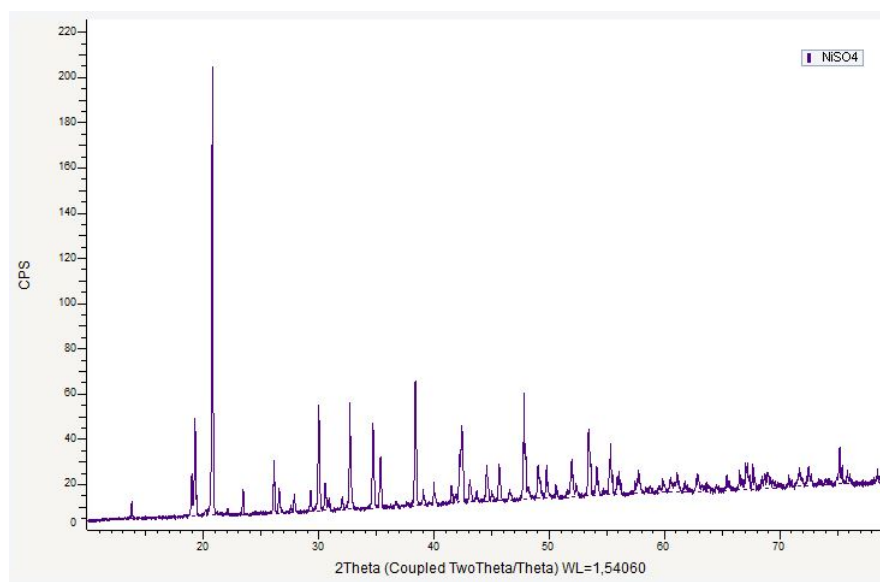


FIGURE D.6: XRD pattern of Nickel sulfate hexahydrate crystallized from a supersaturated aqueous solution of 3g Na^+ per kg of solution at 25°C.

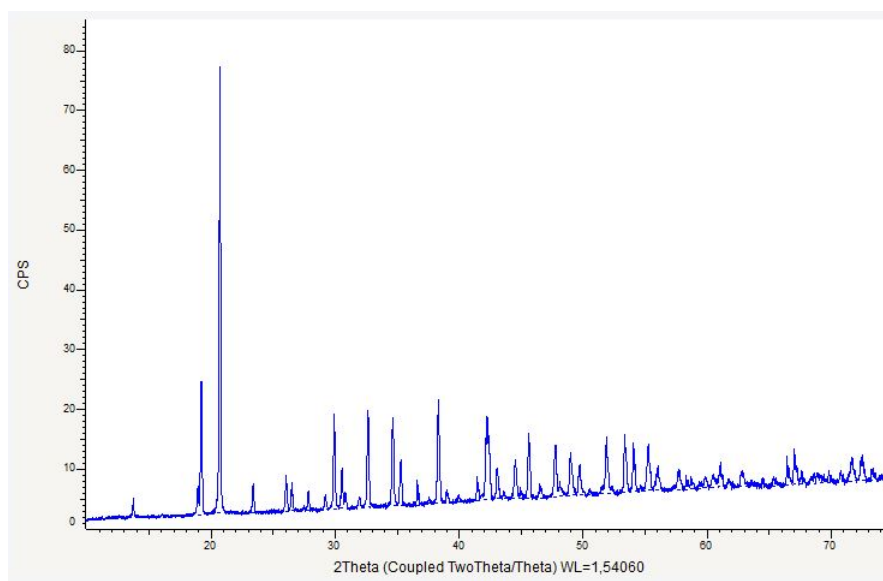


FIGURE D.7: XRD pattern of Nickel sulfate hexahydrate crystallized from a supersaturated aqueous solution of 5g Na^+ per kg of solution at 25°C.

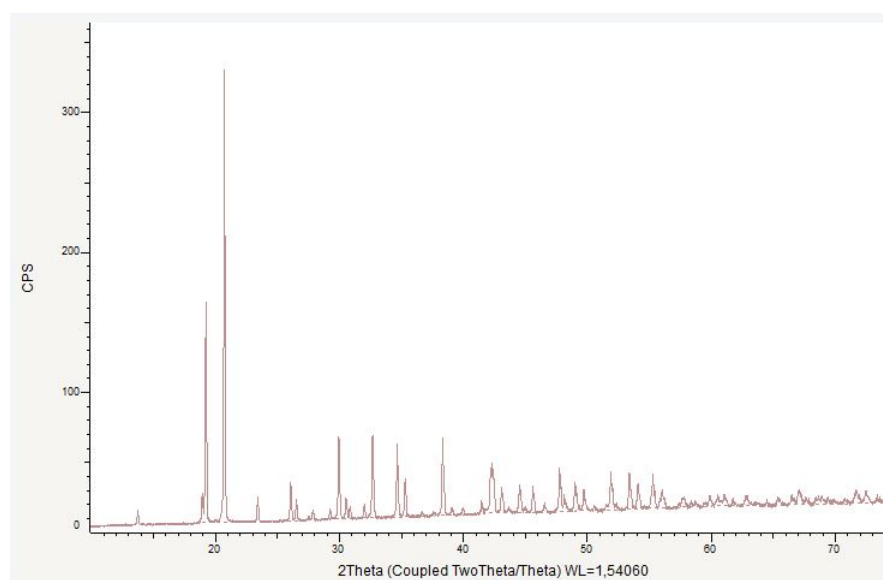


FIGURE D.8: XRD pattern of Nickel sulfate hexahydrate crystallized from a supersaturated aqueous solution of 10g Na^+ per kg of solution at 25°C.

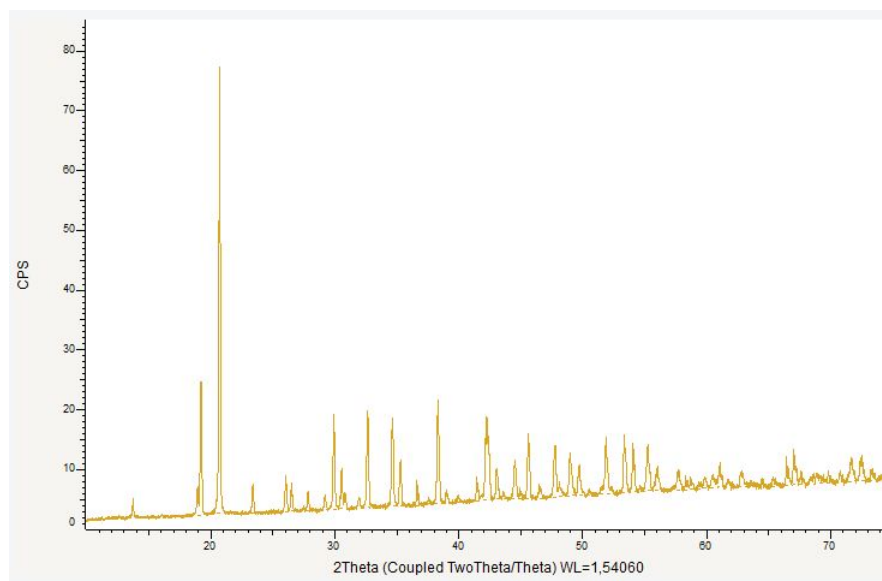


FIGURE D.9: XRD pattern of Nickel sulfate hexahydrate crystallized from a supersaturated aqueous solution of 3g Cl^- per kg of solution at 25°C.

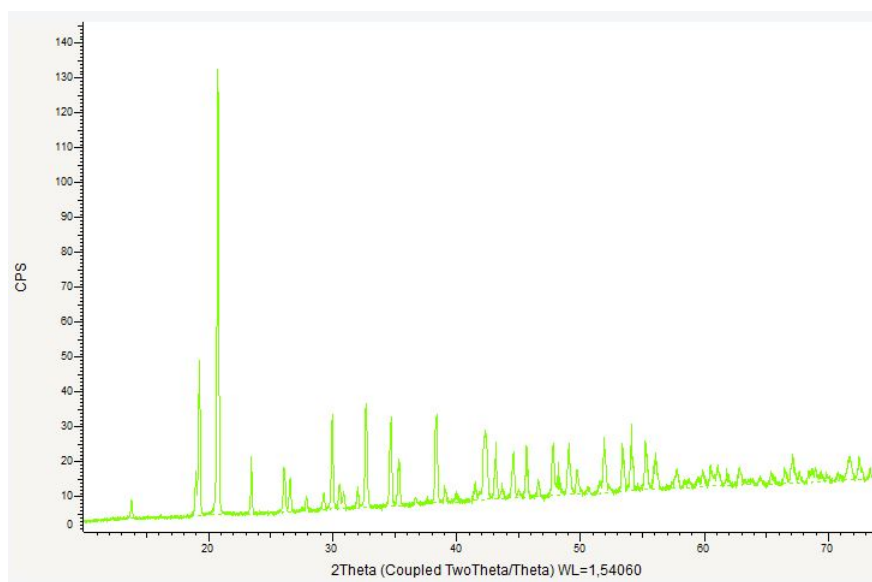


FIGURE D.10: XRD pattern of Nickel sulfate hexahydrate crystallized from a supersaturated aqueous solution of 5g Cl^- per kg of solution at 25°C.

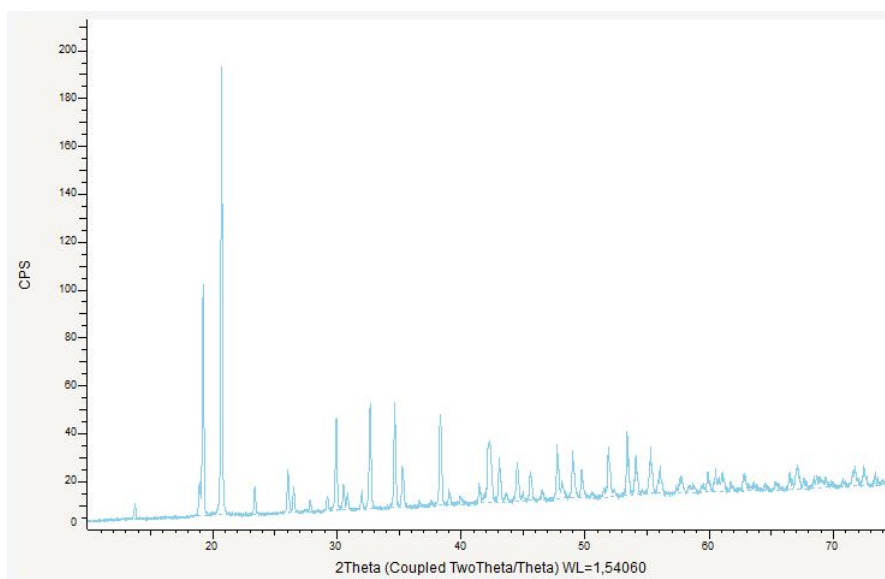


FIGURE D.11: XRD pattern of Nickel sulfate hexahydrate crystallized from a supersaturated aqueous solution of 10g Cl^- per kg of solution at 25°C.

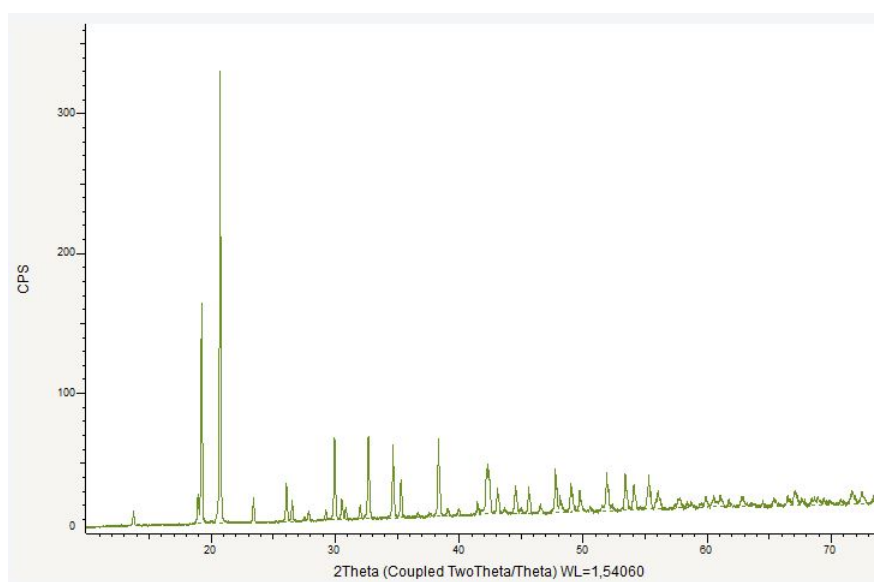


FIGURE D.12: XRD pattern of Nickel sulfate hexahydrate crystallized from a supersaturated aqueous solution of 3g Mg^{2+} per kg of solution at 25°C.

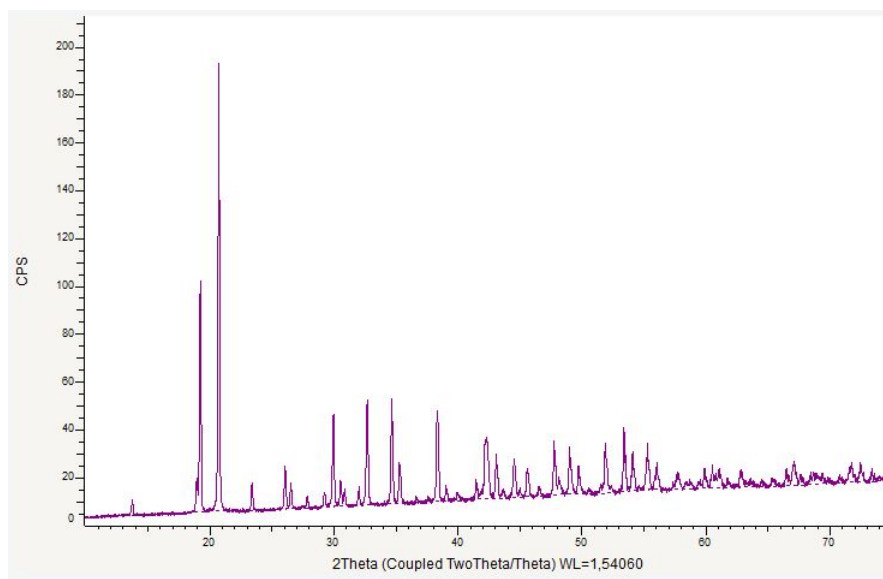


FIGURE D.13: XRD pattern of Nickel sulfate hexahydrate crystallized from a supersaturated aqueous solution of 5g Mg^{2+} per kg of solution at 25°C.

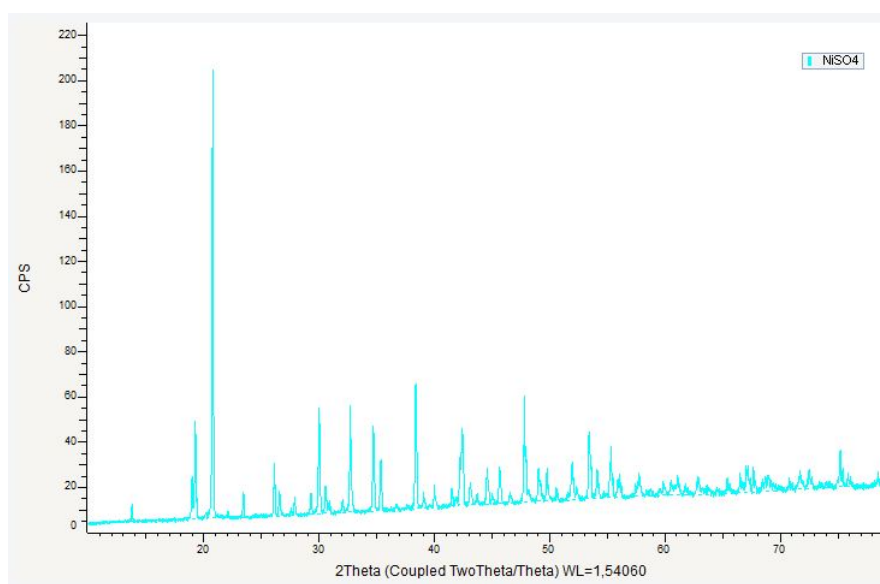


FIGURE D.14: XRD pattern of Nickel sulfate hexahydrate crystallized from a supersaturated aqueous solution of 10g Mg^{2+} per kg of solution at 25°C.

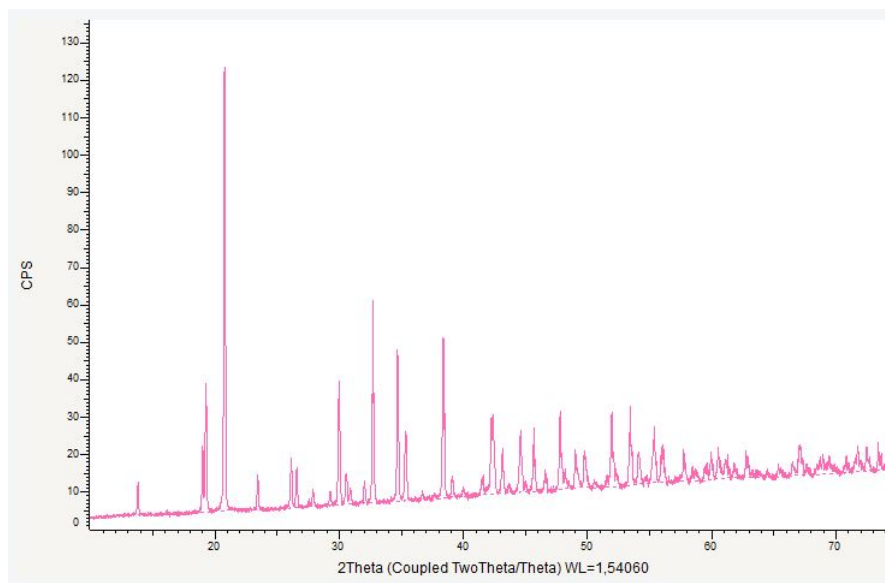


FIGURE D.15: XRD pattern of Nickel sulfate hexahydrate crystallized from a supersaturated aqueous solution of 3g Na^+ , Cl^- , and Mg^{2+} per kg of solution at 25°C.

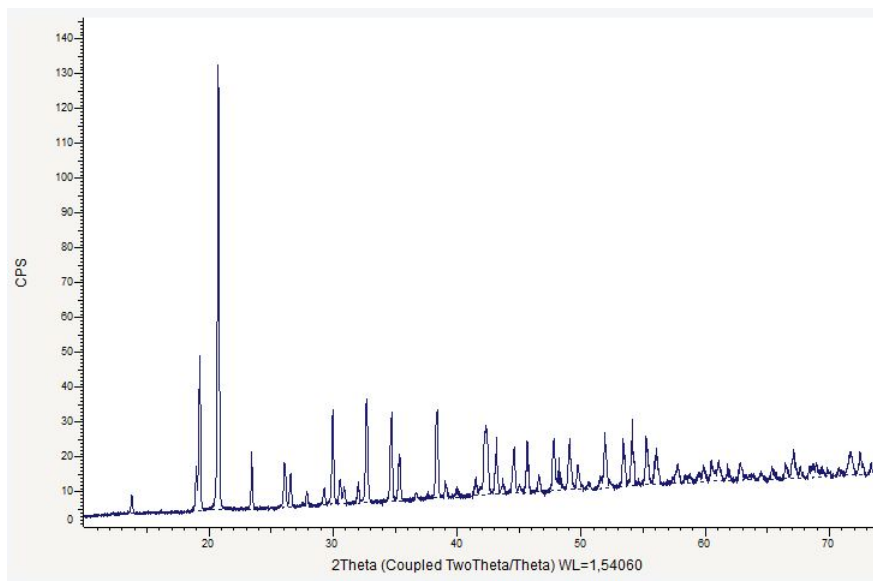


FIGURE D.16: XRD pattern of Nickel sulfate hexahydrate crystallized from a supersaturated aqueous solution of 5g Na^+ , Cl^- , and Mg^{2+} per kg of solution at 25°C.

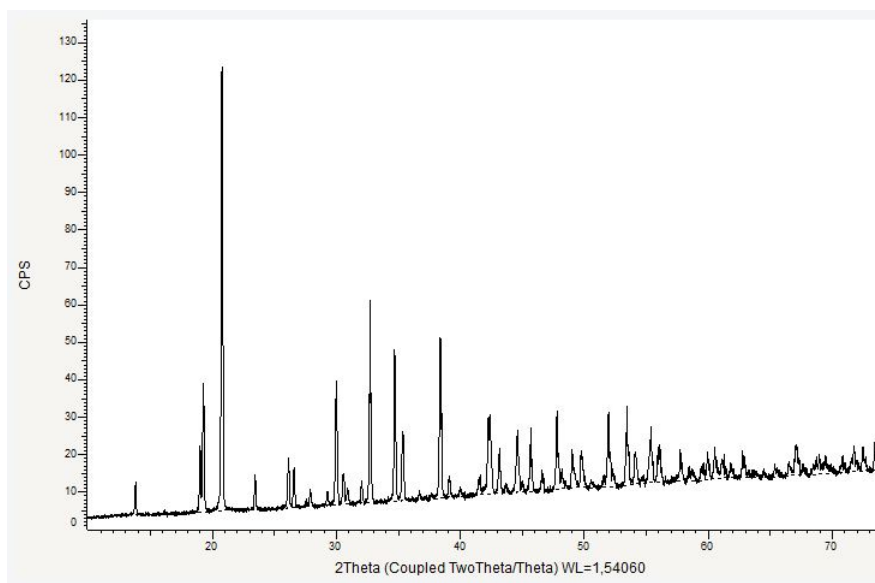
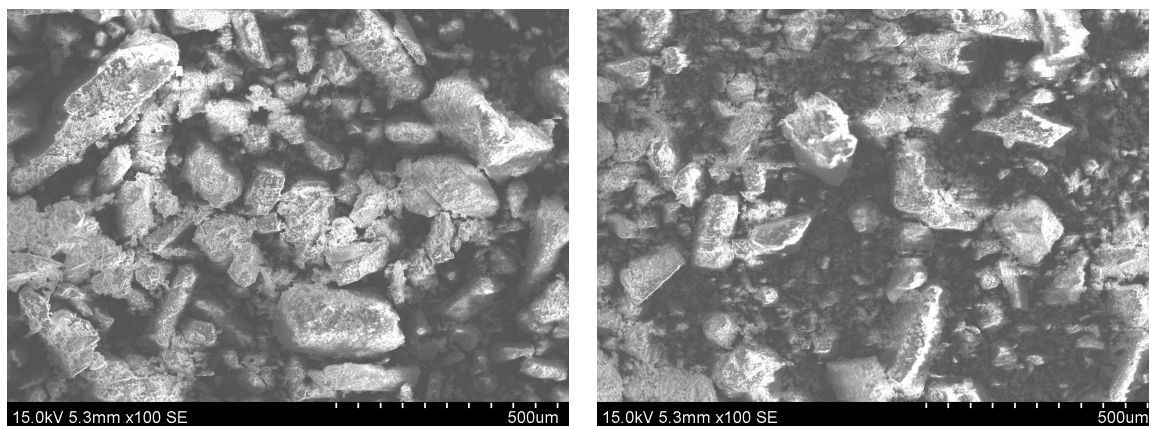


FIGURE D.17: XRD pattern of Nickel sulfate hexahydrate crystallized from a supersaturated aqueous solution of 10g of Na^+ , Cl^- , and Mg^{2+} per kg of solution at 25°C.

Appendix E

Scanning electron microscope pictures

E.1 Na^+ only SEM photographs



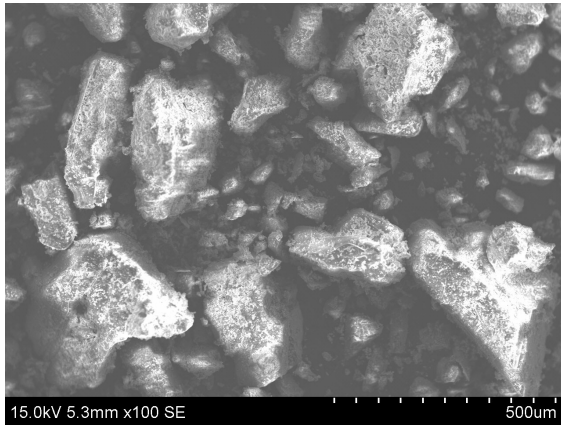
(A) Before partial filtration

(B) After partial filtration

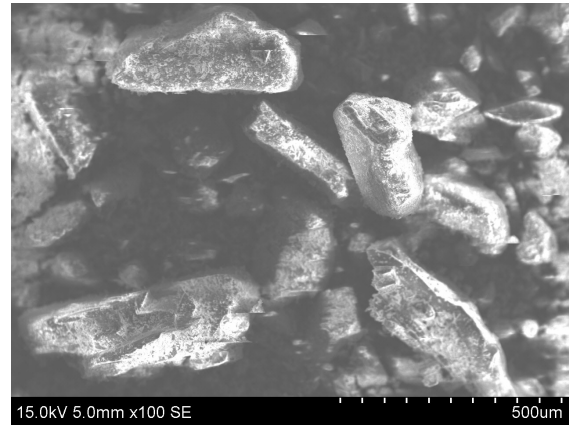
FIGURE E.1: Final crystals from experiment with 3 grams per kg of Na^+ at $25^{\circ}C$ before and after partial filtration. Scale bar of $500 \mu m$ shown as reference

E.2 Cl^- only SEM photographs

E.3 Mg^{2+} only SEM photographs

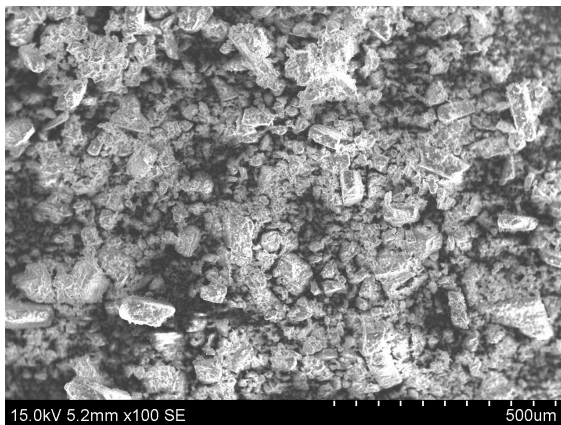


(A) Before partial filtration

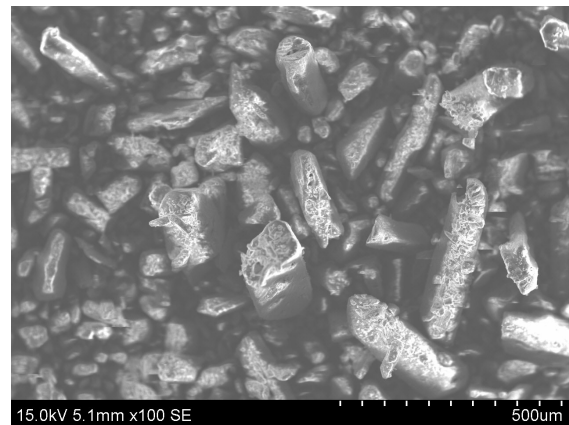


(B) After partial filtration

FIGURE E.2: Final crystals from experiment with 5 grams per kg of Na^+ at 25°C before and after partial filtration. Scale bar of 500 μm shown as reference

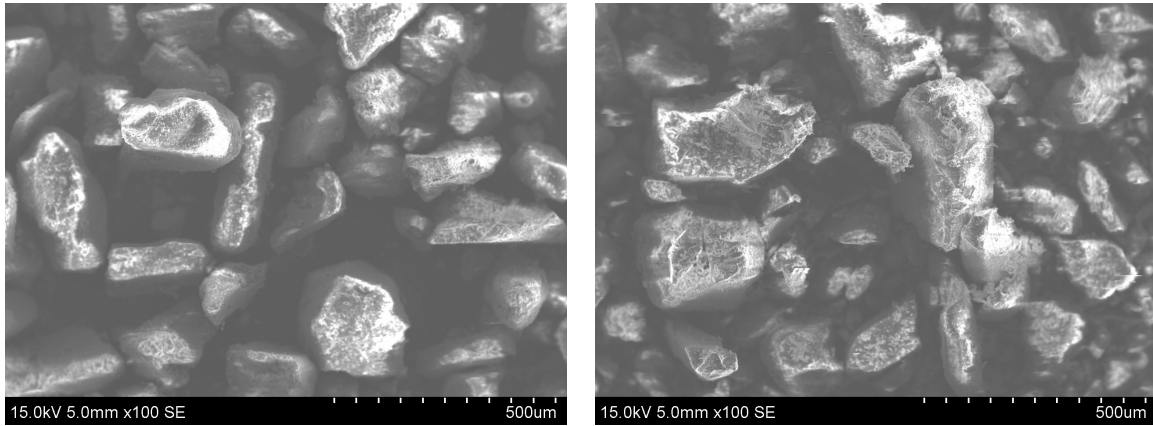


(A) Before partial filtration



(B) After partial filtration

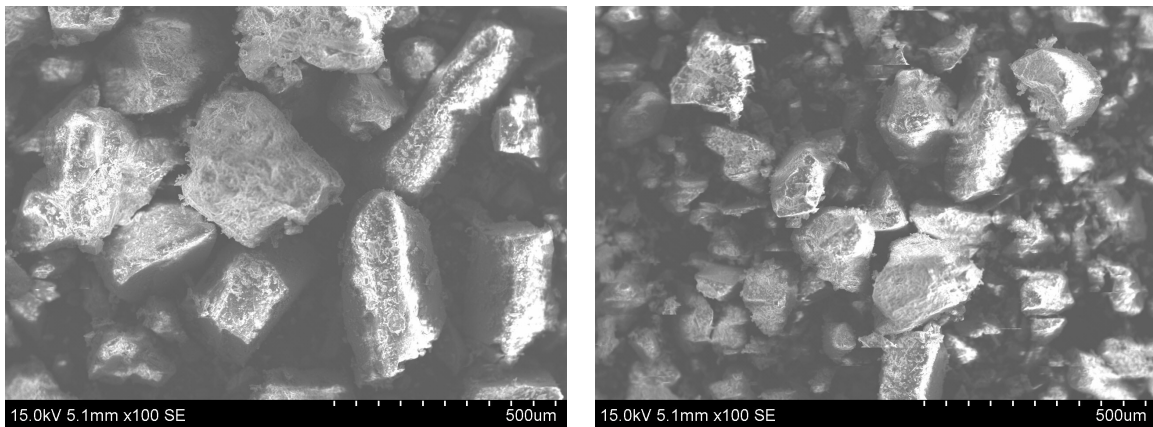
FIGURE E.3: Final crystals from experiment with 10 grams per kg of Na^+ at 25°C before and after partial filtration. Scale bar of 500 μm shown as reference



(A) Before partial filtration

(B) After partial filtration

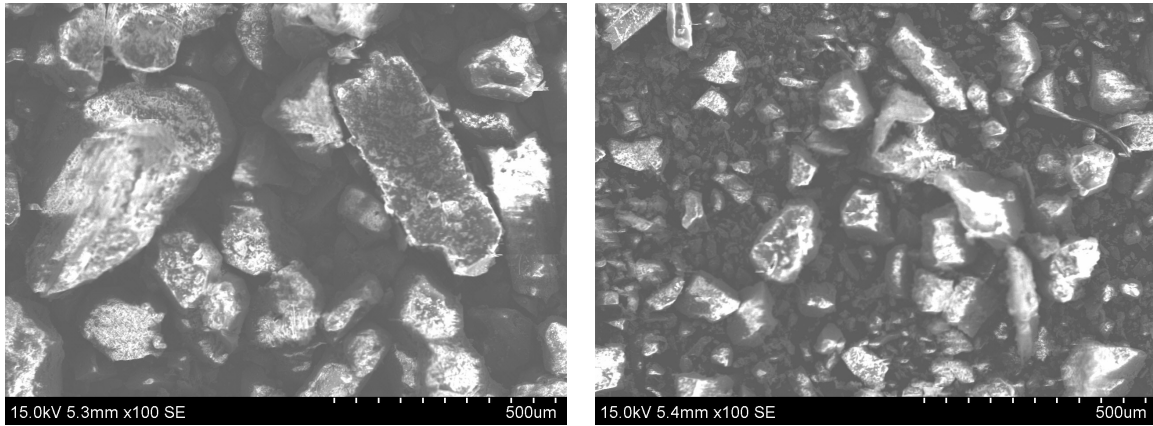
FIGURE E.4: Final crystals from experiment with 3 grams per kg of Cl^- at 25°C before and after partial filtration. Scale bar of 500 μm shown as reference



(A) Before partial filtration

(B) After partial filtration

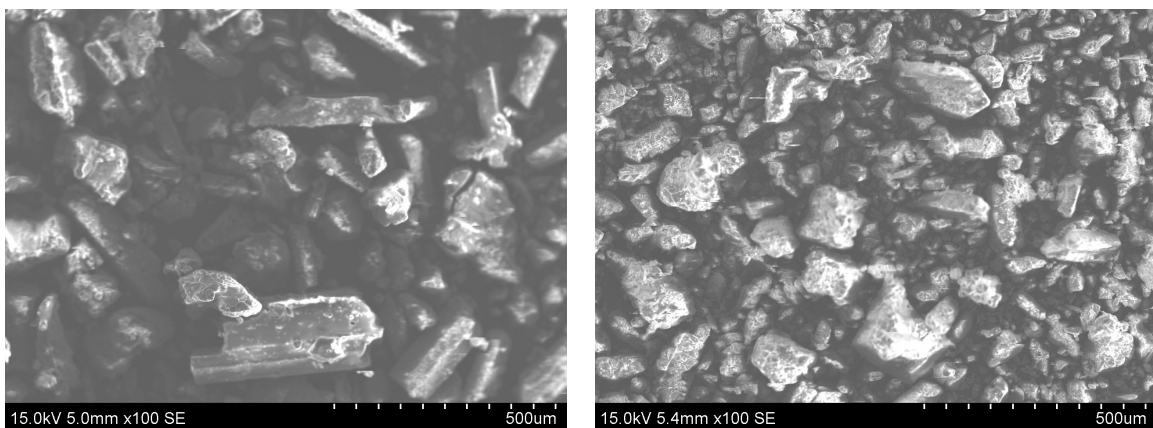
FIGURE E.5: Final crystals from experiment with 5 grams per kg of Cl^- at 25°C before and after partial filtration. Scale bar of 500 μm shown as reference



(A) Before partial filtration

(B) After partial filtration

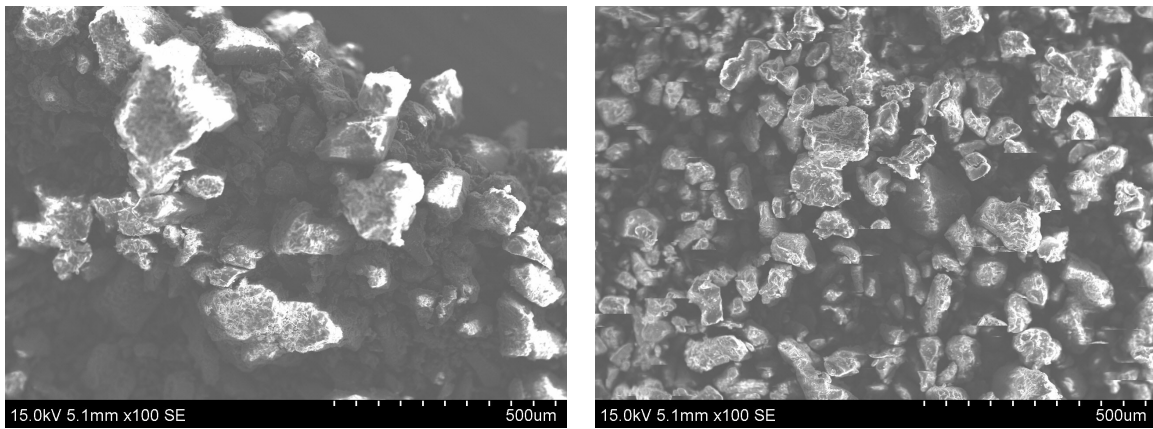
FIGURE E.6: Final crystals from experiment with 10 grams per kg of Cl^- at $25^\circ C$ before and after partial filtration. Scale bar of $500 \mu m$ shown as reference



(A) Before partial filtration

(B) After partial filtration

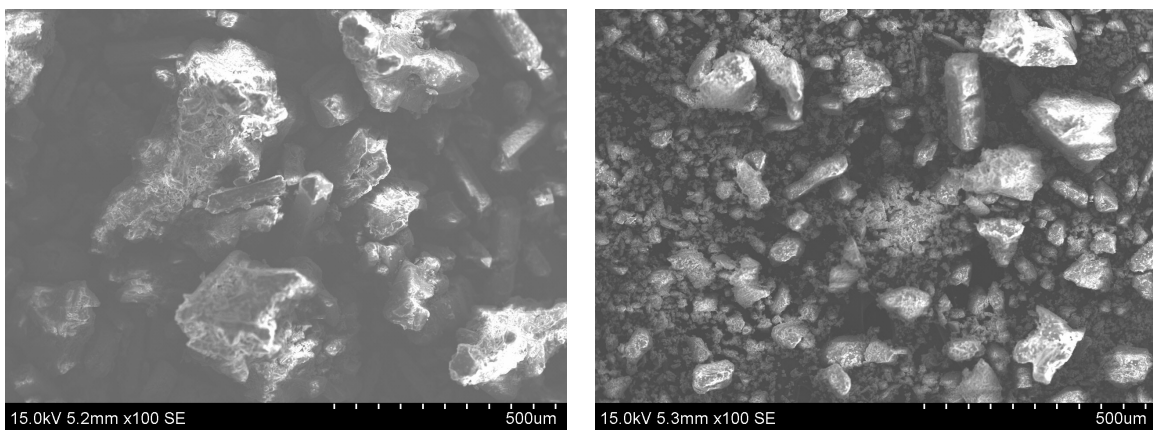
FIGURE E.7: Final crystals from experiment with 3 grams per kg of Mg^{2+} at $25^\circ C$ before and after partial filtration. Scale bar of $500 \mu m$ shown as reference



(A) Before partial filtration

(B) After partial filtration

FIGURE E.8: Final crystals from experiment with 5 grams per kg of Mg^{2+} at $25^{\circ}C$ before and after partial filtration. Scale bar of $500 \mu m$ shown as reference



(A) Before partial filtration

(B) After partial filtration

FIGURE E.9: Final crystals from experiment with 10 grams per kg of Mg^{2+} at $25^{\circ}C$ before and after partial filtration. Scale bar of $500 \mu m$ shown as reference

Appendix F

Health Safety and Environment

All HSE information can be found on NTNU avvik with Riskmanager ID: 23858.

Bibliography

- Andreassen, J.-P. (2015). *Short course in crystallization and precipitation from solution*.
- Beevers, CA t and H Lipson (1932). "The Crystal Structure of Nickel Sulphate Hexahydrate, NiSO₄·6H₂O". In: *Zeitschrift für Kristallographie-Crystalline Materials* 83.1-6, pp. 123–135.
- Berckmans, Gert et al. (2017). "Cost projection of state of the art lithium-ion batteries for electric vehicles up to 2030". In: *Energies* 10.9, p. 1314.
- Buckley, HE (1930). "XXVI. The Crystallization of Potash-alum and the Effect of Certain Added Impurities on its Habit". In: *Zeitschrift für Kristallographie-Crystalline Materials* 73.1-6, pp. 443–464.
- Bøckmann, Oluf (2018). Personal Communication.
- Callen, Herbert B and Theodore A Welton (1951). "Irreversibility and generalized noise". In: *Physical Review* 83.1, p. 34.
- chem.libretexts.org (2017). *vacuum filtration*.
- De Boer, Frank R et al. (1988). "Cohesion in metals". In:
- Garside, J (1971). "The concept of effectiveness factors in crystal growth". In: *Chemical Engineering Science* 26.9, pp. 1425–1431.
- Hassanein, Jusri (2018). "Purification of nickel sulfate by crystallization; Nikkeli-sulfaatin puhdistus kiteyttämällä". en. In: pp. 48+22.
- Haynes, William M (2014). *CRC handbook of chemistry and physics*. CRC press.
- Jibbouri, Sattar et al. (2002). "Effects of additives in solution crystallization". In:
- Kubota, N, M Yokota, and JW Mullin (1996). "Kinetic Models for the Crystal Growth from Aqueous Solution in the Presence of Impurities—Steady and Unsteady State Impurity Actions". In: *Proceeding of the 13th Symposium on Industrial Crystallization, B. Biscans and N. Gabas, Eds., Toulouse, France*, pp. 111–116.
- Kubota, Noriaki and JW Mullin (1995). "A kinetic model for crystal growth from aqueous solution in the presence of impurity". In: *Journal of Crystal Growth* 152.3, pp. 203–208.
- Liebermann, Ernst and Vojtech Fried (1972). "Estimation of the Excess Gibbs Free Energy and Enthalpy of Mixing of Binary Nonassociated Mixtures". In: *Industrial & Engineering Chemistry Fundamentals* 11.3, pp. 350–354.

- Lierhagen, Syverin (2018). Personal Communication.
- Lohninger, Hans (2011). "Sodium Sulfate". In: *Genchem & Inorganic Compounds*.
- Mohameed, HA and J Ulrich (1996). "Influence of the pH-Value on the Growth and Dissolution Rate of Potassium Chloride". In: *Crystal Research and Technology* 31.1, pp. 27–31.
- Mullin, John William (2001). *Crystallization*. Elsevier.
- Myerson, Allan (2002). *Handbook of industrial crystallization*. Butterworth-Heinemann.
- Nitta, Naoki et al. (2015). "Li-ion battery materials: present and future". In: *Materials today* 18.5, pp. 252–264.
- Okorafor, Ogonnaya C (1999). "Solubility and density isotherms for the sodium sulfate- water- methanol system". In: *Journal of Chemical & Engineering Data* 44.3, pp. 488–490.
- Perrot, Pierre (1998). *A to Z of Thermodynamics*. Oxford University Press on Demand.
- Roland, G et al. (2013). "Entropy from State Probabilities: Hydration Entropy of Cations". In: *Journal of physical chemistry*.
- Rousseau, Ed Ronald W (2009). *Handbook of separation process technology*. John Wiley & Sons.